THEORETICAL AND EXPERIMENTAL INVESTIGATION OF MICRO MILLING FOR ADDITIVE MANUFACTURED TITANIUM ALLOY

MUHAMMAD REHAN

PhD

The Hong Kong Polytechnic University

2025

The Hong Kong Polytechnic University

Department of Industrial and Systems Engineering

Theoretical and experimental investigation of micro milling for additive manufactured titanium alloy

Muhammad Rehan

A thesis submitted in partial fulfillment of the requirements for the degree of Doctor of Philosophy

August 2024

CERTIFICATE OF ORIGINALITY

I hereby declare that this thesis is entirely my own work. To the best of my knowledge and belief, it does not contain any material previously published or written by another individual, nor any material that has been submitted for the award of any other degree or diploma, except where proper acknowledgment is provided within the text.

Signature: ----------

Student's Name: Muhammad Rehan

ABSTRACT

Additive Manufacturing (AM) has garnered significant attention due to its ability to produce intricate and complex profiles, lattice structures, and internal and thin-walled structures. Selective Laser Melting (SLM) has emerged as a leading AM method for metals due to its exceptional adaptability in fabricating complex metallic parts, offering flexibility in shapes and geometries. This is especially beneficial for titanium alloys, as the rapid cooling inherent in SLM transforms the stable Ti6Al4V phase into α' martensite within a hexagonal close-packed (HCP) crystal structure. The improved mechanical and microstructural properties of Ti6Al4V produced by SLM have garnered significant interest among metal machining researchers. Consequently, the study of SLM-fabricated Ti6Al4V and its machining characteristics is a focal point in advanced manufacturing.

Despite the significant improvements in the mechanical and microstructural properties of Ti6Al4V produced by SLM, challenges remain in achieving the required surface finish and precise geometry for critical applications, underscoring the importance of post-processing techniques. Micro-milling is a promising method for producing intricate parts with high accuracy, but it presents challenges such as deteriorated surface quality, burr formation, and accelerated tool wear. These issues necessitate careful investigation of influences of machining parameters on micro-milling performances and also the machining effects on the microstructure changes on the machined surface.

This thesis aims to address these machining difficulties by integrating micro- milling with SLM technology, leveraging the advantages of both methods. The performance of micro-milling was evaluated in terms of surface roughness, tool wear, chip morphology, and burr formation through comparative experimentation on SLM Ti6Al4V and wrought Ti6Al4V. The results reveal the micro-milling mechanism and demonstrate superior machinability of SLM Ti6Al4V.

A 3D finite element model (FEM) was developed to simulate the shearing process, incorporating complexities such as tool rotation and interactions between the cutting tool and workpiece surfaces. This model helps in understanding the impact of machining parameters on surface defects, chip morphology, and cutting forces of SLM titanium alloys and is successfully validated with experimental results. On the other hand, this study explores the application of a magnetic field to enhance machining performance. The application of an external magnetic field aligns paramagnetic particles, improving thermal conductivity and reducing surface roughness by 22%. Scanning Electron Microscopy (SEM) images confirm fewer surface defects and reduced tool wear in micro-milling SLM Ti6Al4V with a magnetic field. These insights provide valuable information for applying magnetic fields in the micro-milling of additive manufactured parts, advancing the field of precision machining. Overall, this thesis advances the integration of micro-milling with SLM technology and develops a validated 3D finite element model, with suggesting a magnetic field assistance into micro-milling of SLM Ti6Al4V to resolve machining difficulties, offering significant contributions to understanding the machining mechanism of micro-milling of AM, and further increasing the surface quality of AM parts.

Publication

Journal Papers

1- **Rehan, M**., He, T., Khalil, A. K., Tahir, D., Yip, W. S., & To, S. S. (2024). Experimental Investigation of the Micro-Milling of Additively Manufactured Titanium Alloy: Selective Laser Melting and Wrought Ti6Al4V. *Chinese Journal of Mechanical Engineering*, 37(1), 136.

2- **Rehan, M.,** Zhao, T., Yip, W. S., & To, S. S. (2024). Microstructure and machinability of selective laser melted titanium alloy in micro-milling. *Journal of Materials Research and Technology*, 33, 8491-8502.

3- **Rehan, M.,** Tahir, D., Guo, P., Yip, W. S., & To, S. S. (2025). Magnetic field assisted micro-milling of selective laser melted titanium alloy. *Journal of Manufacturing Processes*, 134, 494-504.

4- **Muhammad Rehan**, Tao He, Wai Sze Yip, Sandy Suet To, Danish Tahir, Ahmed K. Khalil. "3D Finite Element modelling and experimental investigation of micro milling of Ti6Al4V fabricated by laser powder bed fusion," *Results in Engineering*, (*Accepted)*.

5- **Muhammad Rehan**, Muhammad Sana, Muhammad Umar Farooq, Wai Sze Yip, Sandy Suet To, Mehdi Tlija." Understanding surface evolution and cutting force during micro milling of Ti6Al4V using supervised machine learning, *Journal of Manufacturing Processes, (under-review).*

6- **Muhammad Rehan**, Najeeb Ullahah, Muhammad Umar Farooq, Wai Sze Yip, Sandy Suet To. "Comprehensive Review of Micro-Milling: Fundamental Mechanics, Challenges, and Future Prospective", *International journal of advanced manufacturing process, (under-review).*

Conference Papers

1- **Rehan, M.**, Yip, W. S., & To, S. S. (2024, October). Experimental investigation of microstructure, tool wear, and burr formation of micro-milling of selective laser melting Ti6Al4V. In Seventh International Conference on Mechanical Manufacturing and Industrial Engineering **(MMIE 2024)** (Vol. 13290, pp. 111-117). SPIE.

2- Muhammad Rehan1, Wai Sze Yip, Sandy Suet To(2024). Experimental investigation of micro-milling of selective laser melted and wrought titanium alloys, euspen's 24th International Conference & Exhibition, Dublin, IE, June 2024 (Accepted).

Book Chapters

The importance of machining parameters toward sustainable micro-milling process *(Accepted, publisher: springer, expected date of publish: 1st Jan 2025)*

Collaborations

1- He, T., Yip, W. S., Yan, E. H., Tang, J., **Rehan, M.**, Teng, L., ... & To, S. (2024). 3D printing for ultra-precision machining: current status, opportunities, and future perspectives. *Frontiers of Mechanical Engineering*, 19(4), 23.

2- Jin, X., He, T., To, S., Guo, F., Rong, L., Kong, X., **Rehan, M.**, ... & Zhang, S. (2024). Investigation and formulation of cobalt content of ultra-thin diamond blades and dicing performance manufactured by fused deposition modeling and sintering (FDMS). *International Journal of Refractory Metals and Hard Materials*, 121, 106663.

3- Khalil, A. K., Yip, W. S., **Rehan, M.**, & To, S. (2023). A novel magnetic field assisted diamond turning of Ti-6Al-4 V alloy for sustainable ultra-precision machining. *Materials Today Communications*, 35, 105829

Acknowledgments

I would like to express my deepest gratitude to my chief supervisor, Prof. Sandy Suet To, for her exceptional supervision and for giving me the opportunity to be one of her students. Her continuous encouragement and support allowed me to explore new ideas in my research and experience the excitement of my Ph.D. journey. I am also grateful for her unwavering dedication to encouraging us to learn, work hard, and plan diligently, which has had a significant impact on my studies and the completion of this thesis. My heartfelt thanks go to Dr. Yip Wai Sze, my co-supervisor, for her invaluable guidance. Without her patient and persistent support, this thesis would not have been possible.

I would also like to thank The Hong Kong Polytechnic University (PolyU) and all the staff members in the State Key Laboratory of Ultra-precision Machining Technology for their support throughout my Ph.D. study. Special thanks to my classmates and friends who are also working hard to complete their Ph.D. studies. Their shared knowledge and research approaches have been instrumental in helping me continuously improve my research.

A special thanks to my beloved parents and family who have patiently awaited my graduation day for several years. Their unwavering support and encouragement have been invaluable. I also extend my sincere gratitude to my spouse for her immense support and patience during my postgraduate studies. Her unwavering support and countless sacrifices have been crucial in helping me reach this point. Without such a supportive family, I would not have achieved this milestone.

Table of Contents

List of Figures

List of Tables

Chapter 1

Introduction

Titanium grade 5 (Ti6Al4V) is crucial across several manufacturing industries due to its exceptional properties. Its high strength-to-weight ratio, durability, and superior resistance to corrosion and erosion make it an invaluable material in aerospace, automotive, and marine industries, where performance and reliability are paramount. In the medical sector, its non-reactive nature and biocompatibility have led to its widespread use in implants, medical instruments, and dental applications. Additionally, its low elastic modulus and nonmagnetic properties are particularly beneficial in producing precision instruments and devices in healthcare and scientific research. The alloy's versatility extends to the production of optical instruments and mirrors for both ground-based and space telescopes, where lightweight and high-strength materials are essential. Thus, Ti6Al4V's unique characteristics enable its broad application, enhancing performance and innovation across multiple sectors.

Additive manufacturing (AM) has garnered significant attention due to its efficiency, adaptability, cost-effectiveness, and environmental sustainability. AM eliminates the need for dies and specialized tooling, enabling the creation of intricate geometries without additional equipment. This approach not only reduces production time but also minimizes material wastage compared to traditional manufacturing methods. Selective Laser Melting (SLM) is particularly favored for fabricating metallic components due to its numerous advantages, including rapid production, diverse material options, direct CAD production, adaptability to intricate geometries, and the ability to form internal structures. The rapid cooling and solidification processes in SLM refine microstructures and induce the formation of a martensitic α’ phase, thereby enhancing mechanical properties such as strength, hardness, and corrosion resistance. However, challenges remain in achieving the desired precision and

surface roughness. Even with process optimization, the surface roughness of SLM metal parts typically ranges from 5μm to 10μm, necessitating post-machining processes. Micro-milling, a precision machining technique, offers a promising solution for these challenges. This technology enables the fabrication of high-precision products by removing small amounts of material, thereby improving surface characteristics, and achieving high geometrical precision and low surface roughness. Micro-milling can generate more precise details on parts, making it an essential process for enhancing the quality of AM components.

Despite the numerous benefits and potential applications of Ti6Al4V, its low thermal conductivity, strain hardening, high strength at elevated temperatures, and high chemical activity make machining this titanium alloy extremely challenging. Additionally, machining AM metallic parts presents unique difficulties compared to their wrought counterparts due to their heterogeneous microstructure, high residual stresses, and phase transformations induced by rapid solidification. The complex interplay between the powder bed, molten pool, and laser beam during SLM processes results in unique microstructural characteristics, such as the formation of fine columnar grains, a metastable α′ martensitic phase, and internal porosities. These factors lead to unpredictable variations in mechanical properties, which significantly influence chip formation, cutting forces, and tool wear mechanisms during micro-milling. Furthermore, the high strain rates and localized heating in micro-milling exacerbate work hardening and alter the material's deformation behavior at the cutting interface. Understanding these fundamental challenges is critical for optimizing machining parameters and developing predictive models to enhance the micro-machinability of SLM Ti6Al4V.

In ultra-precision machining, not only the material characteristics but also machining conditions such as feed rate, depth of cut, cutting speed, and material removal rate play critical roles. Tool specifications are equally important, making ultra-precision machining highly challenging. Finite Element Modeling (FEM) has proven to be an effective tool for simulating

and studying these processes for decades. FEM-based simulations can efficiently and accurately model complex problems, serving as viable alternatives to physical experiments and saving both time and resources while improving process performance. Despite the advancements in FEM, there is a notable lack of research on the finite element modelling of micro-milling to predict cutting forces, chip characteristics, and surface quality specifically for wrought and additively manufactured Ti6Al4V. Most existing studies focus on orthogonal cutting and tend to oversimplify the complexities of high-speed micro milling, often neglecting factors such as tool rotation and the intricate interactions between the workpiece and the cutting tool's rake and flank surfaces. Both 2D and 3D orthogonal models fall short in accurately capturing the shearing mechanisms involved. This study aims to address these gaps by presenting a comprehensive 3D model that considers the constraints of orthogonal cutting and provides a more accurate simulation of the micro milling process.

The application of a magnetic field in ultra-precision machining has emerged as a promising technique to enhance machining performance and surface quality, particularly for challenging materials like Ti6Al4V. Magnetic fields can significantly influence paramagnetic particles, which typically exhibit adhesive properties due to van der Waals forces and dipole-dipole interactions in the absence of a magnetic field. When exposed to a magnetic field, these particles' dipole moments align with the field, altering the material properties. Building on these principles, magnetic field-induced particle alignment shows potential for enhancing thermal conductivity during the machining of titanium alloys, which are paramagnetic and responsive to magnetic fields. This study conducts a comparative analysis by micro-milling SLM Ti6Al4V in the presence of a magnetic field using cubic boron nitride (CBN) tools, and then comparing the results to those obtained without the magnetic field. The analysis focuses on improvements in machining performance, including surface quality and tool wear, when a magnetic field is applied.

1.1 Research Objectives

A comprehensive study is carried out to explore and improve the process of micro milling for Ti6Al4V with following objectives:

1- To study the machinability of additive manufactured Titanium alloy through micro-milling.

Given the escalating demand for titanium products in precision applications and the inherent challenges associated with the machinability of titanium, there is a pressing need for advanced manufacturing methodologies. These methodologies should harness the capabilities of different advanced manufacturing techniques while mitigating the shortcomings of each. In response to this need, this research aims to conduct a comparative study to investigate the micro milling of Ti6Al4V manufactured via additive manufacturing. The goal is to achieve superior results in terms of surface quality and tool wear compared to traditional ultra-precision machining methods.

2- To develop three-dimensional Finite Element Models (FEM) to investigate the material removal process during micro milling of SLM Ti6Al4V and assess the influence of various machining conditions on surface quality, chips morphology and cutting forces.

Micro milling involves a complex material removal process characterized by phenomena such as plowing and shearing, which are intricately linked to machining conditions including feed rate, depth of cut, and tool geometry. The machining of hard materials like Ti6Al4V further complicates this process. Therefore, Finite Element Modeling (FEM) emerges as a valuable tool to comprehensively analyze the tool-workpiece interaction during micro milling. The outcomes of the FEM simulations will be compared with experimental results, focusing on surface quality, chip morphology, and cutting forces, to validate the accuracy and effectiveness of the models in capturing the intricacies of the micro milling process.

3- To investigate the machinability of additively manufactured Ti6Al4V in magnetic-assisted micro milling.

Ti6Al4V is known for its low thermal conductivity, which causes significant challenges in ultra-precision machining. Previous studies have suggested that applying an external magnetic field can enhance the thermal conductivity of titanium alloys, which are classified as paramagnetic materials. By reducing the cutting temperature during micro milling, the heat generated can be more effectively dispersed, leading to lower tool wear and improved surface quality. This research conducted a comprehensive analysis of the transverse distribution of micro-milled slots both in the presence and absence of a magnetic field. Comparative results are presented to evaluate the impact of the magnetic field on the machinability of additively manufactured Ti6Al4V.

1.2 Organization of the thesis

The thesis consists of six chapters, each contributing to the overall flow and structure of the research:

Chapter 1 serves as an introductory segment to the thesis, delineating the research background of micro milling of additively manufactured Titanium alloy i.e., TiAl4V. Within this chapter, the current research gap in the field is elucidated, accompanied by a comprehensive discussion on the planned methodology for the study.

Chapter 2 comprises the literature review section, where a comprehensive compilation of relevant reference materials pertaining to the research study is presented. This section covers fundamental concepts related to ultra-precision machining and micro milling, as well as an exploration of the challenges inherent in micro milling processes. Additionally, it discusses the characteristics and applications of titanium alloys, especially Ti6Al4V, with a particular focus on manufacturing techniques including additive manufacturing and ultra-precision machining.

Furthermore, the chapter includes a comparative analysis between Selective Laser Melting (SLM) Ti6Al4V and wrought Ti6Al4V, alongside an introduction to combined manufacturing approaches that integrate additive manufacturing and ultra-precision machining.

Chapter 3 presents a detailed report on the application of the Selective Laser Melting (SLM) technique integrated with ultra-precision machining. Experimental investigations are conducted to validate the concept of integrating SLM and micro milling. A comparative study is undertaken to assess tool wear, surface roughness, chip morphology, and burr formation. Furthermore, a comprehensive analysis is conducted in the later section to examine the effect of microstructure and grain orientation on tool wear during micro milling of Ti6Al4V.

Chapter 4 delves into the finite element modelling of the micro milling process of SLM Ti6Al4V. It presents a comparative analysis between the finite element simulation results and experimental findings, particularly focusing on chip morphology, cutting forces, and surface characterization of micro slots generated through micro milling. Additionally, this section explores the impact of variations in machining conditions on the micro milling parameters.

Chapter 5 investigates the efficacy of magnetic fields on the outcomes of micro milling of SLM Ti6Al4V, focusing on enhanced surface quality and reduced tool wear. It provides a thorough analysis of the transverse profile of machined micro-milled slots to elucidate the material removal process during the rotation of micro tools at various stages.

Chapter 6 serves as the conclusion of the thesis, encapsulating the summaries of the research conducted throughout. It outlines the contributions of the study to the existing field of ultra-precision machining, highlighting its significance and potential implications. Additionally, this chapter describes future research plans and extended works related to the

ultra-precision machining of additively manufactured Ti6Al4V, providing a roadmap for further exploration and advancement in the field.

Chapter 2

Literature Review

2.1 Ultra-precision machining

As the demand for exemplary surface quality characterized by nanometric surface roughness and sub-micrometric form error escalates, the significance of ultra-precision machining (UPM) as a pragmatic and cost-efficient solution becomes increasingly apparent. Within the domain of mechanical machining, UPM emerges as a highly promising methodology, distinguished by its notable advantages including heightened efficiency, adaptability, and cost-effectiveness. This approach facilitates the production of superior surfaces renowned for their sub-micrometric form accuracy and nanometric surface roughness, all achieved at a judicious expenditure [7]. UPM attains machining form accuracy levels surpassing 0.2 μm and surface roughness of less than 10 nm, while boasting a resolution and repeatability of under 10 nm. In comparison to conventional machining modalities, UPM exhibits markedly enhanced accuracy, with surface roughness exceeding conventional methods by a factor of 1000 and form accuracy being 100 times more precise [8, 9]. The term "ultra-precision" encapsulates not only the meticulous measures of profile accuracy and surface quality but also acknowledges the complexities associated with meeting predefined benchmarks at specified technical thresholds. In select applications, ultra-precision machining confronts the formidable task of achieving nano-level precision, where machining accuracy approaches a few nanometers, even amidst surface roughness already attaining the sub-nanometer scale [10].

The application of optics holds paramount importance across a spectrum of industries including lighting, telecommunications, medical facilities, automotive, military, and aerospace. This significance is underscored by an ever-increasing demand for optical components

characterized by enhanced performance, heightened reliability, extended longevity, and miniaturization. As a response to these demands, optical elements have undergone specialized refinements, functional advancements, and increased intricacy [11, 12]. The rapid advancement of information and multimedia technologies in recent decades has further accentuated the relevance of high-quality optical elements. This has fuelled a significant market potential, particularly for optical elements manufactured through ultra-precision machining (UPM). In 2012, the optical element market commanded a valuation of $3.6 billion. Projections indicate a substantial growth trajectory, with anticipated market value surging to $12.3 billion by 2019 [9]. Ultra-precision machining (UPM), representing a pinnacle in advanced manufacturing methodologies, provides a pragmatic approach to fabricating precise components. Distinguished by its capability to accommodate small-scale topologies, UPM facilitates the creation of surfaces characterized by non-rotational symmetry. This technology finds widespread application across critical sectors such as optics and medicine, where the demand for precision goods is paramount. UPM exhibits remarkable prowess in achieving sub-micrometer form accuracy and nanometric surface roughness, attributes crucial for meeting stringent quality standards in these sectors. However, it is pertinent to note that the costs associated with UPM machining are relatively higher compared to conventional machining techniques. Nevertheless, this premium investment is justified by the unparalleled precision afforded by UPM. Surfaces fabricated through UPM boast form accuracy and surface roughness metrics that surpass those achieved by conventional machining techniques by factors of 100 and 1000, respectively [13].

UPM technology encompasses these primary categories: single-point diamond turning (SPDT), ultra-precision grinding, ultra-precision micro milling, and ultra-precision raster grinding. Among these, ultra-precision micro milling stands out for its unique capability to produce machined components with the final shape in a single cutting step, eliminating the

need for subsequent machining operations. This method allows for the controlled manipulation of surface geometries, enabling continuous variation in a precisely controllable manner.

2.2 Micro milling and its challenges

The contemporary landscape underscores an escalating requirement for scaled-down products and devices, emblematic of the prevailing pursuit of solutions characterized by diminution in size alongside attributes of enhanced speed, reduced weight, and cost-effectiveness [6, 14]. This overarching trend has precipitated a sustained drive towards the downsizing of materials, devices, systems, and manufacturing methodologies, traversing multiple industrial sectors across macroscopic, microscopic, and nanoscopic scales [6]. These transformative developments resonate notably within domains including electronics, aerospace, medicine, and energy.

Micro- milling stands out as a remarkably adaptable method within the domain of mechanical micromachining. Its multifaceted capabilities render it particularly advantageous for the fabrication of intricate features, notably those integral to implants and medical equipment [15]. Widely embraced across precision-centric industries such as aerospace, electronics, and biomedical sectors, micro- milling is commonly construed as a refined iteration of conventional milling processes. Within the micro-milling paradigm, workpiece dimensions typically span from 0.1mm to 10 mm, enabling the attainment of geometric features as fine as 0.01mm. Noteworthy is the minute scale of micro- milling cutters, exhibiting diameters ranging from 25µm to 1000µm [16]. The difference between macro and micro cutting is illustrated in Figure 2.1. The impact of the tool edge radius (r_0) can be neglected when the depth of cut exceeds the radius of the edge of the tool. This radius, however, affects the cutting mechanism while doing micronuts. Slide due to contact between tool and workpiece and plough owing to tool edge are considered to be primary cutting mechanisms, particularly in situations where elastic recovery occurs in the flank face of the workpiece [2].

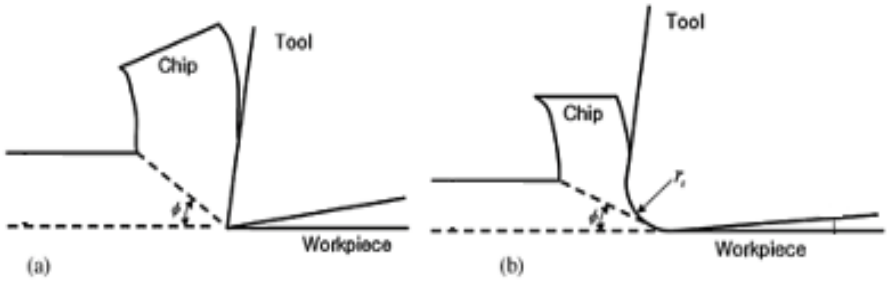

Figure 2. 1 difference between macro and micro milling; a- macro milling, b- micro milling [2]

The concept of size effect pertains to the nuanced variations during dynamics and physical process observed as the undeformed chip thickness (UCT) is in range of cutting-edge radius during micro cutting. Within the domain of micro cutting, size-effect phenomena are widely acknowledged and typically encompass three fundamental aspects. Firstly, as the UCT diminishes to a scale comparable to or smaller than the grain size of phases within the workpiece material, the material's response to machining may exhibit non-uniformity. Secondly, when the UCT approaches or falls short of the cutting-edge radius, the micro mill's effective rake angle tends to become highly negative, resulting in concurrent ploughing and shearing of the workpiece material. Lastly, chip formation may fail to occur when the UCT in micro cutting dwindles below a specified threshold, denoted as the minimum undeformed chip thickness (MUCT). Consequently, the MUCT emerges as a pivotal determinant delineating material removal behavior between both micro as well as macro milling[6].

In the realm of micro machining, the parameter known as undeformed chip thickness (UCT), denoted as h, typically ranges from 0.1 to 50 μm , markedly smaller than the corresponding range in macro processes, spanning from 0.1 to 10 mm [17-19] . As the UCT diminishes below a critical threshold termed hm, the conventional chip formation characteristic of macro machining gives way to alternative material removal mechanisms such as rubbing or ploughing [64]. Contrary macro cutting operations entail UCT values significantly larger, ranging from 10 to 10000 times the corresponding h_m values. Consequently, the transition from macro to micro machining magnifies the significance of behaviors previously considered

negligible, thereby yielding distinct and more intricate material removal dynamics within the micro cutting process. These dynamics are shaped not only by the diverse relationships between h and h_m but also by the varying loading conditions dictated by the geometrical attributes of the contact zone between the cutting edge tips and the workpiece [16, 20]. In the realm of orthogonal micro cutting, material responses exhibit distinctive patterns delineated by the interplay of various h–h_m relationships, as extensively explored in scholarly literature [6]. These patterns manifest across three primary stages: (i) elastic deformation occurring in case h becomes significantly less than h_m, (ii) elastoplastic deformation is observed as h becomes closer but still remains less than h_m, and (iii) chip formation is prominent as h surpasses h_m. During the elastic phase, the workpiece material experiences purely elastic deformation near the point of contact with the cutting edge, leading to complete restoration of its original shape post-micro-rubbing. Experimental data suggests that the chip thickness h during this phase, akin to the inward depth in tribology, typically registers in nanometre range [21]. This phenomenon is explained in figure2.2.

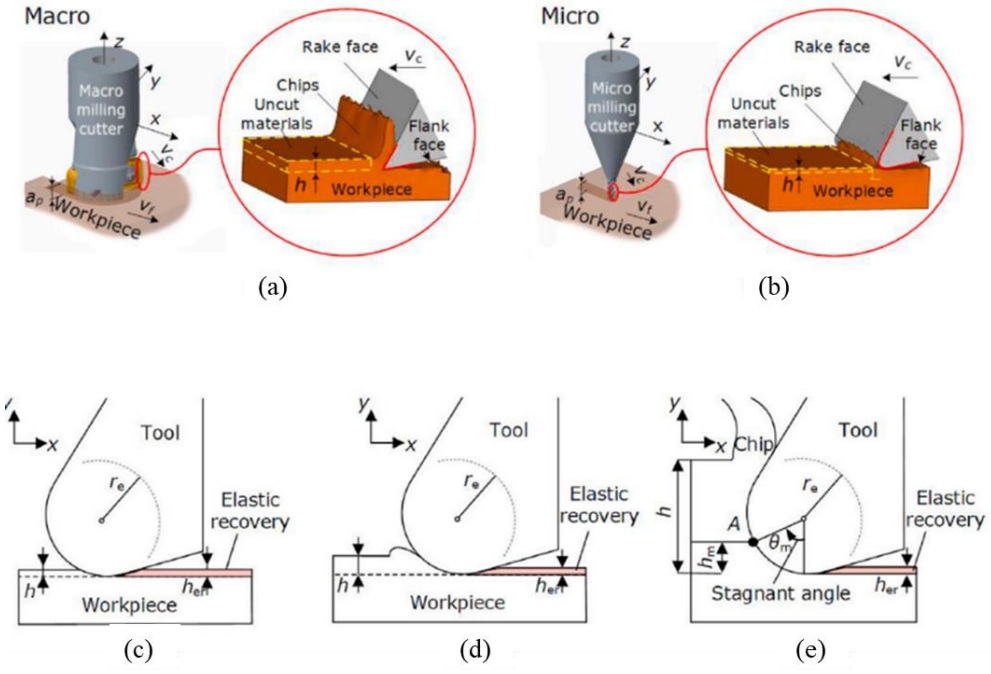

Figure 2. 2: Material removal phenomenon: (a) macro milling, and (b). micro milling; Orthogonal demonstration of micro cutting and micro milling processes:(c) elastic-deformation region, (d). mixed elastic–plastic deformation region (e) Chip generation during orthogonal micro cutting [6]

Transitioning to the elastic-plastic phase, the process entails elastic-plastic deformation characterized by ploughing, wherein a significant portion of the material collects and advances towards the cutting edge [22]. As this material rack up reaches a critical threshold, some of the accumulated material undergoes partial disintegration due to successive material flows, migrating forward and subsequently undergoing physical compression or even chemical bonding with the machined surface. Concurrently, extrusion of materials occurs beyond the cutting edge, initiating a cyclical process wherein materials across the cutting tip piles up and repeat the aforementioned sequence [23]. During the process of chip generation , aside from the ploughed material across the cutting edge (rounded), which eventually constitutes the upper layer of the newly machined surface, an additional material flow emerges due to the increased UCT in stage (iii) [24]. Here, working material is propelled (upwards) along the rake of cutting edge and smoothly separates from the bulk material as the direction of material slippage aligns through the rake face.

Downsizing milling operations to a microscale introduces a host of challenges. Factors such as vibration, deflection, temperature, and the microstructure of the workpiece, often negligible in macroscopic contexts, assume paramount importance. Consequently, achieving desired performance levels in micro- milling necessitates heightened effort compared to macro-milling. This challenge is further exacerbated when dealing with recalcitrant materials like titanium alloys, prevalent in medical devices and implants. With the increasing potential of utilizing micro-parts as cellular-level therapeutic implements, interest in micro-machining of titanium alloys is on the rise. However, machining titanium alloys presents formidable hurdles, primarily due to the accelerated tool wear resulting from titanium's reactivity with tool materials and its subpar thermal conductivity. Additionally, research in the domain of micromachining titanium alloys remains in its infancy, posing significant barriers to its widespread industrial application. [25].

Challenges of micro milling

Micro mill cutters, due to their diminutive size, are susceptible to extensive tool wear, leading to the production of subpar surfaces. The geometric configuration of micro-milling, as depicted in Figure 2.3, exhibits distinctive characteristics compared to macro-milling. With the reduction in cutting tool dimensions, the cutting process undergoes notable alterations, magnifying the significance of certain parameters previously inconsequential in macro milling. Limitations in manufacturing procedures preclude proportional enhancement of cutting tool sharpness with decreasing tool diameter. The cutting edge radius, typically ranging from 0.5 to 5µm, often exceeds the feed per tooth. A pronounced negative rake angle induces elastic-plastic effects, while the minimum chip thickness governs chip formation. Instances of ploughing occur, and chip generation ceases when the uncut chip thickness falls below the minimum threshold. Furthermore, micro-milling operations exhibit run-out ranging from 1 to 5µm, limiting cutting to a single edge [8]. These inherent characteristics of micro-milling engender uncertainties in the cutting process, complicating the attainment of requisite process outputs [26]

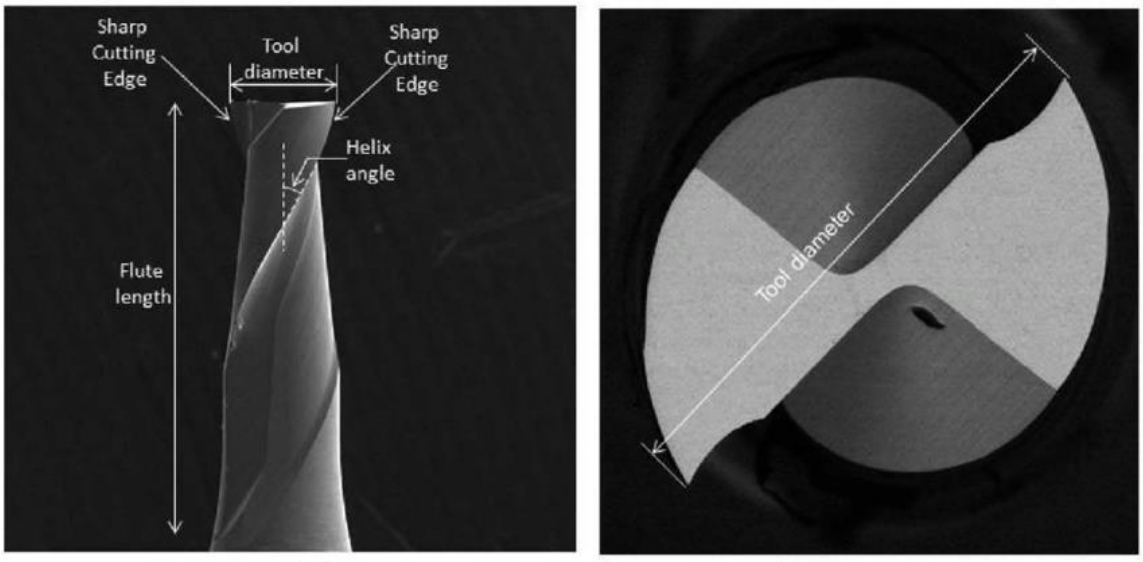

Figure 2. 3 SEM image of the micro mill clearly indicating the tool geometry [3].

The spindle and tool holder characteristics exert the most significant influence on tool run-out. Micro-milling operations experience substantial force variations due to minor runout, which minimally affects the cutting force profile seen in conventional milling. Notably, the ratio of tool run-out to tool diameter (ro/r) escalates significantly in micro-milling compared to conventional methods. Accounting for tool run-out greatly facilitates the assessment of cutting force dynamics across a broad spectrum of cutting parameters, essential for optimizing micro-milling conditions [27]. In conventional milling, the sharp edges of the cutters degrade over time due to material loss, leading to crater formation and eventual cutting edge failure. Monitoring wear aids in predicting when a tool will no longer meet quality standards [28] . In contrast, micro-tool failures typically stem from the breakage of small shafts when chips clog or cutting blades dull, initiating the failure mechanism. The critical concern with micro-tools lies in how cutting force evolves throughout the cutting process, as there exists a correlation between usage (wear) and stress [29]. Employing traditional machines for micro-machining often results in premature failure or erratic tool life. The expense of miniature tools is considerable. Workpieces are often discarded if a tool breaks during machining, as restarting the machine and inspecting the piece entail significant time investments. Efficient micro-machining necessitates high spindle speeds (exceeding 10,000 rpm) to maintain adequate feed rates despite employing very low feed rates per tooth. However, this solution is costly, typically involving the acquisition of specialized high-speed spindle machine tools. Additionally, transferring components between machines is imperative for processes utilizing cutting tools of varying sizes [29].

Micro-machining encounters intricate wear and tool failure mechanisms, where higher feed-per-tooth settings lead to unpredictable and diminished tool longevity, contrasting with adequate tool life at lower feed-per-tooth rates. Over the past two decades, conventional end milling methodologies have been extensively investigated. Numerous studies have focused on

simulating cutting mechanisms, analyzing cutting force properties, and identifying tool failure patterns. Despite the divergent wear and breakage mechanisms observed in micro--milling operations compared to traditional milling, the fundamental characteristics of cutting force parameters remain largely consistent [29]. Among the paramount variables in micro-milling, cutting force stands out as crucial. The relationship between tool wear and system stability is intrinsically tied to the cutting forces generated during machining processes. Utilizing cutting force as a pivotal process parameter can significantly enhance cutting conditions, thereby economically improving the quality of machined components and extending tool life. Precisely predicting cutting forces across various process parameters is imperative [26]. To surmount these challenges and enhance both the quality of micro-milled components and machining productivity, models elucidating the mechanics and dynamics of micro--milling play a crucial role. These models enable the anticipation of machining process behavior prior to costly real-world experimentation and trial-and-error methods. Monitoring the machining process and selecting optimal cutting settings hinge heavily on forecasting and measuring cutting forces during micro--milling[30]. Given the sub-micrometre/nanometre scale of surface topography in micro-features, achieving precise control over machined surfaces poses significant technological hurdles. Micro- milling surfaces play a critical role in friction, lubrication, and overall functional performance. Notably, micro-milling of titanium alloys, particularly for implants, can yield free-form surfaces known to enhance biocompatibility. Hence, surface quality considerations must accompany part features and tolerances to ensure the production of functional micro-products. The control of surface finish in microfeatures is achieved through a range of methodologies, including optimization of process parameters, utilization of modeling and simulation to understand surface production, and evaluation of lubrication effects [15, 31]. Burr development presents a significant concern in micromachining, influenced by factors such as the ductility of the workpiece material, cutter geometry, cutting settings, tool

wear, and workpiece shape [32]. Particularly in the micromachining of hard materials, burrs tend to arise more frequently due to heightened tool wear. However, surface polishing and refining microfeatures are constrained by expensive methods or potential damage to microstructures [33]. Extensive research on micro-milling indicates that while complete elimination of burr formation is challenging, it can be mitigated to an acceptable level through careful selection of process parameters and tool geometry [34]. Effective improvement of surface quality in microfeatures necessitates consideration and management of both surface roughness and burr formation [15, 35].

Concluding the section we get that Micro-milling is characterized by its ability to achieve extremely high precision and surface quality due to the small size of the cutting tools and the fine features they can produce. However, this comes at the cost of reduced material removal rates and productivity. The primary factors contributing to this trade-off include [36]:

1. **Tool Size and Rigidity**: Micro- mills are less rigid due to their small diameters, which limits their cutting depth and feed rate.
2. **Thermal and Mechanical Stability**: Smaller tools generate less heat per unit time but are more prone to thermal and mechanical deformation at higher speeds.
3. **Surface Quality vs. Feed Rate**: In micro-milling, increasing the feed rate often compromises surface finish and dimensional accuracy, as tool deflection and vibration become significant.
4. **Tool Wear and Life**: Due to the high aspect ratio of micro-tools, wear occurs more quickly, further reducing their effective cutting efficiency and productivity.

Scenarios Where Micro-Milling Presents an Advantage

Micro-milling excels in applications where precision and quality outweigh productivity, such as [36, 37]:

- **Medical Devices**: Components such as stents, surgical instruments, and implants require extremely tight tolerances and biocompatible surface finishes.
- **Microelectronics**: Features like fine connectors, microchannels, and precise housings demand high accuracy and intricate geometries that are achievable only with micro-milling.
- **Aerospace and Automotive Sectors**: Applications involving micro-textured surfaces for drag reduction or weight savings benefit from the precision and surface integrity of micro-milling.
- **Tooling and Mold Manufacturing**: Micro-milling is crucial for producing molds with intricate details for applications like microfluidics, optical lenses, or miniaturized plastic parts.
- **Research and Prototyping**: The flexibility of micro-milling allows researchers to fabricate small, detailed components without investing in mass production tools.

2.3 Additive Manufacturing

Additive manufacturing (AM) known as rapid prototyping (RA) has been defined by ASTM (F42, technical committee) as follows:

"Process of joining materials to make objects from three-dimensional (3D) model data, usually layer upon layer, contrary to subtractive manufacturing methodologies [58, 59]".

Additive Manufacturing (AM), also known as Rapid Prototyping (RP), is a layer-by-layer manufacturing technique renowned for its capacity to produce near-net-shape complex geometrical parts of Ti6Al4V using CAD models [39, 40]. This technology has revolutionized manufacturing by offering design flexibility and significantly reducing product lead times. Initially limited to prototyping and porous parts, advancements in AM technology now enable the production of dense parts with vastly improved quality, such as tool inserts, dies, and medical implants. In recent years, a plethora of enhanced AM technologies have emerged,

offering numerous advantages over conventional machining methods, including faster production times, elimination of molds and tooling, efficient material utilization, and the ability to create complex shapes and customize products [39, 41].

Originally introduced for creating non-functional models and prototypes using polymers, AM has now shifted its focus towards producing functional metallic parts for industrial applications. Utilizing near-net-shape methods, AM can fabricate complex 3D geometries that were previously unachievable through conventional manufacturing techniques. While post-processing may be necessary, the versatility and efficiency of AM in producing intricate metallic components or assemblies are on the rise [42, 43]. The application of Metallic Additive Manufacturing (MAM) in functional components is expanding rapidly, as depicted by the graphs in figure 2.4 illustrating the percentage use of MAM across various industries. Among the numerous AM technologies available, Selective Laser Melting (SLM) and Electron Beam Melting (EBM) stand out as the most suitable and preferred methods for creating intricate metallic products [43].

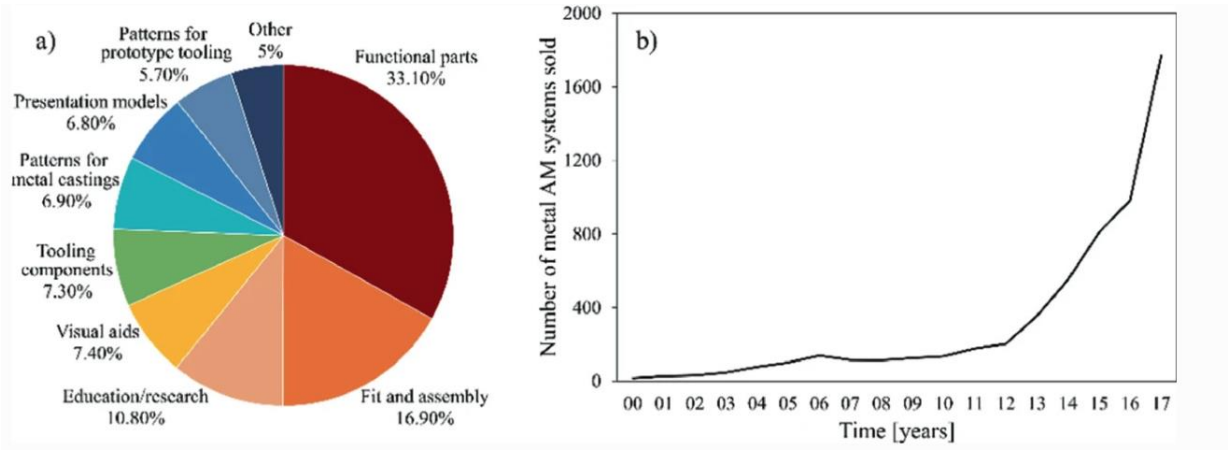

Figure 2. 4 Application purpose of AM since 2000. a- percentage usage b- number of systems sold [51]

Additive manufacturing has emerged as a transformative solution for producing complex metal geometries that were previously challenging to manufacture using conventional methods, such as metal forming. Moreover, additive manufacturing offers the advantage of

improved and refined mechanical properties [39, 44]. Current technology has advanced to the point where it can fabricate thin walls and intricate features at a level as fine as 0.2mm [45]. Among the various metal additive manufacturing technologies available, Selective Laser Melting (SLM) stands out as the most suitable for creating complex metal parts. By utilizing high laser power, SLM can fabricate nearly fully dense parts, with a density level reaching up to 99.8%, layer by layer. Additionally, SLM has the capability to generate porous workpieces and does not require any fixtures or supporting tools for manufacturing complex shapes [46, 47].

In comparison to other manufacturing methods, including machining, additive manufacturing (AM) exhibits superiority in three key aspects. Firstly, AM possesses the capability to fabricate novel and intricate geometries that are unattainable through conventional methods, particularly for hard materials such as Ti6Al4V. Secondly, AM has the potential to minimize the environmental footprints of products from cradle to gate by eliminating the need for tools, scrap, and dies associated with traditional manufacturing techniques. For instance, conventional machining methods for titanium and aluminum parts in aircraft result in a significant 'buy to fly' ratio ranging from 12:1 to 25:1, leading to substantial material and energy wastage along with environmental emissions [48]. Additionally, products manufactured by AM offer enhanced serviceability and environmental safety, making them ideal for applications in industries such as aerospace, where weight reduction is critical for improved fuel performance. Aircraft components like seat buckles, deck minter arms, brackets, and hinges have been successfully replaced with AM-produced parts, resulting in significant weight savings. Moreover, AM offers remarkable advantages and versatility in the choice of materials, along with the ability to rapidly prototype complex shapes with functional designs [49]. Industries requiring lightweight components, such as power production, automotive, aerospace, and medical sectors, often necessitate the inclusion of thin-walled features in their

designs to meet strength and fatigue requirements. However, subtractive methods typically involve the removal of nearly 95% of bulk material to achieve the final product geometry, resulting in significant material wastage, particularly for expensive materials like titanium and nickel alloys. AM addresses this challenge by enabling the deposition of only the necessary amount of material to create thin features, thus controlling material wastage to a significant extent. Furthermore, AM eliminates costs associated with inventory management [50, 51]. The concept of near-net-shape manufacturing for hard materials like titanium and nickel super alloys was introduced through AM to overcome the challenges of high stresses, material wastage, and long lead times associated with conventional fabrication methods, as compared to steels and aluminum. While AM effectively addresses these shortcomings, challenges related to dimensional accuracy and surface requirements remain to be fully resolved [52].

2.3.1 Electron Beam Melting

The operational principle of Electron Beam Melting (EBM) is depicted in Figure 2.5, resembling the working principle of a scanning electron microscope (SEM). Electrons are emitted from a heated tungsten filament positioned at the top of the column. These electrons are then collimated and accelerated to high kinetic energy levels (60KeV). Two magnets located at the bottom of the column aid in controlling the electron beam, with one coil serving as a magnetic lens to focus the beam, while the second coil assists in positioning the focused electron onto the platform at specific locations [53]. Notably, the electron gun remains fixed, and beam deflection is achieved solely through the use of coils, eliminating the need for mechanical parts. The beam diameter can be reduced to as small as 0.1mm using a current ranging from 1-50mA. Within the middle of the machine, a thin layer of powder is formed with the assistance of two hoppers. A racking mechanism is employed to evenly distribute the powder for each layer, typically ranging in thickness from 0.05-0.02mm. Subsequently, a computer numerically controlled beam scans according to a programmed sequence. Initially, a

high-speed beam (~10 m/s) is utilized multiple times to preheat the powder, followed by a slower beam of approximately 0.5 m/s to melt the powder. This process is repeated for each new powder layer until the desired product is completed. To maintain an inert atmosphere and prevent the accumulation of charges within the chamber, a high vacuum is applied along with helium gas, facilitating the processing of high-performance alloys. Upon completion of all layers, the built part is cooled within the chamber [53-55].

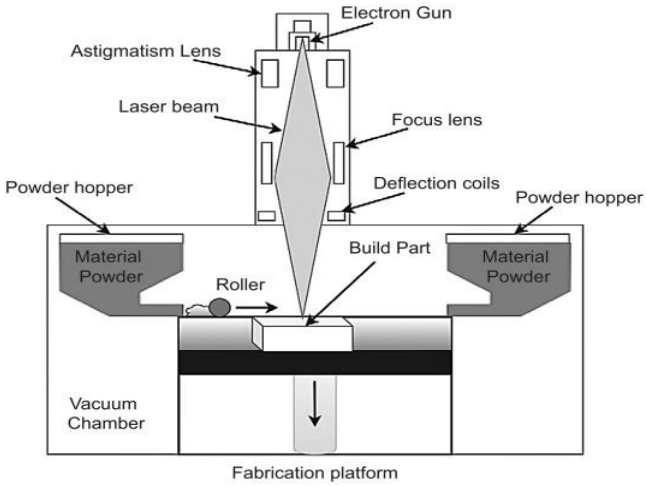

Figure 2. 5 The schematic illustration of the electron beam melting (EBM) process [1]

EBM has found significant applications in the manufacturing sector, particularly in aerospace, where it offers the flexibility of both prototyping and low-volume production. It has streamlined the testing and installation processes by facilitating the creation of fully functional parts, thereby overcoming the time and cost limitations associated with conventional methods like machining. Additionally, EBM has played a pivotal role in the design of lightweight cellular structures, enhancing the efficiency of aerospace components. In addition to its contributions to the aerospace industry, EBM is garnering attention in the field of medical implants. It has revolutionized the production of implants by enabling the fabrication of patient-specific parts using customized data, thereby eliminating the need for post-processing. This capability not only provides greater freedom in design but also allows for controlled porosity, ensuring that the functional characteristics of the implants closely mimic natural anatomy.

Thus, EBM holds promise for advancing the field of medical implantology by enhancing customization and functional integration [53].

2.3.2 Selective Laser Melting

Selective Laser Melting (SLM) utilizes the energy of a high-intensity mobile laser beam to selectively melt the powder layer and form a metal part, as illustrated in Figure 2.6 [56]. The process begins with the horizontal spreading of powder on the build plate, facilitated by a roller that evenly distributes the powdered metal material. Subsequently, the laser is employed to melt the powder in accordance with 2D instructions provided by software. Utilizing 3D data, the laser is precisely controlled to melt the powder of each specific layer according to the 3D model. Following this, the platform is incrementally lifted, reducing the thickness of the layer, and the process is repeated to generate the subsequent layers until the desired product is completed. To prevent the reaction of highly reactive metals like titanium with impurities, an inert atmosphere is generated within the chamber. The gas pressure inside the chamber is maintained higher than atmospheric air pressure, ensuring the exclusion of oxygen and preventing oxidation at high temperatures. However, it is crucial to remove the gas at the appropriate time to prevent its entrapment inside the component, which could result in porosity and compromise the performance of functional components. The performance of the final product is heavily reliant on process parameters such as scan speed, scan interval, laser power, scan strategy, and scan speed [57, 58].

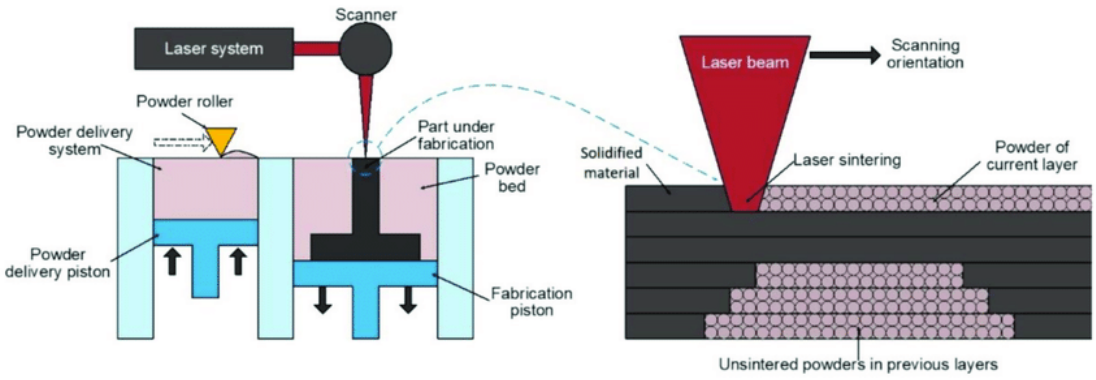

Figure 2. 6 The schematic illustration of the selective laser melting (SLM) process [4].

The layer-by-layer production principle of SLM enables the bulk manufacturing of complex profiles and geometries, offering versatility in the fabrication of both dense and porous products. This adaptability makes the SLM process highly suitable for applications across various industries, including aerospace, automotive, and biomedical fields. In aerospace and automotive sectors, SLM can produce intricate components with high precision, meeting the demanding requirements of these industries for lightweight yet durable parts. Similarly, in the biomedical field, SLM allows for the creation of customized implants and prosthetics with complex structures tailored to individual patient needs. Thus, the inherent flexibility of SLM makes it a valuable manufacturing technique for a wide range of applications requiring intricate and customizable components.

SLM is equally well-suited for production in small batches, offering flexibility in manufacturing quantities. It boasts the capability to process a wide variety of materials, although challenges may arise, particularly with the manufacturing of high melting temperature alloys [58-60]. Despite these challenges, SLM offers numerous advantages over conventional manufacturing methods. These include reduced tooling requirements, resulting in time and cost savings, as well as environmental friendliness. Moreover, SLM-produced parts often exhibit superior mechanical properties, and the process enables customization and control over the atmospheric conditions during fabrication [57, 60]. Overall, these advantages position SLM as a highly efficient and versatile additive manufacturing technique with broad applicability across industries.

SLM-produced Ti6Al4V parts exhibit superior mechanical properties compared to their wrought counterparts, with enhancements observed in yield strength, tensile strength, and hardness. This improvement can be attributed to the unique microstructure of parts generated through high cooling rates during the SLM process. The microstructure of Ti6Al4V parts produced by SLM is highly dependent on laser power, leading to distinctions in corrosion

resistance [61]. Typically, the microstructure is anisotropic, consisting of acicular α′ martensite alongside columnar prior β grains [62]. The formation of non-equilibrium phases with very fine-grained microstructures, such as acicular martensitic structure (α′), is achieved due to the high heating and cooling rates (approximately 10^3 - 10^6 K/s) inherent in SLM, contributing to the superior mechanical properties observed [58, 63]. To achieve a balance in mechanical properties and enhance ductility, post-processing in the form of heat treatment is recommended. This treatment helps transform the metastable martensite structure into a biphasic α-β structure. However, it's worth noting that SLM-manufactured parts may suffer from poor surface finish and dimensional inaccuracies due to the presence of un-melted powder residue and laser marks on the surface. These factors can impact the performance of functional parts, necessitating post-machining to improve surface roughness and geometrical tolerances [62].

2.4 Characteristics of Ti6Al4V and its applications

Titanium, with its atomic number 22, represents a transitional metal renowned for its distinctive properties. Typically silver in color and possessing a highly lustrous texture, titanium and its alloys have garnered considerable attention across modern industries [64]. Among these alloys, Ti6Al4V (grade 5) emerges as one of the most prevalent, finding extensive application in aerospace, marine, power generation, automotive, and chemical sectors. The exceptional properties of Ti6Al4V stem from its unique crystalline structure, setting it apart from other materials within its category. Characterized by a crystalline arrangement predominantly comprised of hexagonal closest packed (HCP) α phase at ambient temperatures, Ti6Al4V also exhibits a minor proportion of body-centered cubic crystalline (BCC) β phase [64, 65]. Based on its composition, the deformation behavior of titanium predominantly reflects the characteristics of the hexagonal closest packed (HCP) α phase at lower operating temperatures. However, under high temperature conditions such as during machining processes, the influence of the body-centered cubic crystalline (BCC) β phase becomes

pertinent. Elevated temperatures lead to an increase in the proportion of the β phase [65]. Notably lightweight, titanium offers exceptional strength and boasts outstanding mechanical attributes, including corrosion resistance, fatigue resistance, and toughness even at elevated temperatures. Titanium alloys also exhibit notable hardness. These combined properties render the alloy well-suited for the aforementioned applications [64, 66]. Further details regarding the mechanical and physical properties of various titanium alloys are provided in Table 2.1.

Table 2. 1 Mechanical properties of Titanium alloys

Material	Modulus, GPa	Ultimate tensile strength, MPa	Yield Strength, MPa	Elongation, %	Density, g/cc
Cp Ti-I	102	240	170	24	4.5
Cp Ti-II	102	345	275	20	4.5
Cp Ti-III	102	450	380	18	4.5
Cp Ti-IV	104	550	483	15	4.5
Ti6Al4V-ELI	113	860	795	10	4.4
Ti6Al4V	113	930	860	10	4.4
Ti6Al7Nb	114	900-1050	880-950	8-15	4.4
Ti5Al2.5Fe	112	1020	895	15	4.4
Ti15Zr4Nb2Ta0.2Pd	94-99	715-919	693-806	18-28	4.4
Ti-29Nb13Ta4.6Zr	80	911	864	13.2	4.4

Applications of Ti6Al4V in Medical and Implants

Over the past few decades, Ti6Al4V has emerged as a prominent choice for medical applications. Compared to other ferrous materials utilized in the medical field, Ti6Al4V exhibits the highest strength-to-weight ratio. Its durability, longevity, and non-toxic nature make it particularly suitable for use as implants within the human body [64, 66]. Studies have indicated that titanium implants can endure for over twenty years when employed as rods,

plates, cages, or pins within the human body. In comparison to stainless steel (316 LSS), cobalt alloy, and CoCrMo, Ti6Al4V boasts a low modulus of elasticity and high load-bearing capacity, alongside the aforementioned properties. Furthermore, it demonstrates enhanced compatibility with body tissues and bones, rendering it well-suited for various implants such as tooth and knee replacements, as well as hip joints [64, 67] . Additionally, it finds application in bone plates, screws, nails, and maxillofacial surgery due to its bio-adhesion and biocompatibility. Surgical instruments and prostheses are also commonly crafted from titanium [64, 68]. Another advantage of titanium over other materials is its non-ferromagnetic nature, ensuring safety during magnetic resonance imaging (MRI) and nuclear magnetic resonance imaging (NMRI) procedures. These superior characteristics position titanium and its alloys as promising materials for manufacturing stents used in blood vessels [67]. The medical sector necessitates metals that are non-reactive with the human body and pose no harm to health. Titanium alloys stand out as one of the most well-known metals utilized in the medical industry, with titanium alloys being implanted in patients worldwide each year. With the increasing demand for joint replacements due to factors such as strenuous physical activities, injuries from accidents, and aging, titanium alloys remain a preferred choice. Medical authorities and designers assert that only a select few materials inherently meet the stringent requirements for medical applications, with titanium alloys being among the most specific [69].

Applications of Ti6Al4V in Aerospace:

Titanium alloys, including the well-known Ti-6Al-4V grade, boast a range of unique advantages such as wear resistance and biocompatibility, making them indispensable in various industries including aerospace, automotive, medical, marine, and sports equipment [70, 71]. Particularly in aerospace applications, titanium has gained significant traction. The Soviet Union was the pioneer in producing titanium parts in the 20th century, recognizing its strategic

importance, which subsequently influenced other nations to adopt titanium for military and civilian purposes [72]

In recent years, the industry's performance has seen a notable uptick, largely due to the integration of titanium alloys in engine components, thereby enhancing the performance of aircraft engines. Titanium alloys are extensively utilized in the aviation sector for manufacturing engine parts, primarily owing to their ability to reduce weight and maintain temperature stability during operation. Notably, aircraft models such as the Boeing 777, 787, and Airbus A380 have incorporated titanium alloys, particularly beta titanium alloy in engine components like landing gear. For instance, Boeing's 787 employs Ti-5Al-5V-5Mo-3Cr (Ti-5553), renowned for its superior strength and hardness, whereas the A380 and 777 utilize Ti-10V-2Fe-3Al (Ti 10-2-3), offering weight savings compared to conventional Ti6Al4V grade. Additionally, titanium alloys find application in the interior components of jet engines, such as turbine compressor blades, albeit they are avoided in high-temperature areas to mitigate combustion-related issues [73].

Applications of Ti6Al4V in Marine:

Corrosion is one of the issues that threatens the parts used in navigation, and researchers face a great challenge in maintaining these elements to improve the navigation industry. The best option for the navigation industry is titanium alloys because they are resistant to corrosion and give parts a longer life span. When the parts are exposed to a corrosive environment and saltwater, they are at risk of rapid failure and cannot carry out their intended function [74]. Titanium alloys are resistant to the process of corrosion in navigation. And the infrastructure of the maritime sector, which is crucial for protecting components from corrosion, extends their useful lives, and delivers other services [75]. Most of these issues have been resolved and the navigation process has improved since the use of titanium alloys in this industry.

2.5 Properties of SLM Ti6Al4V comparative to wrought Ti6Al4V

Selective Laser Melting (SLM) Ti6Al4V and wrought Ti6Al4V exhibit unique characteristics and properties influenced by their respective manufacturing processes, wherein cooling rate plays a significant role. In SLM Ti6Al4V, the microstructure is predominantly composed of columnar β grains and α′ martensite, a consequence of the rapid cooling rate during fabrication. This rapid solidification process results in a distinctive microstructural arrangement, further refined through precise control over laser power and scanning speed [76, 77]. As a result, SLM Ti6Al4V showcases exceptional microhardness and smooth surfaces akin to bulk Ti6Al4V alloy. However, the presence of robust martensite imparts SLM Ti6Al4V with notably high tensile strength while compromising ductility [78, 79]. According to Murr et al. [80], this enhanced strength and hardness observed in SLM Ti-6Al-4V primarily stem from the presence of martensite phase regimes within its microstructure. This microstructural characteristic significantly reduces the ductility of SLM Ti-6Al-4V in comparison to wrought Ti-6Al-4V, which is attributed to its distinctive microstructure and porosity. Similar results has been reported by Shunmugavel et al.[76]. In contrast, wrought Ti6Al4V, produced through conventional methods such as casting and forging, experiences a slower cooling rate during processing [79]. This gradual cooling allows for the formation of equiaxed grains and a more uniform microstructure. Although wrought Ti6Al4V may demonstrate lower tensile strength and hardness compared to SLM Ti6Al4V, it typically exhibits greater ductility due to its microstructural characteristics. Despite SLM Ti6Al4V's advantages in terms of strength and surface finish, it may experience reduced fatigue life due to factors like microstructural features, porosity, surface finish, and residual stress [81, 82]. This underscores the importance of cooling rate in determining material properties and performance. Moreover, the implementation of post-processing techniques like hot isostatic pressing (HIP) can enhance the fatigue strength of SLM Ti6Al4V, albeit at the expense of ductility [81, 83]. Ultimately, the

choice between SLM Ti6Al4V and wrought Ti6Al4V hinges on the specific requirements of the application, considering factors such as strength, ductility, and production efficiency. Each variant offers unique advantages and trade-offs, necessitating thoughtful consideration when selecting the appropriate material for a given engineering application. Even though near net shape components can be fabricated using the AM technology, the surface finish of the components created are poor. Surface quality of additive manufactured components is often found to be affected by non-uniform distribution of powders, delamination between the layers and rippling effect caused by the shear force of laser on the liquefied powder particles [15]. Thus, in order to eliminate these defects and improve the surface quality of additive manufactured components, a final touch of finish machining is always required [16, 17].

2.6 Machining difficulties of Ti6Al4V:

While Titanium alloys, particularly Ti6Al4V, are esteemed materials for critical applications, they pose challenges in both subtractive and additive manufacturing processes. Their low specific heat and thermal conductivity render them difficult to machine, leading to excessive heat generation at the tool-material interface and slow heat dissipation rates. This phenomenon results in work hardening and significant tool degradation, compounded by issues such as oxidation and residual stresses, categorizing Titanium alloys as difficult-to-cut materials [66, 84, 85].

In subtractive manufacturing methods, tool wear emerges as a prominent challenge, exacerbated by high thermal stresses, variable chip thickness, and elevated load pressures. This ultimately diminishes material removal rates, escalating machining costs [66, 86]. Surface quality and productivity are paramount considerations in product generation via machining processes, with higher productivity correlating with increased material removal rates. However, high cutting speeds of Titanium alloys are hindered by challenges such as

catastrophic tool failure, microstructure variations, and poor surface roughness, impacting product quality and performance [87].

Overall, the subtractive manufacturing of Ti6Al4V faces formidable challenges due to its poor thermal conductivity and susceptibility to strain hardening, resulting in high costs, material wastage, and extended lead times. Additionally, its machining presents further complexities due to factors such as low heat conduction, chemical reactivity, and strain hardening, leading to rapid tool wear and inferior surface finishes[44, 88-90]. These challenges are particularly pronounced in ultra-precision machining of micro-products, where excessive material wastage and tool wear contribute to substantial costs [90, 91]. Furthermore, the generation of complex profiles, thin-walled structures, and aspherical curves using machining techniques remains exceedingly challenging for such hard materials [92]. Consequently, Titanium alloys encounter limitations in precision machining, constraining their applications in ultra-precision settings [93, 94].

2.7 Limitations of AM for processing Ti6Al4V

The additive manufacturing (AM) of Ti6Al4V is a complex process influenced by various factors, including the specific technique employed, operating/input conditions, post-heat treatment methods, and development orientation [95-97]. Both microstructure and hardness of the resulting parts are closely linked to these operating variables. Post-heat treatment can refine the microstructure, leading to improvements in ductility [95, 98]. However, achieving the desired outcome in AM is challenging due to the control of input parameters. These parameters encompass a range of variables, including powder type, feeding method, and energy type, among others [85]. Managing these parameters effectively is crucial to ensure the quality and performance of the final Ti6Al4V components produced through additive manufacturing processes[99].

2.8 Micro machining of AM components:

In recent years, a novel approach known combined manufacturing has emerged to capitalize on the strengths of various manufacturing techniques while mitigating their individual limitations and environmental impacts [52, 100]. In many instances AM is complemented by supplementary processes aimed at enhancing surface characteristics, microstructure, dimensional accuracy, and physical properties [52], this process is shown in figure 2.7 [5]. This integration facilitates the production of high-quality components within shorter timeframes. Despite significant progress in AM with regards to repeatability and material integrity, certain factors such as porous surface morphology, metallurgical imperfections, inadequate surface finish, and dimensional inaccuracies persist as impediments to broader applications [49, 51, 100]. Additionally, upon removal from the build plate, these components often exhibit residual stresses [101]. Consequently, post-machining operations become imperative for achieving precise geometrical tolerances, with milling commonly employed to rectify errors and refine surface finish [49, 102]. Furthermore, operations such as polishing or grinding may be necessary to eliminate porous surfaces and metallurgical flaws, thus enhancing surface quality subsequent to removal from the build plate [51]. The residual stresses can be alleviated through post-heat treatment procedures [101]. By integrating metal additive manufacturing (MAM) with subtractive techniques, offers enhanced flexibility and addresses concerns regarding excessive material wastage typically associated with conventional methods [52, 100]. Figure 2.8 shows the application of combining UPM and 3D printing for Optics [5].

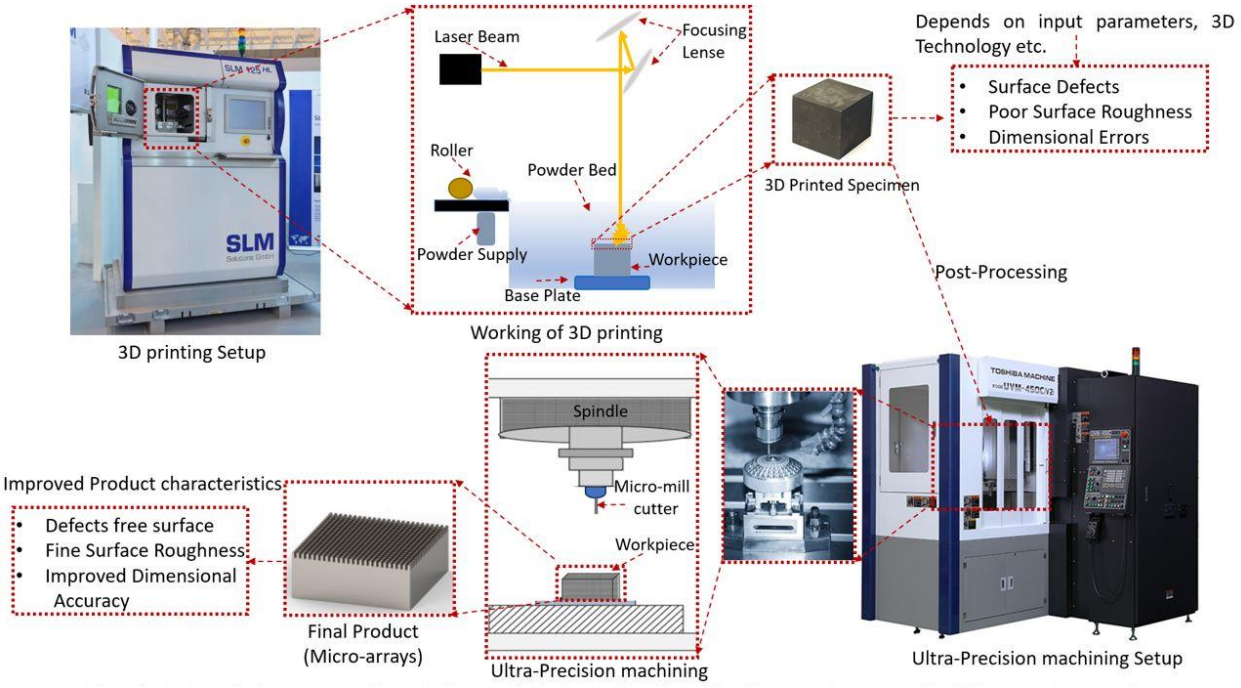

Figure 2. 7 Combined manufacturing process (selective laser melting (SLM) and micro milling) [5]

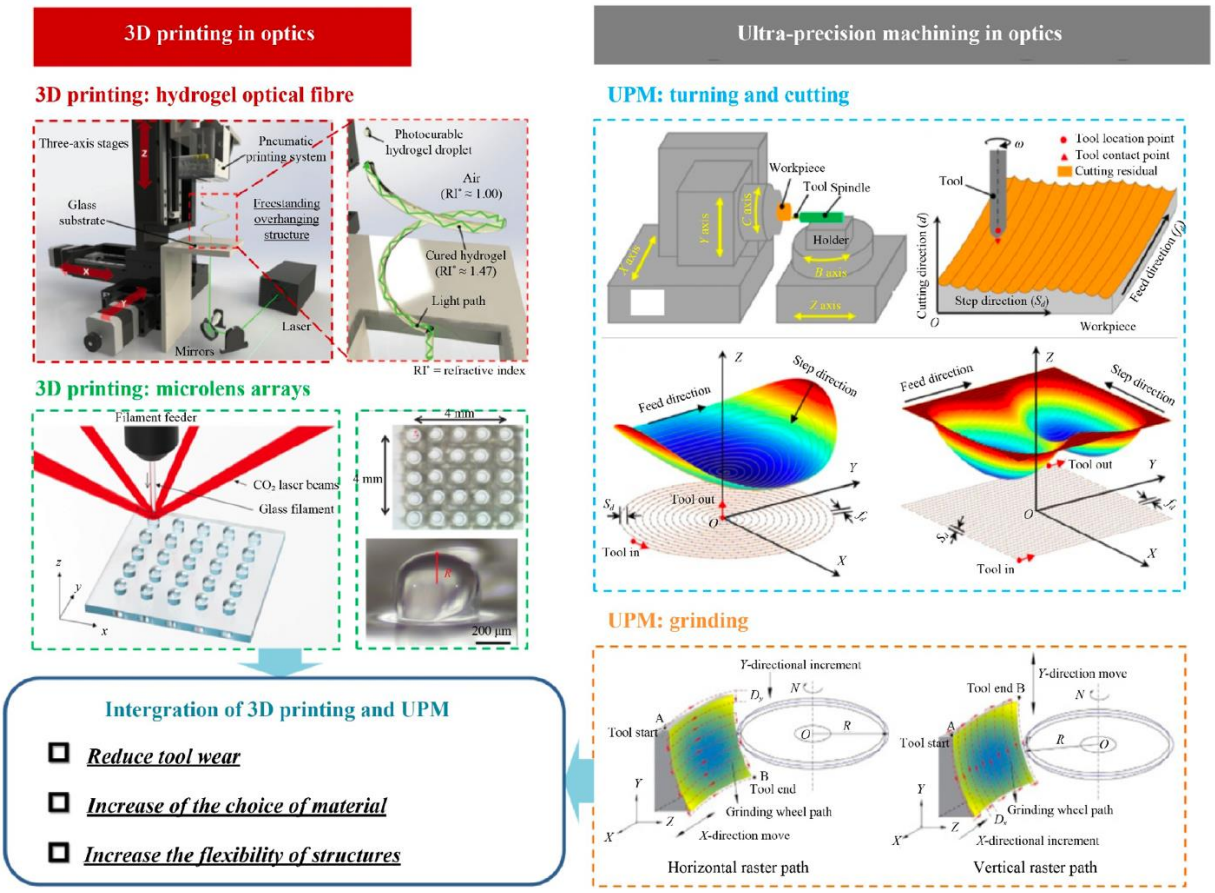

Figure 2. 8 Combining 3D printing and UPM for optics [5]

Modern industries place significant emphasis on sustainable and environmentally responsible manufacturing practices. This entails stringent measures to minimize energy and material wastage, as well as mitigate environmental degradation. International regulations and agreements mandate companies to adopt cleaner and sustainable production methods. In the machining of hard materials, cooling liquids are commonly used to improve surface finish and extend tool life by reducing heat at the cutting point. However, the use of cutting fluids leads to the deposition of residual chemical particles on the machined surface. These particles pose environmental hazards, contributing to soil and water pollution, thereby undermining the principles of sustainable manufacturing. Many cutting fluids contain compounds such as polychlorinated biphenyls (PCBs), heavy metals, and polycyclic aromatic hydrocarbons (PAHs), which pose risks to human health upon prolonged exposure [67].

In recent studies, researchers such as Zdenka and Stefania [103] have investigated the manufacturing of hard materials like Ti6Al4V. They conducted experiments to assess the machinability of additively manufactured (AM) Ti6Al4V using uncoated tungsten carbide tools, with electron beam melting (EBM) and Direct Metal Laser Sintering (DMLS) employed as AM techniques. Their research involved micro-milling to analyze burr formation, surface roughness, and microstructural variations. Similarly, Hojati et al. [104] conducted a study focusing on the effectiveness of micro-milling on additively manufactured Ti6Al4V, specifically examining surface quality, burr geometry, cutting forces, and specific cutting energy. A comparative analysis was performed with the machining of extruded Ti6Al4V. Despite the higher hardness of AM parts, there was no significant difference observed in cutting forces; however, AM parts exhibited superior surface quality. The study revealed that for chip thicknesses less than 7.4μm, the cutting forces and specific cutting energy of extruded Ti6Al4V exceeded those of AM. Additionally, when comparing burr formation, micro-milling of AM Ti6Al4V resulted in enlarged wavy continuous formations.

Bonaiti et al. [44] conducted a study focusing on the surface quality, cutting forces, and chip formation of Ti-6Al-4V alloy manufactured via Laser Engineered Net Shaping (LENS) additive manufacturing. The researchers also conducted hardness tests to further assess the material properties. Similarly, Oliveira et al. [105] conducted a comparative analysis of the machinability of Selective Laser Melting (SLM) and wrought Ti6Al4V using uncoated carbide end mill cutters. Their study investigated parameters such as cutting forces, surface roughness, and chip characteristics. The results indicated that SLM Ti6Al4V exhibited superior surface roughness during micro-milling, accompanied by lower cutting forces and reduced burrs. Additionally, SLM Ti6Al4V demonstrated enhanced mechanical properties, including strength and hardness, attributed to the formation of α' martensite microstructure resulting from rapid cooling during additive manufacturing. Rysava et al. [106] conducted a study evaluating the performance of two distinct micro-milling strategies utilizing uncoated end mill cutters on additively manufactured Ti6Al4V. Varghesea et al. [107] investigated the machining of porous additively manufactured Ti6Al4V using coated tungsten carbide milling tools. Their research delved into the effects of machining conditions on surface roughness, cutting forces, and microhardness (reference 93). In a separate study, Dang et al. [102] explored high-speed milling employing a ceramic (Al2O3/Si3N4) tool for machining Ti6Al4V fabricated via Direct Metal Laser Sintering (DMLS). The investigation of tool wear was conducted utilizing techniques such as energy dispersive spectroscopy (EDS) and scanning electron microscopy (SEM). Their findings revealed a relatively weak stability of ceramic tools in additive manufacturing environments, with prominent diffusion and adhesion wear observed. Thermal cracks were evident on the diffusion interface due to disparate thermal expansion coefficients between the tool substrate and diffusion surface. Additionally, crater formations near the tool edge were observed. Su et al. [108] conducted a comparative analysis of the machinability between Selective Laser Melting (SLM) and wrought Ti6Al4V utilizing polycrystalline

diamond (PCD) tools. Their comprehensive study investigated various aspects including tool wear, surface roughness, cutting forces, microstructure, and hardness. The findings revealed that SLM Ti6Al4V exhibited superior surface quality and lower cutting forces during dry machining compared to conventional Ti6Al4V. The study also elucidated a cutting phenomenon involving plasticity, brittleness, and hardness, attributing the reduced cutting forces to improved surface finish. In a related context, Atkins et al. [93] conducted experiments on the fabrication of additive manufacturing (AM) mirrors using diamond tools, focusing on various materials including Ti6Al4V. Their research highlighted the potential enhancement of optical performance through the reduction of porosity in AM components. Laser powder bed fusion and electron beam powder bed fusion were employed for the production of AM parts. While there have been studies exploring micro-machining of AM Ti6Al4V utilizing both coated and uncoated tools, it's noteworthy that only one study has utilized diamond tools for additive manufactured Ti6Al4V.

Sommer et al. [109] conducted a study, which involved the combination of laser powder bed fusion and high-speed milling, without the use of any lubricant. The research focused on correlating tool wear and surface roughness during the high-speed milling of additively manufactured components. The study achieved a surface roughness below 3µm, while microscopy of the flank face revealed a wear of 100µm. Proposing improvements to the milling process, the study suggested utilizing optimized tool start positions and adjusting the number of built layers. Furthermore, for undercut additive manufactured surfaces, the study recommended employing maximum milling angles of 30◦ for roughening and 40◦ for finishing purposes. Khaliq et al. [110] emphasize the challenges associated with micromachining difficult-to-machine materials, particularly titanium, wherein achieving superior surface quality, minimizing stresses, and extending tool life pose significant obstacles. The material's poor thermal conductivity and high hardness contribute to premature tool failure. Furthermore,

in micro-machining additive manufactured titanium alloys, the necessity of lubricant/coolant to mitigate tool wear becomes inevitable. The authors conducted an analysis of tool wear using coated tungsten carbide mills under various feed rates and cutting speeds, specifically under minimum quantity lubrication (MQL) conditions. Similarly, Danish et al. [111] investigated the micro-machinability of additively manufactured materials for generating complex profiles under different cooling conditions, namely minimum quantity lubrication (MQL), dry chilled air, and flooded cooling. Their analysis revealed that MQL yielded superior results in terms of surface roughness, cutting forces, tool wear, and burr width.

Bordin et al. [112] examined tool wear during the turning process of additively manufactured Ti6Al4V and observed that elevated cutting speeds and feed rates led to significant tool wear. They concluded that employing cryogenic cooling could diminish adhesive wear mechanisms, thereby extending tool life compared to dry machining. In a related study, Bruschi et al. [113] analyzed the wear behavior of machined additively manufactured Ti6Al4V intended for biomedical applications. Tests were conducted under varied machining parameters and cooling techniques in controlled environments to assess wear behavior within the human body. Their findings indicated that cryogenic cooling during machining exhibited superior wear performance, resulting in improved surface conditions (reference 99). Furthermore, in a separate investigation, Bruschi et al. [114] evaluated the micro-milling performance on additively manufactured Ti6Al4V under different lubricating conditions and machining parameters, focusing on surface quality, microstructure, and nano-hardness. Dry machining yielded comparable results to Minimum Quantity Lubrication (MQL), advocating for an environmentally friendly approach. In a comparative analysis, Airao et al. [115] scrutinized tool wear and surface characteristics between wrought Ti6Al4V and Selective Laser Melting (SLM) Ti6Al4V. Wrought Ti6Al4V, characterized by equiaxed grains, displayed a ductile behavior leading to adhesive tool wear, the formation of built-up edges (BUE), and

suboptimal surface topography. In contrast, SLM Ti6Al4V, with a lamella microstructure featuring higher hardness, exhibited reduced adhesive tool wear and BUE formation. However, it also demonstrated increased tool abrasion and higher surface roughness.

The mechanical properties of additive manufacturing (AM) parts exhibit an inherent anisotropic nature, wherein the microstructure is contingent upon the build-up direction. This characteristic presents notable implications during machining processes. In a study conducted by Lizzul et al., they investigated tool wear during the milling of AM Ti6Al4V (fabricated via laser powder bed fusion) across four distinct build-up directions. Through both qualitative and quantitative analyses of the machined surface and chip morphology, they assessed tool wear. Their findings revealed that specimens prepared vertically demonstrated a 40% improvement in machinability compared to horizontally manufactured parts [116]. Furthermore, Lizzul et al. [117] fabricated prisms of Ti6Al4V using laser powder bed fusion and examined the effect of build-up direction during machining. Interestingly, their results indicated that horizontal build-up direction conferred superior machinability.

Summary

Additive manufacturing (AM) currently faces challenges in achieving the precision required for critical applications, particularly in terms of geometrical accuracy and surface roughness. Even after process optimization, the roughness (Ra) of AM metal parts typically ranges from 5 to 10μm [44]. Consequently, post-machining processes are often necessary to meet stringent requirements. Ultra-precision machining, characterized by the removal of small quantities of material to achieve high geometrical accuracy and surface roughness, offers a solution to this challenge. Combining these two advanced manufacturing technologies can yield superior results. AM addresses issues related to generating complex and thin profiles while enhancing mechanical properties, reducing tool wear, and minimizing material wastage. Meanwhile, ultra-precision machining ensures precision and surface quality, facilitating

sustainable production practices by minimizing extensive material removal during the main manufacturing process. However, ultra-precision machining of hard materials like Ti6Al4V often necessitates the excessive use of cutting fluid to reduce cutting temperatures and enhance tool life. This practice poses environmental pollution risks and hazards to machinists, along with significant costs associated with fluid maintenance, storage, and disposal. Despite these challenges, the growing demand for precision components made from Ti6Al4V underscores the urgency for researchers to develop sustainable manufacturing methods for cleaner production in ultra-precision machining. From the literature review, it is evident that the existing research on micromachining techniques, particularly using coated and uncoated tools on additively manufactured Ti6Al4V, remains insufficient, especially concerning micro-precision milling. This area has not been explored to its full potential. This study presents a strategy for developing combined manufacturing processes for one of the most challenging materials prevalent in the manufacturing industry. The research focuses on evaluating the machinability of Ti6Al4V produced through Selective Laser Melting (SLM). By creating fully dense workpieces via SLM, the study ensures optimal material integrity. Subsequently, ultra-precision milling will be applied to heat-treated SLM parts to assess various machinability parameters, including surface roughness, form accuracy, cutting forces, tool wear, and chip morphology. To uphold environmental sustainability, only a minimal mist of lubricating oil will be utilized. This methodology aims to minimize material waste, reduce tool wear, and maintain low lubrication conditions, thereby fostering a sustainable manufacturing process.

Chapter 3

An experimental investigation on micro-milling of additively manufactured titanium alloys: selective laser melting and wrought Ti6Al4V.

3.1 Introduction

Titanium grade 5 (Ti6Al4V) is renowned for its exceptional properties, including a high strength-to-weight ratio, durability, superior resistance to corrosion and erosion, and low elastic modulus. Additionally, this alloy is non-reactive and ductile . These characteristics make Ti6Al4V preferable to nickel-based alloys for critical applications, a preference that has persisted for decades . In recent years, the alloy's nonmagnetic nature and corrosion resistance have led to its increased use in healthcare and medical fields . Ti6Al4V is employed in a wide range of applications, including medical endoscopes, dental optical instruments, and inspection mirrors [88, 89, 118, 119] . Furthermore, astronomical instruments, whether ground-based or space-bound, require optical mirror surfaces with low mass-to-strength ratios, making titanium alloys an ideal choice . However, manufacturing titanium alloy components through traditional methods often presents significant challenges. These include complex processing procedures, suboptimal forming effects, high processing costs, and considerable material waste. Such issues can reduce efficiency and increase overall production costs, thereby affecting the economic viability of using titanium alloys [120, 121].

Additive manufacturing (AM), commonly known as 3D printing, has garnered substantial attention due to its efficiency, versatility, cost-effectiveness, and environmental benefits. This technique employs a laser beam to melt metallic powder, which then solidifies based on a computer-aided design (CAD) model [122, 123]. Unlike traditional manufacturing

methods, AM eliminates the need for dies and specialized tools, enabling the creation of complex geometries without additional equipment. This capability not only shortens production times but also significantly reduces material waste [124-126]. Modern AM technology is capable of producing thin walls and features down to 0.2mm [45]. Selective Laser Melting (SLM) is the preferred method for fabricating Ti6Al4V components due to its numerous advantages, including rapid production, a variety of material options, direct CAD production, adaptability to intricate geometries, and the ability to form internal structures. Additionally, the rapid cooling and solidification in SLM refine microstructures and induce the formation of a martensitic α' phase, significantly enhancing mechanical properties such as strength, hardness, and corrosion resistance [105]. However, there are still challenges regarding precision and surface roughness [105, 115, 116].. Even after process optimization, the surface roughness of SLM metal parts ranges from 5μm to 10μm [23], necessitating post-machining processes for AM components [44, 115]. Micro-milling, a precision machining technique, presents a promising solution for these challenges . It enables the generation of precise details and improved surface characteristics on parts. By removing a small amount of material, micro-milling achieves high geometrical precision and low surface roughness [105, 106].

Despite the numerous benefits and potential applications of Ti6Al4V, machining this titanium alloy remains challenging due to its low thermal conductivity, strain hardening, high strength at elevated temperatures, and high chemical reactivity [127-130]. Machining additively manufactured (AM) metallic parts presents additional challenges compared to wrought alloys. The complexities of the powder bed, molten pool, and laser beam dynamics during AM processes complicate the understanding of underlying thermophysical and metallurgical phenomena [131, 132]. Micro-machining further intensifies these difficulties due to the increased sensitivity to variations in AM process parameters and cooling rates, which affect the delicate microstructure. Moreover, micro-machining faces issues related to size

effects, machine tool vibrations, and tool-workpiece interactions. Size effects arise from various factors such as workpiece characteristics, microstructure, process variables, and tool geometry. Chip formation in micro-machining also modifies process behaviour [131, 133].

The machinability of a material is intricately linked to its mechanical properties, which are shaped by the manufacturing method employed and the ensuing microstructural characteristics [44, 105]. Extensive research endeavours have been undertaken to explore the impact of manufacturing techniques on microstructural evolution and, by extension, their influence on precision machining. Sharma et al. [134] delved into the intricate relationship between microstructural attributes like grain size, phase fraction, and morphology, and their impact on machining characteristics and tool wear during high-speed machining of Ti-6Al-4V. Their findings unveiled a noteworthy correlation between these microstructural features and parameters such as cutting forces, sub-surface alterations, and patterns of wear.

Airao et al. [115], on the other hand, conducted a comparative analysis of the micro-milling outcomes between SLM-produced Ti6Al4V and its wrought counterpart. They observed that the wrought alloy, characterized by equiaxed grains, exhibited higher levels of adhesive wear, built-up edge (BUE) formation, and inferior surface finish. In contrast, the SLM Ti6Al4V, featuring a lamellar structure and heightened hardness, showcased reduced tool wear and BUE formation, albeit with a slight increase in surface roughness due to abrasion. Notably, the cutting-edge radius of the wrought alloy experienced a more pronounced expansion (18-37%) compared to the SLM variant (10-34%), and the SLM Ti6Al4V achieved an average surface roughness that was 8-10.6% smoother than its wrought counterpart. Ji et al. [135] investigated the impact of spindle speed and feed rate on micro-milling performance for both SLM and wrought IN718. Their study revealed that alterations in these machining parameters resulted in heightened levels of tool wear, surface roughness, and microhardness, particularly notable when machining the wrought IN718.

The demand for titanium parts in the precision industry is increasing, yet producing precision parts using both additive manufacturing (AM) and machining processes remains challenging [20-22, 25]. The primary objective of current research is to address these challenges and enhance the production of Ti6Al4V for precision applications. This study proposes an integrated approach that combines micro-milling with AM, leveraging the strengths of both technologies to mitigate their respective limitations. In this research, micro-milling is employed as a post-process following selective laser melting (SLM) to improve the surface characteristics and dimensional tolerances associated with AM. This approach enhances machining flexibility and addresses the issue of extensive tool wear in micro-manufacturing. The study specifically focuses on micro-milling AM-fabricated Ti6Al4V using cubic boron nitride (CBN) micro mills. The results are compared to those obtained from commercially available wrought Ti6Al4V, examining factors such as surface roughness, tool wear, burr formation, and chip morphology. The later part of the study focuses on examining the influence of microstructure and grain orientation on the performance of high-speed micro-milling of titanium in terms of tool wear, with particular attention to how these factors are affected by different manufacturing methods. Additionally, the study investigates the effect of feed rate to enhance the understanding of micro-milling. Systematic analysis of the micro-machineability of both samples is conducted, evaluating profile quality, chip formation, and tool wear.

3.2 Experimentation

To investigate the machinability of additively manufactured Titanium grade 5 (Ti6Al4V), we fabricated two types of specimens: one through 3D printing using selective laser melting (SLM) and the other using commercially available wrought titanium alloy. The wrought titanium alloy specimen was selected as the control group due to the maturity of the current casting processes for titanium alloys, which are widely used in comparative analyses

by researchers. Each specimen measured 25 mm x 25 mm x 25 mm. The chemical compositions of both materials are provided in Table 1. For the SLM specimen, the powder particle size ranged from 15 to 53 μm. The manufacturing process parameters included a laser power of 340 W, a scanning speed of 1250 mm/min, a hatch spacing of 0.3 mm, and a layer thickness of 60 μm. The mechanical properties of SLM processed alloys such as tensile strength, hardness, ductility, and fatigue resistance are highly sensitive to process parameters. Therefore, the parameters were carefully optimized to achieve a density of 99.9%, ensuring the material is suitable for high-performance applications in industries such as aerospace, biomedical, and automotive. After fabrication, the part underwent vacuum annealing at 800°C for 3 hours in an inert argon atmosphere to eliminate residual stresses, ensuring that these stresses did not influence the machining results [105, 136].

Table 3. 1 Composition of wrought and Ti6Al4V fabricated by AM

Element		Ti	Al	V	Fe	C	O	N	H
Percentage	Wrought	Balance	6.28	4.05	0.18	0.032	0.159	0.006	0.0021
Composition	AM	Balance	6.01	4.08	0.042	0.006	0.097	0.005	0.003

For the experiments, a five-axis high-precision machine, the Toshiba UVM-450C(V2), was employed. This machine offers a resolution of 0.01 μm for the X, Y, and Z axes. To evaluate the machinability of SLM Ti6Al4V, a series of micro-grooves, each 10 mm in length and with a width equal to the tool diameter, were machined. The cutting parameters and their respective levels are detailed in Table 3.2. Taguchi L16 design of experimentation has been used to conduct the study. Two-fluted cubic boron nitride (CBN) micro-flat end mill cutters were used, each having cutting diameter (D) of 600μm with the cutting length of 1.5 mm . The cross-section of the tool was examined using a scanning electron microscope (SEM), specifically the Hitachi TM3000, at various magnifications. The micro slots were generated across the build direction of the specimen. The SEM images are provided in Figure 3.1 for reference. To ensure

consistent experimental conditions, a new tool was used for each sample. Prior to the experiments, the surface of the workpiece was plane milled using a two-fluted end mill cutter with a 2 mm diameter. This standard practice helps achieve a precise depth of cut for the experiments and removes any oxide layer present on the surface. For lubrication, Klubercut CO (6-102), a biodegradable vegetable oil, was used. For phase identification, an X-ray diffractometer (Rigaku SmartLab) equipped with a 9 kW rotating anode X-ray source (λ~1.54 Å) was utilized. Each groove was examined using an optical profiling system (Zygo NexviewTM) to measure surface roughness and generate surface topography. Additionally, the Hitachi tabletop microscope (TM3000) was used to inspect the tool edge, the machined surface, and the chip geometry. Processed tools were cleaned well using ultrasonic cleaner and alcohol solution. A non-contact measurement method via the optical profiling system was adopted to assess the surface roughness of each groove. Five readings were taken for each groove, and the average value is reported. These measurements were taken approximately along the center line of each groove. Figure 3.1 illustrates the machining setup, the cutting sequence, and the tool's geometry

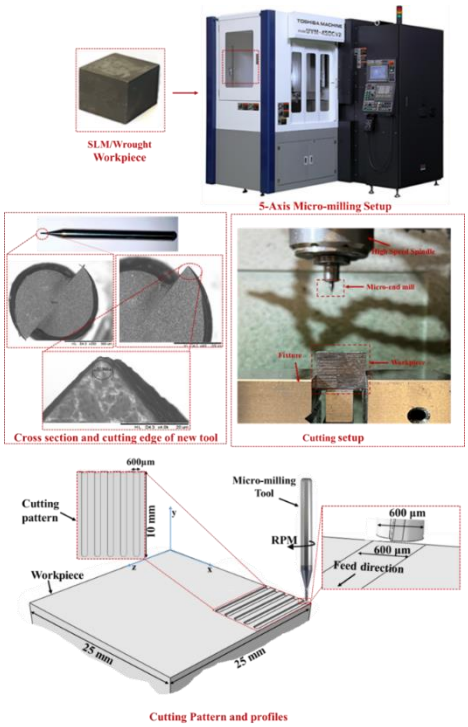

Figure 3. 1 Experimental setup showing micro milling setup, geometry of tool and cutting profiles

Table 3. 2 Machining Parameters of micro-milling

Cutting parameter	**Values**
Spindle speed (rpm)	60K,65K, 70K,75k
Depth of cut (μm)	10,15, 20, 25
Feed rate (μm/flute)	1, 2, 3, 4

Characteristics of the specimens

As previously stated, this study involves two types of specimens manufactured using distinct methods: SLM (Selective Laser Melting) and wrought. The surface morphology, X-ray diffraction (XRD) patterns, and microhardness of both types of specimens (as received) before any further processing are depicted in Figure 3.2. Phase detection was conducted using Crystal Impact Match software. In terms of surface morphology, the SLM work part exhibits a wavier pattern characterized by dimples and bumps of varying sizes, while the wrought specimen displays a linear pattern with spikes. This disparity can be attributed to differences in manufacturing techniques and post-treatment processes, specifically the heat treatment for the SLM specimen and machining for the wrought specimen.

The X-ray diffraction (XRD) results indicate that the α-phase is predominant in the SLM specimen, whereas the α + β phase structure is prominent in the wrought Ti6Al4V. The microhardness of each specimen was measured using a universal microhardness tester with a 1kgf load and a 10-second dwell time. The microhardness values for SLM Ti6Al4V and wrought Ti6Al4V were found to be 370 HV and 325 HV, respectively. Keist and Palmer [94] have indicated a direct relationship between mechanical properties and microhardness; thus, the ultimate tensile strength and yield strength of SLM Ti6Al4V are higher than those of wrought Ti6Al4V. The comparatively higher hardness value for SLM Ti6Al4V is attributed to the finer structure of the α’ + α phase. This higher strength and hardness exhibited by the SLM

specimen indicate resistance to plastic deformation for AM manufactured components [104, 137].

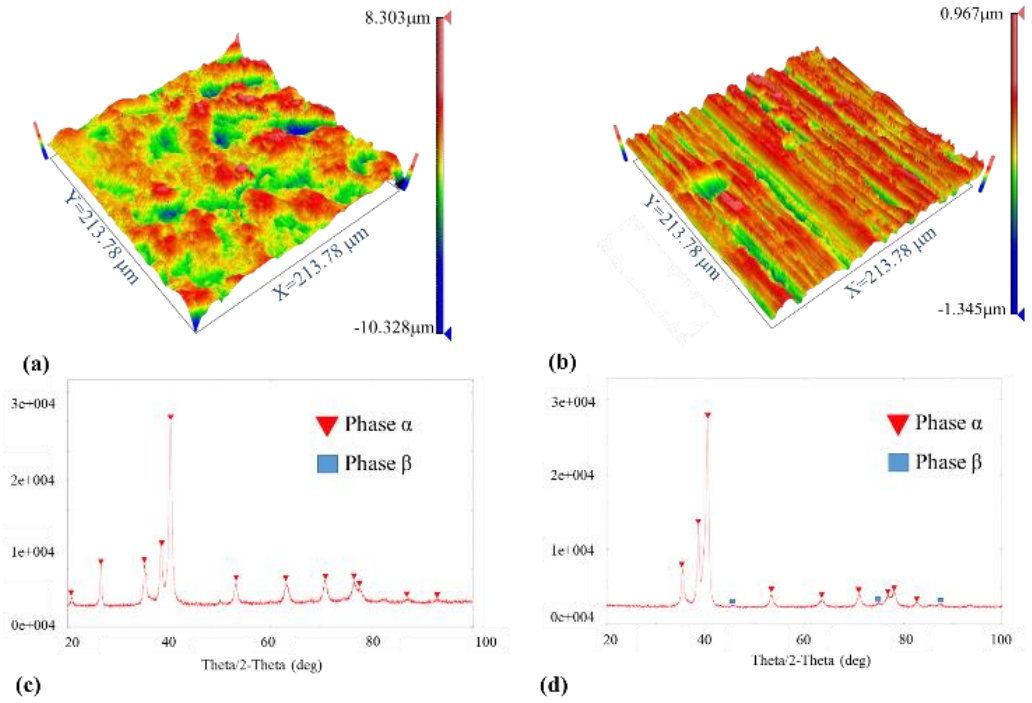

Figure 3. 2 Surface morphologies of (a) SLM Ti6Al4V, (b) Wrought Ti6Al4V; XRD of (c) SLM Ti6Al4V , (d) Wrought Ti6Al4V;

Figure 3.3 presents the microstructure and EBSD results of our specimens. Figure 3.3(a1), depicting SLM Ti6Al4V, reveals a defect-free surface devoid of pores, keyholes, and fusion defects, indicating excellent build quality and near-complete density. It highlights distinct β grain boundaries, marked by dashed lines, within which acicular α' martensitic phases are embedded. During the initial thermal cycle of heating and cooling, primary α' precipitates along the β grain boundaries. This microstructural feature results from the material's complex thermal gradient, ranging from 10^4 to 10^5 K/s, during solidification[138-140]. The microstructural pattern of SLM Ti6Al4V is markedly different from that of wrought samples shown in Figure 3.3 (b1 & b2) , exhibiting a unique grain growth pattern. Figures 3.3 (a2) and (b2) provide more magnified views to study further minor details. SEM images reveal needle-

like α' phase structures, with grain sizes ranging from 50 to 80 μm, and laminar grains averaging 40 to 60 μm. The microstructure is characterized by acicular α′ martensite phases uniformly distributed throughout the hexagonal close-packed (hcp) crystal structure, typical of supersaturated solid solutions [141-143] . These acicular martensites, varying in size and exhibiting a large aspect ratio, are dispersed across the primary β grains, as depicted. In subsequent thermal cycles, primary α' reverts to β and liquid phases when temperatures exceed the phase transition range. Upon cooling below the martensite start temperature (Ms), the liquid transforms back to primary acicular α', and the remaining β phase converts to secondary and tertiary acicular α' [144, 145]. Due to the high and rapid cooling rates, a hierarchy of martensitic structures forms, including primary, secondary, and tertiary α′ martensite, which are labeled in Figure 3.3 (a2) [144] . The orientation of the α′ martensite is either parallel or perpendicular, with primary acicular α' appearing as long columnar structures and secondary and tertiary phases progressively finer. At higher magnification, traces of the β phase become visible as flat particles along the α' needle boundaries [145, 146]. The β phase is distinguishable by its brighter appearance, due to the higher atomic mass of vanadium compared to titanium. The β phase contains a greater concentration of vanadium than the α phase [62, 147]. The rapid cooling rates in the SLM process inhibit vanadium segregation in the molten pool, leading to α' needles with higher vanadium content . Although α and α' phases share the same crystalline structure and morphology, they cannot be differentiated by X-ray diffraction (XRD), optical microscopy, or scanning electron microscopy (SEM). The β → α transformation during cooling preserves the β phase only at the edges of the original β grains . The Widmanstätten structure, is formed by the directional solidification of the α phase along specific planes within the β phase during intermediate cooling rates [148, 149]. Below the β transus temperature, the α phase precipitates as laths, expanding within the β grain boundaries. These laths grow in parallel within colonies, creating the distinctive lamellar Widmanstätten pattern, which

significantly influences the alloy's mechanical attributes, such as ductility and fracture toughness [150, 151] . The average dimension of these structures is noted to be 2.3μm, with a room temperature phase composition of 95% α and 5% β. The fine α/α′ microstructure prevalent in SLM Ti6Al4V alloys is credited for the material's superior tensile strength, resulting in high strength and toughness, markedly contributing to the alloy's mechanical integrity [152, 153].

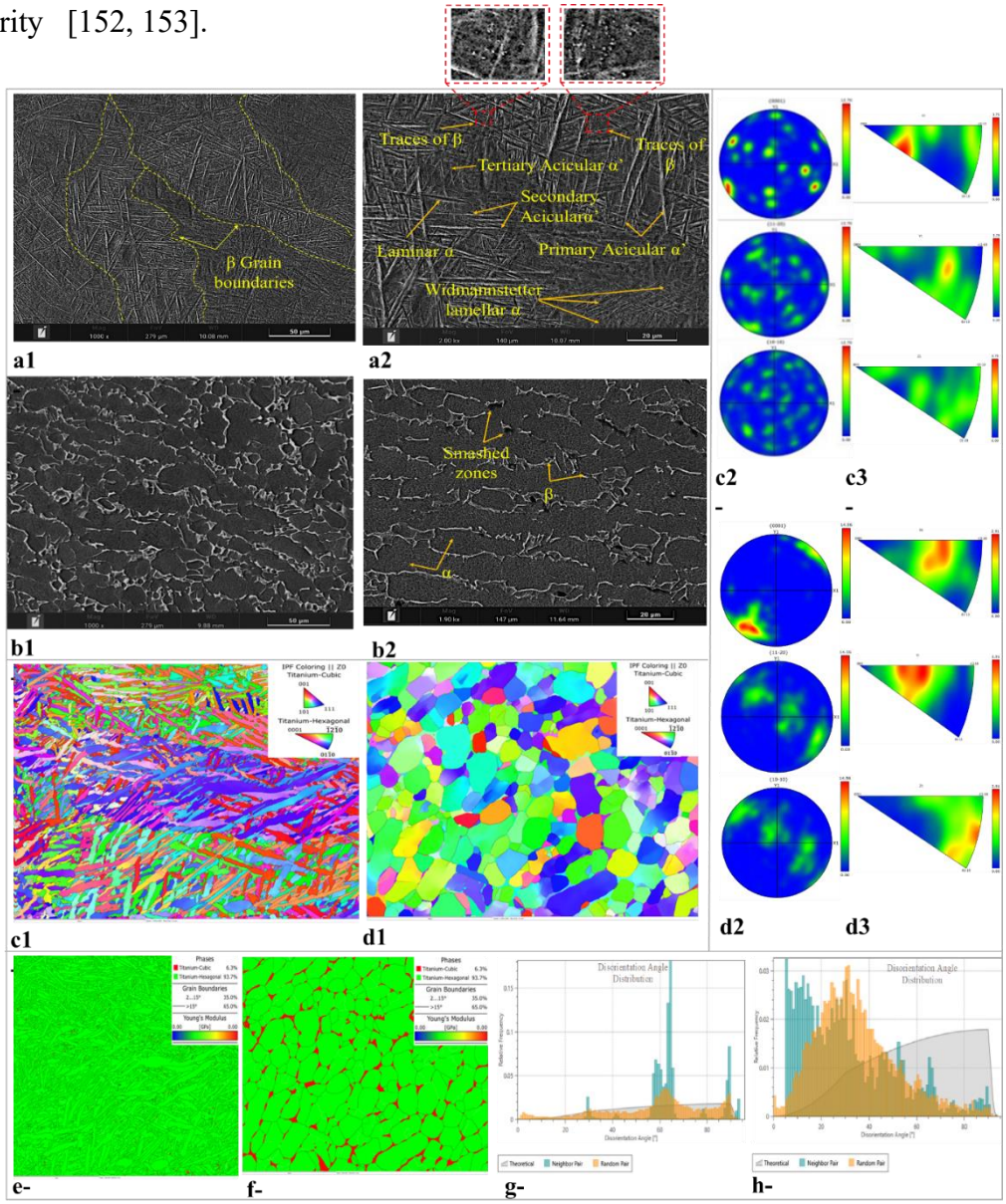

Figure 3. 3 SEM of specimens: a1-a2, SLM Ti6Al4V; b1-b2 Wrought Ti6Al4V, EBSD of specimens: c1-c4, SLM Ti6Al4; d1-d3, Wrought Ti6Al4V; phase mapping: e, SLM Ti6Al4V, f ; wrought Ti6Al4V; grain orientation distribution: g, SLM Ti6Al4V, h ; wrought Ti6Al4V

The microstructural characteristics of wrought Ti6Al4V differ significantly from those seen in Selective Laser Melting (SLM) samples, as illustrated in the inverse pole figure (IPF+ Zo). highlights the presence of equiaxed α grains, identifiable as dark regions within the microstructure. In addition, the intergranular β phases, enriched with vanadium, appear as distinct bright regions along the boundaries of the α grains. This combination of α grains and intergranular β phases forms a bimodal structure [154]. This bimodal microstructure arises during hot deformation, where the β phase transforms into the α phase through diffusion-controlled nucleation and growth [155]. This specific microstructure is evident when the heat treatment temperature is below the β-transus temperature but within the α + β region [156, 157]. In metallurgy, phase transformations are crucial in determining the microstructure and mechanical properties of materials. For wrought Ti6Al4V, the equiaxed α grains significantly impact the mechanical properties of the titanium alloy, with an average α grain size of about 20 μm. This grain size is larger than that reported by Shunmugavel et al. [155], which was 14 μm. The phase transformation in Ti6Al4V follows Burger's orientation relationship, where the respective close-packed planes (5α /β) and close-packed directions (<1120> α /<111> β) are parallel. This transformation occurs during both cooling (β to α) and heating (α to β), involving the transition between a high-temperature body-centered cubic (bcc) phase β and a low-temperature hexagonal close-packed α phase. This orientation relationship highlights the complex structural changes in Ti6Al4V during thermal cycling [158, 159].

Figure 3.3 (c&d) presents phase mapping for both samples, highlighting grain orientation and phase distribution. The absence of blank or dark regions throughout the grain structure indicates no zero solutions or defects, confirming the high quality of the EBSD analysis. The Ti6Al4V alloy, a binary titanium composition, exhibits a hexagonal close-packed alpha (α) phase stable up to 882°C and a body-centered cubic beta (β) phase stable above 882°C. Figure 3.3e illustrates that the SLM Ti6Al4V sample predominantly comprises the α

phase (99.7%), evident in the green areas, with a minimal presence of the β phase (0.3%) in red. In contrast, the wrought Ti6Al4V sample contains a higher proportion of the β phase (6.3%) alongside 93.7% α phase. This variation results from the distinct thermal and microstructural characteristics inherent to each manufacturing method. The rapid cooling in SLM "quenches" the alloy into the α phase, inhibiting significant β phase formation. Additionally, SLM promotes a finer, more uniform grain structure, which inherently restricts β phase development at grain boundaries. Moreover, the residual stresses and defects induced by the SLM process further influence its unique phase composition. These factors collectively contribute to the lower β phase content in SLM-produced Ti6Al4V compared to its wrought counterpart. Notably, the crystallographic texture of the samples is almost random and does not show any sign of pattern development. However, there is a significant increase in grain size in the wrought sample.

The disorientation angle quantifies the angular deviation between neighboring grains in a material, serving as an indicator of grain boundary characteristics. High disorientation angles, particularly those over 15 degrees, denote high-angle grain boundaries, which play a crucial role in influencing grain growth, recrystallization, and the material's mechanical properties. In the case of SLM Ti6Al4V in figure 3.3 (g) , the distribution of disorientation angles is skewed towards larger angles, suggesting substantial intergranular rotations due to rapid solidification and a complex microstructure. This trend is evident in the theoretical, neighbor pair, and random pair distributions, with the latter two highlighting the dominance of high-angle grain boundaries and the influence of the bcc-β to hcp α' phase transformation and acicular α' martensite’s. Conversely, wrought Ti6Al4V displays a more varied disorientation angle distribution, encompassing both low and high angles, with a noticeable frequency of higher angles in theoretical distributions (figure 3.3 h). This diversity reflects the material's exposure to deformation processes during manufacturing, which induce a range of

crystallographic orientations. Neighbour pair distributions in wrought Ti6Al4V reveal a balance of low-angle and high-angle grain boundaries, with a tendency towards lower angles. This indicates the diverse grain shapes and orientations resulting from conventional deformation. Random pair distributions span a broad spectrum of angles, mirroring the more traditional microstructure formed through deformation and recrystallization processes.

3.3 Results and Discussion

3.3.1 Tool Wear

This segment of the study delves into a detailed assessment of the influence of fabrication methods, specifically SLM and wrought, on tool wear. Figure 3.4 presents scanning electron microscope (SEM) images of milling tools after micro- milling of SLM and wrought Ti6Al4V after completion of all set of experiments (L16). Before the experiments, each cutter exhibited a smooth and sharp cutting edge, as depicted in Figure 3.1. However, the process of slotting subjects the cutting tool to both mechanical and thermal loading, leading to wear. The SEM images illustrate that tool wear is concentrated around the cutting edge in all instances. The results indicate that there was no catastrophic tool failure during the experimentation on both specimens. However, visible tool wear is evident at the conclusion of each set of grooves. The extent of tool wear is less severe for the SLM specimen compared to the wrought specimen. These observations are further corroborated by the surface generated during each groove. Consequently, it can be inferred that CBN milling tools exhibit commendable machining performance for titanium alloys, particularly SLM Ti6Al4V, in terms of tool wear and surface quality in micro- milling.

In the case of wrought Ti6Al4V, observable chipping off from the cutting edge is evident, accompanied by a loss of sharpness and shape in the tool edge. The extent of tool wear may be linked to the hardness and properties of the material. Figures 3.4a and 3.4c depict minor

wear and abrasion at the cutting edges of the tools used for AM parts, contrasting with the wear exhibited by the tool in Figures 3.4d and 3.4f employed for micro-milling of wrought Ti6Al4V. The occurrence of chipping can be attributed to variations in mechanical properties stemming from differences in microstructure between the two workpieces. Interestingly, the tool used for the AM part was anticipated to experience a higher level of wear due to the greater strength and hardness of the workpiece. However, the results appear contradictory. As illustrated by the XRD analysis in Figure 3.2 (c&d), the SLM specimen exhibits a more uniform crystalline structure, characterized by α'+ α hexagonal close-packed (HCP) phases, in contrast to the α+ β phase composition of wrought Ti6Al4V. This improved machinability of the material is attributed to the reduced plastic flow during cutting, resulting from decreased ductility owing to the more uniform crystalline structure [134].

Additionally, welded micro fragments are observable on the cross-sectional area of each tool. Figure 3.4b illustrates SLM Ti6Al4V with only a few attached segments, while wrought Ti6Al4V in Figure 3.4e displays a considerably higher quantity. These fragments have the potential to adversely impact both the quality of the machined surface and the tool's lifespan in subsequent operations. Abrasive particles such as these can scratch the groove surface and pose a significant risk of tool tip breakage. The elevated temperature experienced during cutting renders the small fraction of β-grains unstable, resulting in a softer wrought Ti6Al4V and increased material adhesion on the cross-section [160]. Consequently, when this adhered material is removed from the tool surface, chipping can occur, as evident in Figure 3.4d. In contrast, SLM Ti6Al4V exhibits greater hardness and a reduced propensity for material adhesion. Consequently, it effectively resists material adhesion on the surface and shows no signs of chipping on the cutting edge.

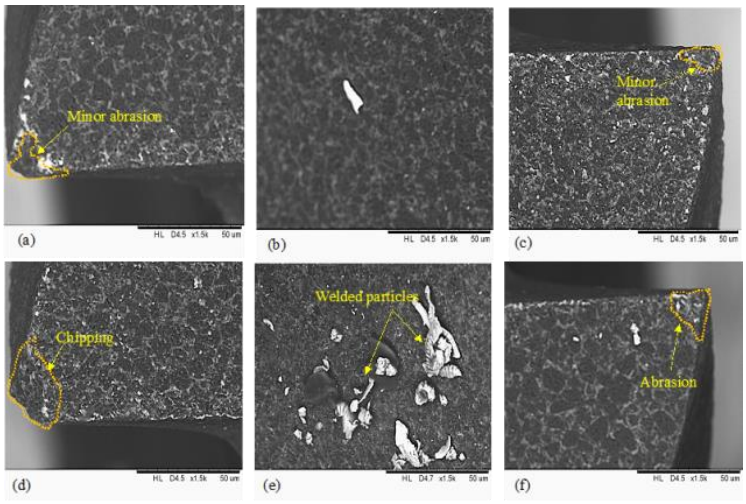

Figure 3. 4 The cutting tool processed on SLMTi6Al4V, (a) left flute, (b) cross section, (c) right flute, the cutting tool processed on wrought Ti6Al4V (d) left flute (e) cross section (f) right flute.

3.3.2 Surface quality

Surface roughness is a critical parameter in assessing the quality of products produced through micro-milling processes, particularly for precision applications where fine surface finishes are imperative, often measured in nanometers. The surface roughness is influenced by various factors including machining parameters, specimen and tool materials, tool geometry, lubrication conditions, and machining vibrations [111, 161].. Figure 3.5 illustrates the average surface roughness obtained in each experimental run (L16). Remarkably, the results for SLM-manufactured Ti6Al4V outperform those of the wrought Ti6Al4V counterpart. Specifically, the minimum surface roughness achieved is 19.21nm for SLM Ti6Al4V and 22.31nm for wrought Ti6Al4V, indicating a 13.9% improvement in surface quality with SLM Ti6Al4V. Throughout the experiments, the surface roughness of SLM Ti6Al4V consistently remains lower than that of wrought Ti6Al4V. The condition of the cutting tool edge significantly influences the surface roughness of micro-milled surfaces. Notably, tool wear was relatively inconspicuous in the case of tools used for SLM parts, as evidenced in the previous analysis. This difference in tool wear may contribute to the superior surface quality observed in SLM-manufactured Ti6Al4V.

The low plastic deformation exhibited by SLM-produced parts, attributed to their high hardness and low ductility, likely contributes to their superior surface quality [108]. In contrast, materials with higher ductility are prone to greater lateral plastic flow during machining, resulting in increased peak-to-valley height in the machined surface profile. Conversely, the reduced lateral plastic flow in SLM Ti6Al4V, owing to its higher hardness, leads to a finer surface finish [79]. The diminished plastic deformation during micro- milling of Ti6Al4V by SLM compared to wrought Ti6Al4V further underscores the better machinability of SLM-manufactured Ti6Al4V components [108]. This enhancement in machinability, coupled with the finer surface finish achieved, underscores the potential advantages of SLM technology in micro-milling applications.

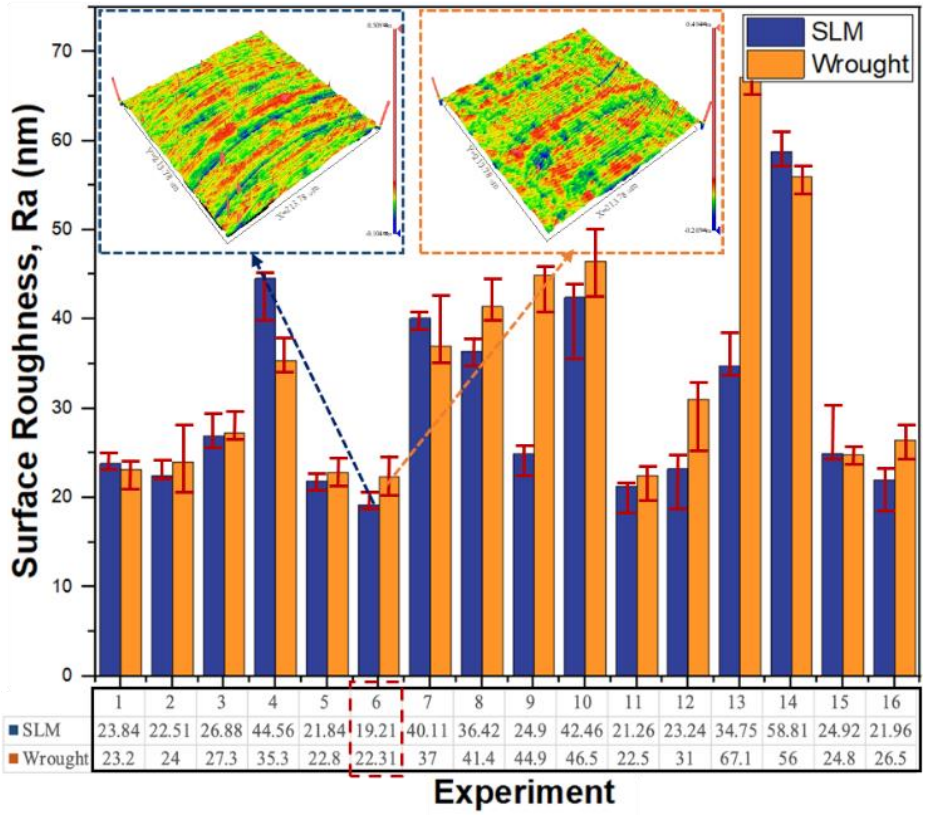

Figure 3. 5 Surface roughness of the machined grooves for each experiment

Burr formation during micro-milling is a significant concern as it directly impacts product efficiency. Factors such as material properties, machining parameters, and tool geometry

influence burr size and formation. The edge radius of the micro tool is particularly critical in micro-milling, where small cutting depths result in significant friction between the chip and the tool's rake face, leading to increased tool wear and material shear deformation. Figure 3.6 gives a demonstration of burr formation during micro-milling process. To mitigate these issues, the cutting depth generally needs to exceed the minimum chip thickness [162]. The condition of the tool also plays a crucial role in burr formation, as a worn-out tool with a weakened cutting edge contributes to burr generation [104, 111]. While burr formation is a significant concern for product quality, it can be controlled or minimized through improved machining strategies and material characteristics. Various approaches have been suggested to address this issue. Kou et al. [162] proposed using adhesive as a supporting material to extend the workpiece boundary, allowing burrs to form on the adhesive rather than the workpiece. Kumar et al. [163] emphasized the importance of burr modeling for minimizing and controlling burr formation. Additionally, optimizing cutting parameter values, applying coatings, utilizing hybrid cooling-lubrication systems, and employing supporting materials are effective methods to minimize and prevent burr formation. Figure 3.7 presents magnified SEM images of groove surfaces machined by micro- milling, depicting burrs produced on both sides of the grooves . One side, known as the down milling side, where cutting and feed occur in the same direction, exhibits greater burr height compared to the other side, known as the up milling side, where cutting is in the opposite direction to feed [164, 165]. This difference in burr height is attributed to the uneven distribution of force along the sides during the cutting process [111].

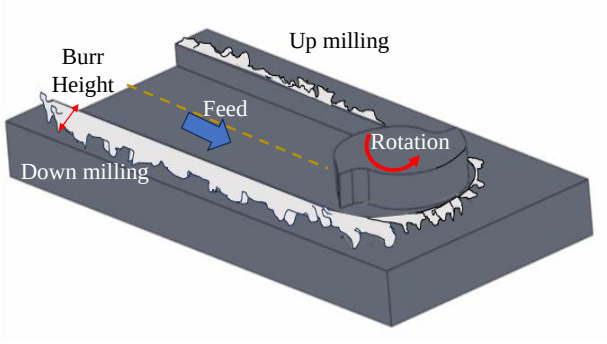

Figure 3. 6 Burr formation during micro milling

Figure 3.7 serves as a valuable tool for analyzing the surface characteristics of grooves from experiments 1, 5, 9, and 13. Notably, in Figure 3.7b, visible tool marks are evident on the surface, while the others appear smooth, lacking such marks. Comparing these surfaces with those of wrought Ti6Al4V (Figure 3.7 a, c, e, g), it's evident that the burrs on SLM Ti6Al4V (Figure 3.7 b, d, f, h) are smaller. The formation of burrs is heavily influenced by the material's shear deformation during machining, where increased shear deformation leads to wider and thicker burrs [104, 160]. Given its lower hardness, wrought Ti6Al4V exhibits more significant plastic deformation, while SLM-produced Ti6Al4V restricts this plastic deformation. Consequently, micro-milling of wrought Ti6Al4V results in larger burrs, whereas SLM Ti6Al4V displays smaller burrs on its machined surface. Moreover, the size and width of burrs directly correlate with the level of tool wear. In our experiments, the tool used for wrought Ti6Al4V showed considerably more severe wear compared to the one used for SLM-produced Ti6Al4V. As cutting-edge wear intensifies, the size of burrs increases along the machined surface.

Based on these findings, it can be concluded that the formation of burrs is contingent upon the manufacturing method of the workpiece, influenced by variations in microstructure, mechanical properties, and the condition of the cutting tool. Wrought Ti6Al4V tends to produce wider and more uniform burrs, whereas SLM Ti6Al4V yields uniform and narrower burrs. Additionally, burr formation in micro-milling is attributed to unexpected material plastic side flow within the milled slots, where there is an unresisted free surface with low support stiffness. The presence of unseparated chips connecting on the top of the machined slot significantly exacerbates burr formation. To mitigate top burr, it is imperative to employ optimal machining strategies.

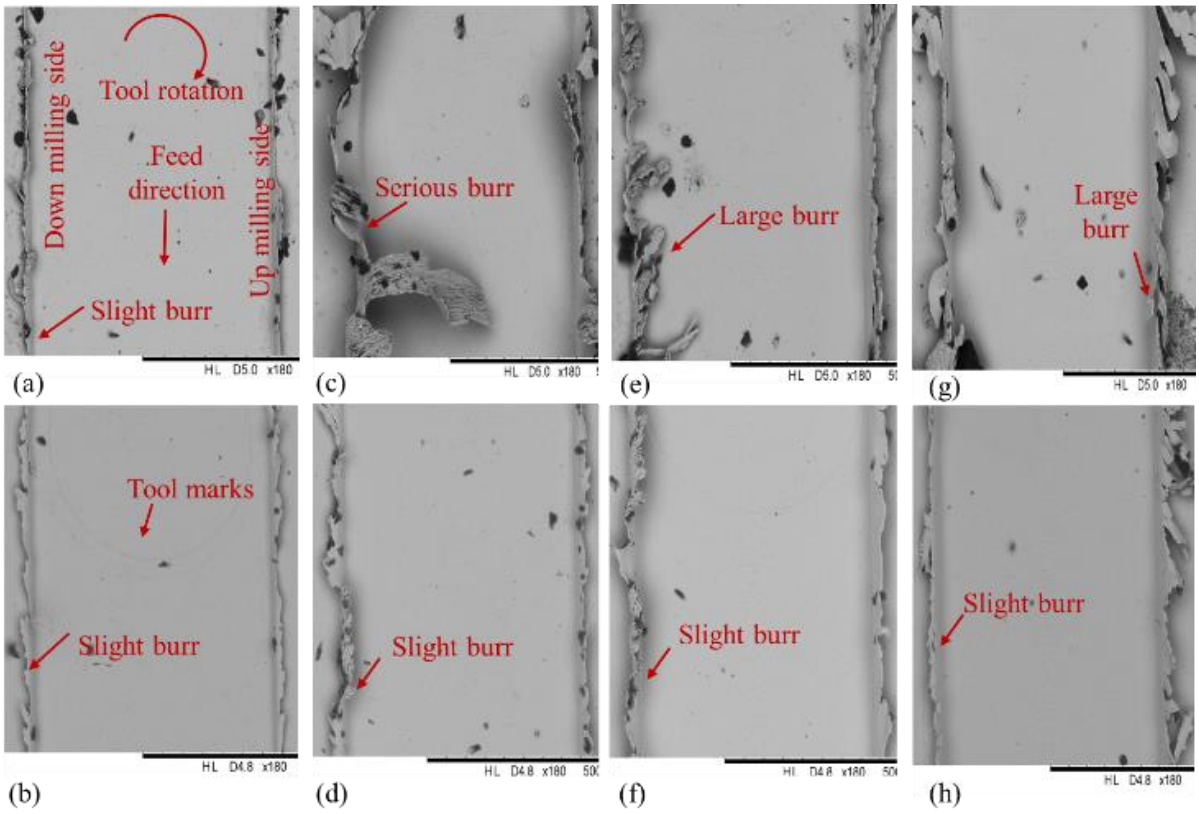

Figure 3. 7 SEM of groove surfaces (a) wrought Ti6Al4V in experiment 1, (b) SLM Ti6Al4V in experiment 1, (c) wrought Ti6Al4V in experiment 5, (d) SLM Ti6Al4V in experiment 5, (e) wrought Ti6Al4V in experiment 9, (f) SLM Ti6Al4V in experiment 9 (g) wrought Ti6Al4V in experiment 13, (h) SLM Ti6Al4V in experiment 13

3.3.3 Chips morphology

In the realm of micro-milling, the process of chip formation holds paramount importance, as it directly influences the dimensions of the chip and the depth of cut, which closely resemble those of the cutting tool's edge and corner radius (re). When the radius of the tool's edge is smaller than the chip thickness, it leads to a critical phenomenon known as the size effect in micro-cutting processes. The minimum chip thickness is defined as the ratio of the feed per tooth to the cutting tool's edge radius, below which chip formation ceases to occur [166, 167]. During the milling operation, the tool encounters a continuously varying chip thickness as it rotates. This process of chip formation during micro-milling is elucidated in Figure 3.8. Ploughing occurs when the undeformed chip thickness falls below the minimum required threshold, adversely affecting surface quality and contributing to the formation of

burrs. Micro-milling can be categorized into three distinct scenarios based on the relationship between the uncut chip thickness (h) and the minimum chip thickness (h_c), as illustrated in Figure 3.8. When h is less than h_c, only plastic-elastic deformation takes place, exacerbating ploughing and increasing tool wear. Chip formation initiates at $h = h_c$, while at h approximately equal to hc, a combination of plastic-elastic and shear deformation ensues. As h surpasses h_c, the workpiece material is chipped away, and elastic recovery becomes negligible [6, 168]. Therefore, it is imperative to ascertain the minimum chip thickness before initiating micro-milling operations for both the cutting tool and the workpiece.

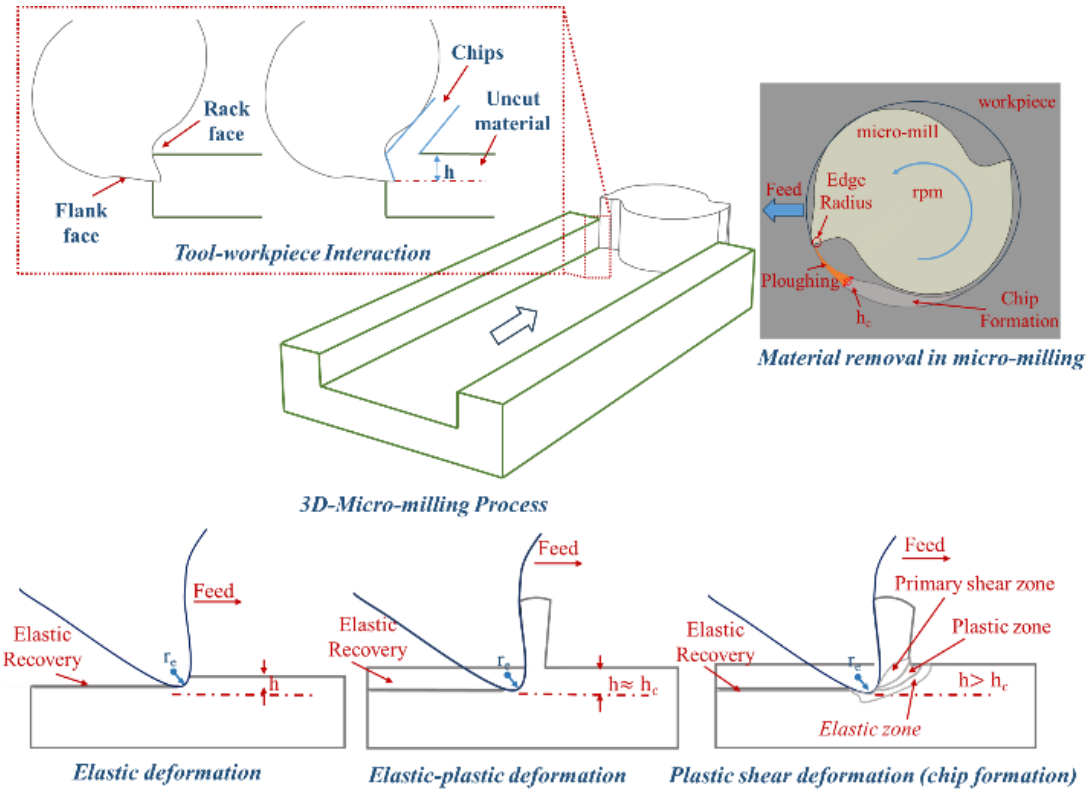

Figure 3. 8 Chips formation during micro-milling of SLM /Wrought Ti6Al4V

In micro-machining, the morphology and geometry of chips are intricately linked to the cutting mechanism, where dominance shifts between ploughing and shearing depending on the uncut chip thickness relative to the critical depth of cut. The characteristics of chips generated during micro-machining are influenced by various factors, including the material of the

workpiece, tool geometry, cutting speed, depth of cut, and lubrication conditions [131, 169]. In the present study, scanning electron microscopy (SEM) was employed to analyze the chips produced during micro- milling of Ti alloys fabricated via SLM and wrought Ti alloys. Figure 3.9 depicts the chip morphology of Ti6Al4V produced by SLM and wrought Ti6Al4V. Chips exhibit two distinct sides: the free surface (Figures 3.9d and 3.9h), typically characterized by a segmented surface, and the contact surface (Figures 6c and 6g). As the chip slides against the rake face of the cutting tool, the contact surface tends to become relatively smoother and shinier. Increased friction, elevated temperatures, and heightened contact pressure contribute to softening this side, resulting in a smoother surface texture [169].

Figures 3.9b, 3.9c, and 3.9d provide a closer look at the chip characteristics under high magnification. Micro-milling of Ti6Al4V by SLM yields chips that exhibit a more continuous, uniform, and consistent appearance, owing to the very fine and uniform α'+ α hexagonal close-packed (HCP) crystalline structure. The contact surface of these chips displays welded microparticles, a phenomenon attributed to the elevated temperatures generated during micro-milling, which lead to the adherence of micro particles to the chip surface [131]. Additionally, the sides of the chips exhibit distinct continuous ridges, a consequence of the high cutting forces and intense plastic deformation induced by elevated temperatures and pressures. Meanwhile, the free surface of the chips displays a pattern of scales known as lamellae. During micro- milling, the increase in temperature enhances ductility while decreasing hardness. Consequently, the heightened plastic strain results in segments of both materials sliding over one another, contributing to the formation of these lamellar structures [62, 131, 170].

In Figures 3.9e and 3.9f, as well as Figures 3.9g and 3.9h, the chip morphology of wrought Ti6Al4V is depicted. Notably, these chips exhibit larger dimensions and serrated patterns, a characteristic often observed in materials with poor thermal conductivity, which experience a reduction in mechanical strength with increasing temperature—a phenomenon

known as thermal softening [131]. The non-uniform strain generated during machining leads to regions of varying shear strains, resulting in tearing occurs [171]. This non-uniform strain distribution may be attributed to the α+ β crystalline structure [172]. Examining the surface of the chips, finer lamellae with narrower patterns are observed compared to those produced by the SLM sample. This variation in serration spacing is attributed to differing mechanical properties and microstructure. Materials with greater ductility and a more uniform microstructure exhibit increased plastic deformation at elevated temperatures, resulting in greater distances between serrations [131]. Despite variations in machining parameters, all chips collected during the process display a consistent formation. Wrought Ti6Al4V tends to produce shorter, discontinuous chips due to its higher hardness, which limits plasticity during micro-milling and reduces lateral plastic flow [30]. Some chips may appear welded together due to non-uniform strain distribution causing cracks and tearing. Consequently, chip morphology plays a crucial role as even minor variations can impact tool wear, surface quality, and machining accuracy. Increased tool wear is often associated with wider, more discontinuous chip formation. In the present study, long continuous chips produced by SLM Ti alloys exhibited less tool wear and superior surface quality compared to wrought Ti6Al4V, which generated wider, shorter chips.

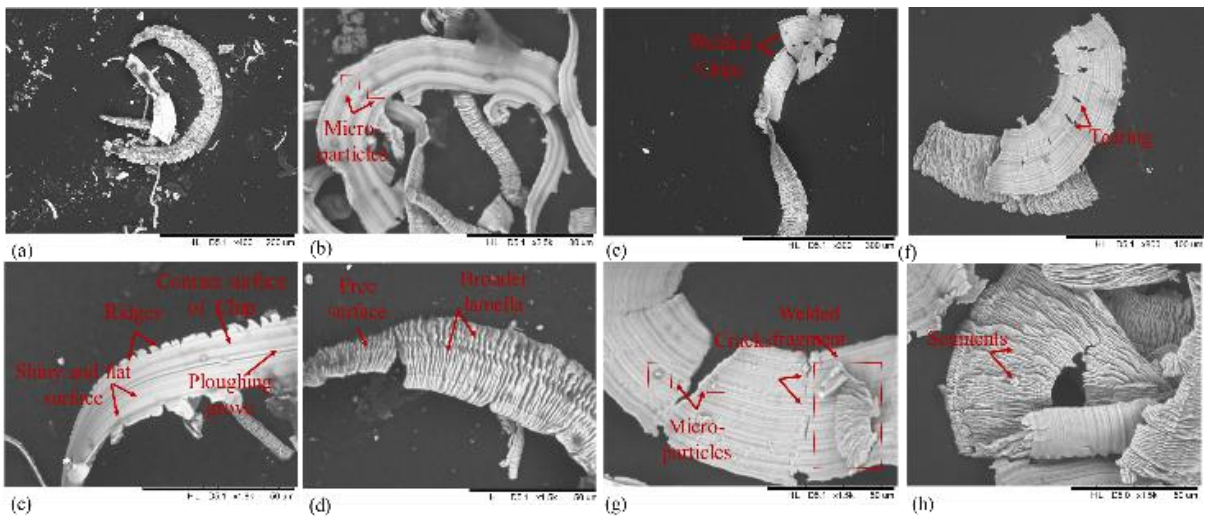

Figure 3. 9 Chips morphologies of SLM Ti6Al4V (a) long continuous chips, (b) magnified chips surface (c) contact surface of chips, and (d) free surface; Chips Morphologies of wrought Ti6Al4V (e) short, welded chips, (f) magnified chips surface (g) contact surface (h) free surface

3.4 Micro-structure and grain orientation

The properties of Ti6Al4V alloy produced by additive manufacturing (AM) notably differ from those manufactured through traditional methods such as forging and casting. Specifically, Ti-6Al-4V fabricated via selective laser melting (SLM) is characterized by α' martensite with a hexagonal closed-packed structure, a result of rapid cooling that transforms the stable β phase into α' martensite. In contrast, conventionally manufactured Ti6Al4V exhibits equiaxed α grains and intergranular β phases, with directional alignment due to deformation in processes like forging. The slower cooling rates in traditional methods lead to coarser grains, allowing for more significant grain growth [39, 105, 116]. The directional and rapid solidification process in SLM, combined with substantial temperature gradients during molten pool surface formation, significantly contributes to the material's anisotropic behavior [173, 174]. Columnar grain growth along specific directions, such as the 〈100〉 orientation aligned with the maximum heat extraction direction, results in a heterogeneous and anisotropic microstructure. A location-specific thermal history is established due to the thermal gradient between the melt pool and previously solidified layers. Lower ultimate tensile stress and yield stress but higher elongation are observed along the longitudinal direction compared to the transverse direction, attributed to the presence of elongated α phase grains (αGB) forming along the boundaries of preceding β grains, serving as weak junction points [175-177]. To address the inherent challenges of residual stresses associated with AM-produced components, post-processing heat treatments are typically employed to stabilize the microstructure, alleviate thermal stresses, reduce porosity, and enhance the mechanical properties of the as-built parts [116, 178]. Despite the better mechanical properties of components fabricated using AM technologies compared to those prepared by forging or rolling, deviations from specified surface finish and geometric tolerances required for critical and precision applications are observed. Thus, post-processing of as-fabricated components is necessary to overcome the

limitations in achieving the desired surface finish and dimensional accuracy using current AM technology [116, 117, 179]. Hence, it is a well-established fact that the machinability of a material is directly influenced by its mechanical properties, which, in turn, are determined by the manufacturing method and the resulting microstructural development. These mechanical properties influenced by microstructural development in conjunction with other factors like thermal conductivity and chemical composition, dictate how a material responds to machining processes. So this part of the research work is focused on this particular aspect.

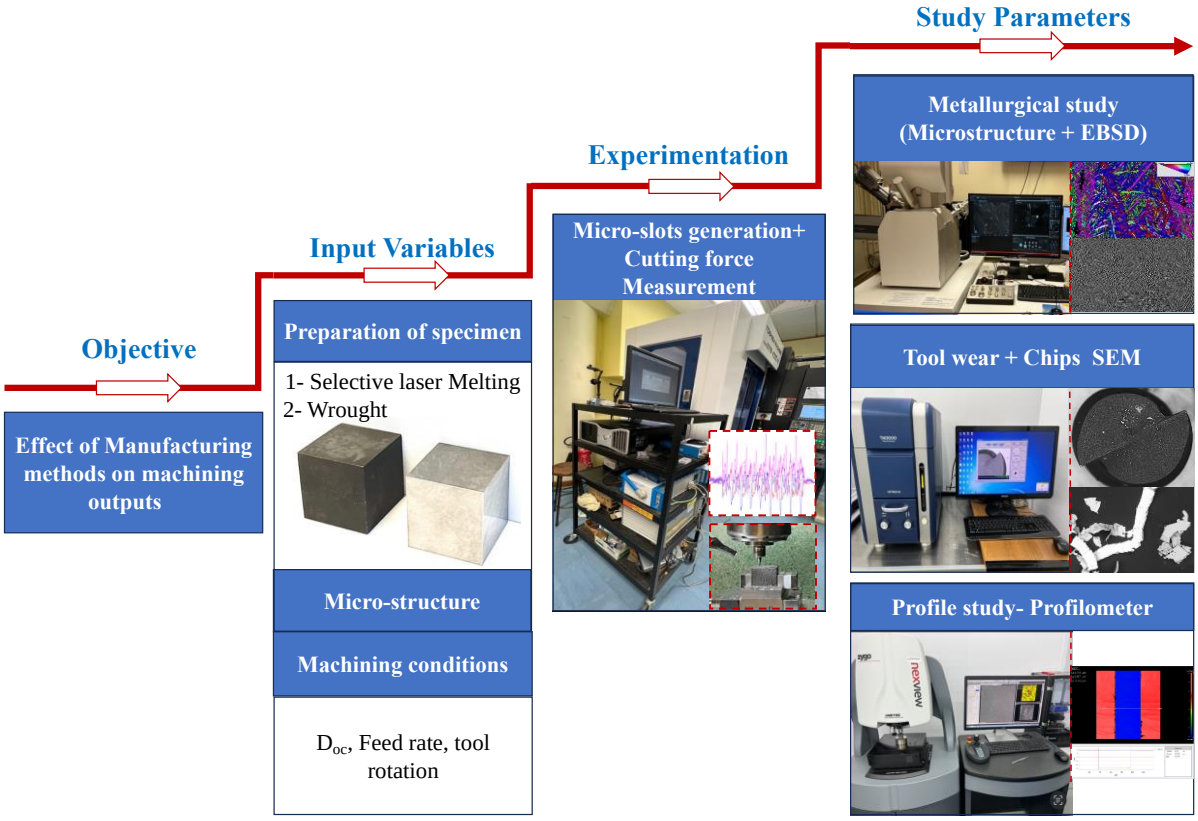

Figure 3. 10 study the effect of microstructure on micro milling.

3.4.1 Micro-structure and grain orientation on micro milling of Titanium alloys

Two specimens of Ti6Al4V titanium alloy, one fabricated by selective laser melting (SLM) and the other using conventional wrought methods, were prepared for micro-milling investigations. Each specimen measured 25mm x 25mm x 25mm. The SLM specimen, created

using a Metal (SLM) - SLM 125HL printer with a powder size of 15-53µm and specified composition, was processed with a laser power of 340W, scanning speed of 1250mm/min, hatch spacing of 0.3mm, and layer thickness of 60µm, followed by vacuum annealing at 800°C for 3 hours in an inert argon atmosphere to remove residual stresses. The mechanical properties of SLM processed alloys such as tensile strength, hardness, ductility, and fatigue resistance are highly sensitive to process parameters. Therefore, the parameters were carefully optimized to achieve a density of 99.9%, ensuring the material is suitable for high-performance applications in industries such as aerospace, biomedical, and automotive. The wrought specimen was provided by Firmakes Titanium Co., Ltd. Microstructural analysis and electron backscatter diffraction (EBSD) were conducted using TESCAN MIRA and Nordly Max3 of Oxford Instruments, respectively, with electropolishing performed in a solution of 5% perchloric acid and 95% glacial acetic acid at 10°C and 60V for 30 seconds. The processed data, visualized using Aztec Crystal of EDAX – TSL software, revealed significant differences in the microstructure and grain orientation, providing insights into how these factors, influenced by manufacturing methods, affect the machinability and performance of titanium alloys in micro-milling. The experimental setup and micro mill tool used for the current experimentation is shown in figures 3.11 and 3.12 respectively.

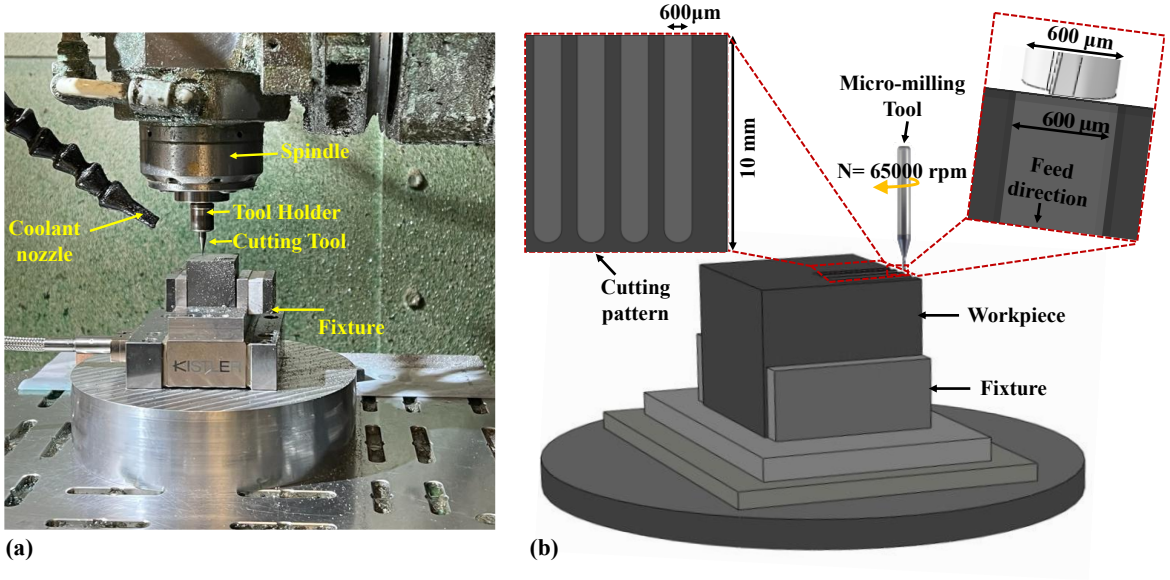

Figure 3. 11 Experimental setup; (a) original setup, (b) 3D demonstration of profile generation

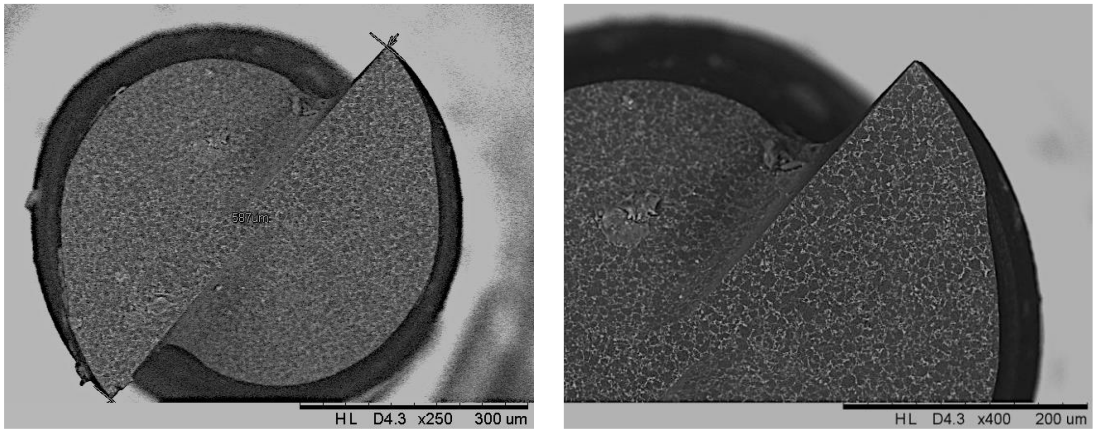

(a) **(b)**

Figure 3. 12 Cutting tool; (a) corss section; (b) cutting edge

3.5 Tool-workpiece interaction:

The amount of plastic strain experienced by a material during the milling process significantly differs from that observed in microhardness tests or uniaxial tensile tests. During milling, the material undergoes severe plastic deformation around the cutting edge, with extremely high strain rates and temperature gradients, as reported by La Monaca et al. . [52]. Additionally, friction between the tool, workpiece, and chip generates substantial heat. The nature of material removal is linked to dislocation slip, and the dislocation-annihilation mechanism can cause significant softening during this process. The rate of dislocation movement or annihilation is closely related to immobile dislocations, vacancies, and grain boundaries (or cellular boundaries). The extremely high temperatures generated by plastic deformation and frictional resistance greatly affect the concentration of vacancies, thereby influencing the dislocation annihilation process [53]. As a result, the strengthening effect of the initial immobile dislocations is partially offset. Furthermore, some precipitates may partially dissolve under such high temperatures, leading to limited precipitation strengthening in the the shear region shear region. The figure 3.13 illustrates the differences in tool-workpiece interaction at the micro level for both materials. The ductility of SLM Ti6Al4V is lower compared to wrought Ti6Al4V.

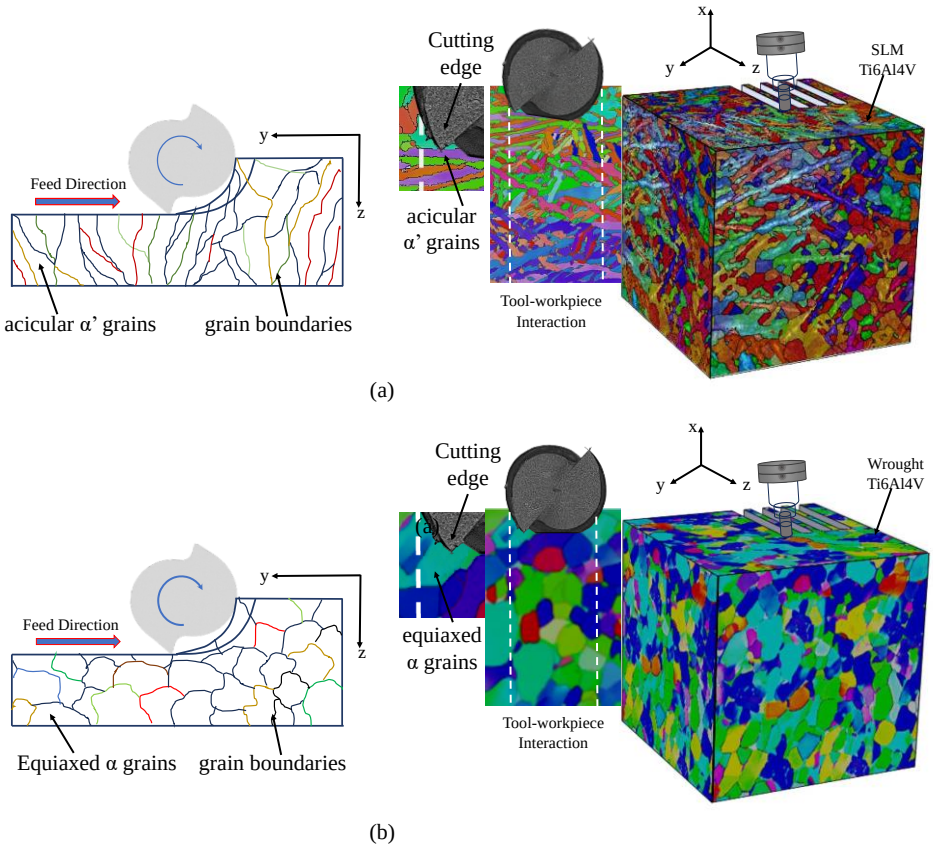

Figure 3. 13 tool workpiece interaction; (a) SLM Ti6Al4V, (b) wrought Ti6Al4V.

During the milling process, the cutting edges endure significant cutting forces and elevated temperatures, resulting in complex interactions with the workpiece. This complexity is further compounded by the high hardness and tensile strength characteristic of Ti6Al4V, leading to plastic deformation during micro-milling. The consequent increase in cutting forces and temperatures profoundly impacts tool wear. Elevated chip temperatures promote heightened friction at the chip-tool interface, causing wear on the end mill's rake face and subsequent increases in machining force and power consumption. Therefore, it becomes imperative to assess rake face wear during machining operations. Additionally, in micromachining, the flank face interfaces directly with the freshly machined surface, significantly affecting product quality [131, 180, 181]. Hence, investigating flank wear is equally crucial in ensuring quality outcomes. Various factors, such as processing parameters, tool and workpiece materials, and cooling conditions, are known to influence tool wear. This study emphasizes that differences

in microstructures primarily account for variations in tool wear among samples under identical cutting conditions. Specifically, the observed differences in tool wear under uniform cutting conditions are closely linked to sample microstructure. Scanning electron microscope (SEM) images are utilized to analyze the dependence of tool wear on the manufacturing method as a function of microstructure. SEM images depicting different views at variable magnifications of the tools, including cross-sections, rake faces, and flank faces, are presented in Figure 3.14 and 3.15. The condition of both tools is clearly distinguishable from each other. Major tool wear mechanisms include abrasion and adhesion for both samples. Comparing the cross-sections of each tool, as illustrated in Figure 3.14a and Figure 3.15a, no significant wear that causes the failure is visibly apparent. Both tools display adhesive wear, attributed to friction between the cutting tool and the workpiece material. During the ploughing process, material slips over the tool surface, adhering to it. In Figure 3.15b, the adhesive layer of workpiece material on the cutting edges is notably more pronounced for wrought Ti6Al4V compared to SLM Ti6Al4V, as depicted in Figure 3.14b. The cutting temperature induced during micromachining of Ti6Al4V typically ranges from 450 to 650°C. Such high temperatures and pressures at the tool-workpiece interface create conditions conducive to material adhesion at the cutting edge [182, 183]. The equiaxed microstructure characteristic of wrought Ti6Al4V, with a higher proportion of β grains, undergoes destabilization under conditions of elevated pressure and temperature, leading to adhesion to the tool and the formation of a layer. Conversely, in SLM Ti6Al4V, the high hardness serves as a barrier to material adhesion onto the tool surface. The grain thickness of SLM Ti6Al4V is significantly less compared to that of wrought Ti6Al4V. Additionally, SLM Ti6Al4V exhibits lower ductility, resulting in easier shearing or pulling out of grains compared to the larger equiaxed grains of α and β phases present in wrought Ti6Al4V.

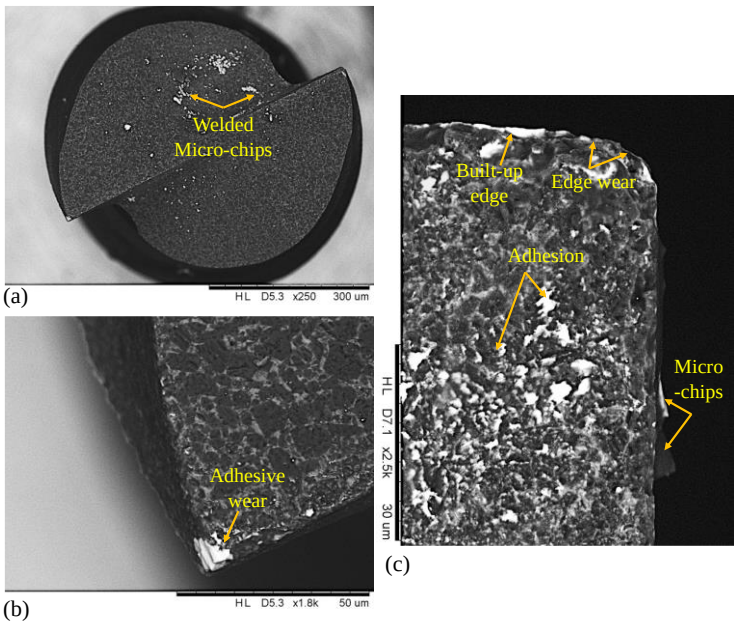

Figure 3. 14 Tool processed on SLM Ti6Al4V ;(a) Cross section (b) cutting edge (c) rake face

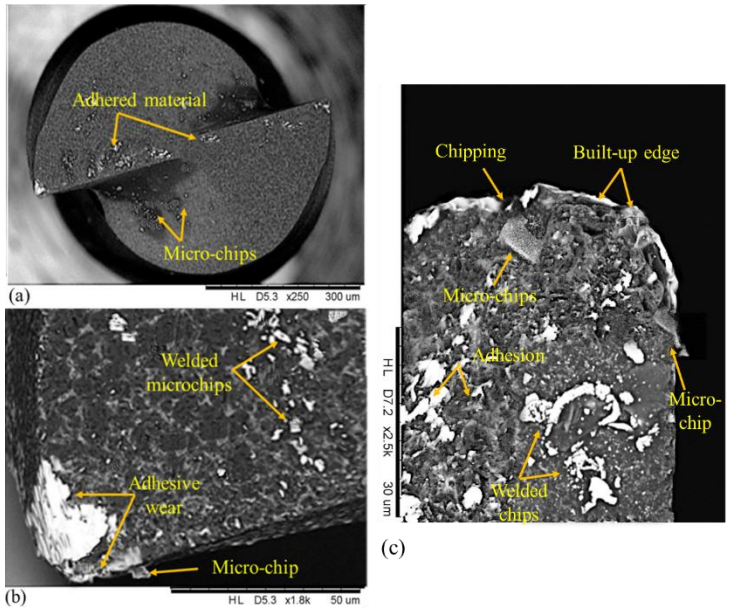

Figure 3. 15 Tool processed on wrought Ti6Al4V ;(a) Cross section (b) cutting edge (c) rake face

These larger grains provide sufficient resistance, leading to greater wear observed on the processed tool. Similar observations regarding the micro-milling of Ti6Al4V with varying microstructures were documented by Ahmadi et al. [184] Upon subsequent machining, removal

of the adhesive layer results in the detachment of some tool material, causing edge chipping or flaking. Consequently, the cutting tool experiences a notable reduction in sharpness. Furthermore, the non-uniformity of material and larger grain size also significantly influence the cutting process. The distribution of grain disorientation angles further impacts process stability. In the case of wrought Ti6Al4V, the disorientation angle distribution range is notably wide, encompassing both low and high-angle boundaries, which may engender a more diverse material response during micro-milling. The existence of low-angle boundaries may precipitate localized stress concentrations, thereby contributing to heightened tool wear. Moreover, the assortment of grain orientations could give rise to more intricate tool wear patterns.

Welded chips are observable in both scenarios. However, the rake face of the tool processed on wrought Ti6Al4V exhibits more extensive coverage compared to that processed on SLM Ti6Al4V, a condition known as built-up edge (BUE). This difference stems from the presence of the beta phase in wrought Ti6Al4V, which, due to the heat generated during cutting, becomes softer and shows a higher tendency to adhere to the workpiece material compared to SLM Ti6Al4V [134, 145] . Sharma and Meena [134] have established that the microstructure of work materials significantly impacts BUE fo rmation in micro-scale machining. The higher hardness and laminar grain structure of SLM Ti6Al4V result in lower ductility, reducing plastic flow and consequently mitigating BUE formation.

As the cutting process continues, the adhered microparticles are gradually chipped off, leading to tool surface chipping, as shown in Figure 3.15c. However, material adhesion enlarges the edge radius, shifting material removal from shearing to ploughing. Ploughing hinders chip flow over the rake face, redirecting it around the enlarged edge radius. In continuous machining, intensified material ploughing due to increased adhesion prevents the material from shearing off as chips [134]. Thus, adhesion, abrasion, and edge chipping are predominant mechanisms for wrought Ti6Al4V. In contrast, SLM Ti6Al4V, with its larger α

colony and partitioning effect, has lower yield stress and diminished resistance, preventing tool chipping . The rapid solidification process in SLM can produce a more homogeneous microstructure and even grain boundary distribution, facilitating smoother material removal and enhancing tool condition.

Welded chips are observable in both scenarios, yet the rake face of the tool processed on wrought Ti6Al4V exhibits a greater degree of coverage compared to that processed on SLM Ti6Al4V, a condition known as built-up edge (BUE). This discrepancy arises from the presence of the beta phase in wrought Ti6Al4V, which, under the influence of heat generated during the cutting process, becomes softer and demonstrates an increased affinity to adhere to the workpiece material compared to SLM Ti6Al4V [134, 145]. Sharma and Meena [134] have determined that the microstructure of work materials significantly influences built-up edge (BUE) formation in micro-scale machining. Given the higher hardness of SLM Ti6Al4V, characterized by laminar grains, its lower ductility results in reduced plastic flow of the material, thereby mitigating BUE formation. As the cutting process progresses, the adhered micro particles are gradually chipped off the surface, leading to the chipping of the tool surface, as depicted in Figure 3.15c. However, material adhesion results in the enlargement of the edge radius, causing a transition in material removal from shearing to ploughing. Ploughing impedes chip flow over the rake face, redirecting it around the enlarged edge radius. In continuous machining, material ploughing intensifies with increasing adhesion, constraining the material from shearing off as chips. Consequently, adhesion, abrasion, and edge chipping emerge as predominant mechanisms for wrought Ti6Al4V. Conversely, SLM Ti6Al4V displays a larger α colony and partitioning effect, resulting in lower yield stress and diminished resistance, thereby precluding chipping of the tool. The rapid solidification process inherent in SLM may lead to the formation of a more homogeneous microstructure and a more even distribution of grain

angle boundaries. This, in turn, could facilitate smoother material removal and, consequently, contribute to better tool condition.

3.6 Conclusions

In conclusion, this study underscores the superior machinability of SLM Ti6Al4V over wrought Ti6Al4V in micro-milling applications. The experimental investigation revealed notable advantages of SLM Ti6Al4V, including lower surface roughness, reduced tool wear, and smaller burr formation compared to its wrought counterpart. Despite the higher hardness of SLM Ti6Al4V, it exhibited improved surface quality with minimal tool wear and burr heights. These findings underscore the potential of micro-milling as a post-processing technique to enhance the surface quality and form accuracy of AM Ti6Al4V. The key highlights of this research are summarized as follows:

1. Significant tool wear was observed in micro-milling of wrought Ti6Al4V compared to SLM Ti6Al4V, with wear concentrated around the cutting edges.
2. SLM Ti6Al4V demonstrated superior surface roughness relative to wrought Ti6Al4V, achieving a minimum roughness value of 19.21nm compared to 22.31nm for wrought Ti6Al4V, representing a 13.9% improvement in surface quality.
3. Micro-milling of SLM Ti6Al4V yielded more continuous, uniform, and identical chips, while wrought Ti6Al4V produced larger chips with serrated patterns.
4. The microstructure of a material, heavily influenced by the manufacturing method, is crucial in determining machining performance. Detailed examinations of tool wear, considering materials with identical compositions, indicate that SLM Ti6Al4V, characterized by a finer microstructure, shows less tool wear compared to the coarser microstructure of wrought Ti6Al4V. The equiaxed microstructure with β grains in wrought Ti6Al4V becomes unstable under high pressure and temperature, resulting in increased adhesion. In contrast, the finer grain structure and lower ductility of SLM

Ti6Al4V facilitate easier grain shearing, thus reducing tool wear. Wrought Ti6Al4V experiences more extensive built-up edge (BUE) formation due to the beta phase, which leads to greater adhesion and tool wear. SLM Ti6Al4V's laminar grain structure and lower ductility mitigate BUE formation, reducing tool surface chipping. The transition from shearing to ploughing due to material adhesion affects chip flow and increases tool wear in wrought Ti6Al4V. Conversely, SLM Ti6Al4V's homogeneous microstructure and even grain boundary distribution enhance material removal and improve tool condition

Chapter 4

3D Finite Element modeling of micro milling of Ti6Al4V fabricated by Selective laser melting technique

4.1 Introduction

To enhance product performance, minimize weight, and optimize costs, there has been a discernible trend towards miniaturization, resulting in the production of small-scale components. The attainment of precise tolerances and dimensions necessitates the utilization of advanced machining methodologies. Industries such as aerospace, automotive, electronics, and biomedicine are increasingly reliant on micro components [183]. Among the various methodologies for micro-machining, micro- milling has garnered considerable attention due to its ability to fabricate intricate 3D micro components with high aspect ratios across a diverse array of materials including metals, alloys, composites, and ceramics [183, 185]. This methodology holds significant promise for the rapid production of complex parts with exceptional accuracy and precision. Micro-milling, also known as end-milling with microtools featuring diameters less than 500 micrometres, presents multifarious challenges such as compromised surface quality, burr formation, accelerated tool wear, and tool breakage, all attributable to size effects [186, 187]. In micro- milling, the sharpness of the flute edge becomes less crucial due to the size effect, given that the feed per tooth falls within the range of 0.5-5 micrometers, a figure akin to the undeformed chip thickness. An augmented effective rake angle induces elastic-plastic deformations in the workpiece, thus complicating material separation. When the undeformed chip thickness falls below this minimum threshold during tool rotation, chip formation may be impeded. Ploughing and elastic recovery contribute to escalated forces, surface roughness, and tool wear, particularly at lower feed rates [188, 189]. Additionally, to mitigate the premature wear and breakage of micro-mills, meticulous

optimization of factors such as tool geometry, cutting speed, chip load, and depth of cut is imperative [190]. Micro-milling precipitates tool or workpiece deformation owing to cutting forces, thereby engendering disruptive chip formation dynamics, cutting forces, and vibrations, potentially undermining machining stability. Consequently, the accurate prediction of cutting forces under diverse process parameters assumes paramount importance [191]. The aforementioned challenges serve to further exacerbate the complexity of predicting cutting forces. Moreover, the configuration of chips generated during the micro-milling process significantly influences surface quality.

For decades, machining processes have been extensively scrutinized through Finite Element (FE) simulation, offering a multitude of advantages. Foremost among these benefits is the capability of FE analysis to forecast and assess various machining process parameters such as cutting temperature, strain, strain rate, and stress, attributes that pose significant challenges for experimental measurement. Leveraging FE-based process simulation enables efficient and accurate modeling and simulation of intricate machining scenarios, facilitated by advancements in computing power. Consequently, these simulations have emerged as credible alternatives to physical experiments, affording savings in both time and resources expended on analysis while concurrently enhancing process performance. Notably, the utilization of three-dimensional FE simulations has proven instrumental in the development and refinement of cutting tool micro-geometries. Despite these advancements, certain challenges persist in FE process simulation research. Within the realm of 3D modeling strategies and micro process representation, acquiring comprehensive material and friction modelling data, and implementing sophisticated meshing methods to optimize simulation precision and computational efficiency pose considerable challenges [192]. Academic research endeavours are actively addressing these challenges by developing accurate models aimed at unravelling complex dynamics. Furthermore, experimental validations are being conducted to augment

model reliability and robustness. For instance, Ucak et al. [193] conducted a comparative study on the orthogonal micro-cutting process involving additively manufactured Ti6Al4V produced through laser powder bed fusion and wrought Ti6Al4V. To simulate this process, they utilized the experimentally derived Johnson-Cook constitutive model for both wrought and Selective laser melting(SLM) Ti6Al4V, and subsequently validated the simulation results through a series of orthogonal micro-cutting tests focusing on cutting force and maximum chip compression. Similarly, Liu et al. [194] delved into the machining of SLM Ti6Al4V, specifically investigating different laser scanning strategies and building directions. They proposed an enhanced constitutive model based on the Johnson-Cook framework, incorporating activation energy effects. Their research also involved a detailed exploration of the impact of various modified coefficients on flow behavior, revealing significant implications for chip morphology and segmentation dynamics .

Serrated chips, characterized by irregular and jagged segments arising from uneven plastic deformation, are frequently observed during the machining of challenging materials such as Ti6Al4V at high speeds, owing to their notable strength and hardness. The formation of serrated chips stems from intricate interplays among material properties, tool geometry, and cutting parameters. An in-depth investigation into serrated chips is pivotal for refining machining strategies to enhance operational efficiency and prolong tool life, consequently impacting machining outcomes such as surface quality and tool wear [195]. Dejian et al. [196] delved into the evolution of chips, examining morphology features and segment parameters during high-speed machining of SLM Ti6Al4V alloys, which exhibit distinct microstructural, mechanical, and machinability characteristics compared to conventional Ti6Al4V alloys. Employing the Johnson-Cook model, they developed an orthogonal cutting model to explore the influence of physical-mechanical properties on shear localization, a key determinant in serrated chip formation in SLMed Ti6Al4V. In contrast to conventional Ti6Al4V with equiaxed

grains, the distinctive behavior of needle-like martensite α′ in SLM Ti6Al4V led to reduced plastic flow and grain distortion within the adiabatic shear band of the chips. Contemporary micro-milling orthogonal cutting models offer a simplified view of the machining process. However, a deeper understanding of the shearing mechanism necessitates a more comprehensive approach, incorporating a three-dimensional simulation modeling method that factors in tool geometry and surface interaction properties. These aspects, often overlooked by the orthogonal cutting model, can be thoroughly explored through this holistic approach. Y et al. [197] utilized mechanics-based Finite Element (FE) modeling to investigate residual stress in the surface and subsurface regions of Ti6Al4V. Their study aimed to develop a three-dimensional micro-milling model specifically tailored for wrought Ti6Al4V. Employing dynamic explicit time incrementation and temperature-displacement transient analysis, FEM modeling delved into the effects of critical uncut chip thickness, tool edge radius, feed per tooth, and axial depth on cutting forces. The comparison between experimental and simulated results revealed a high degree of agreement, suggesting the validity of the approach. Nevertheless, the limitations of orthogonal cutting models in capturing the intricacies of 3D micro-milling underscore the necessity of employing proper 3D models for accurate and precise prediction of cutting characteristics, particularly in SLMed Ti6Al4V micro-milling scenarios

Research on FE modeling of micro- milling for predicting cutting forces, chip characteristics, and residual stresses in both wrought and additively manufactured Ti6Al4V remains scarce. Existing studies predominantly focus on orthogonal cutting, overlooking the complexities of high-speed micro-milling, such as tool rotation and interactions between the workpiece, cutting tool, and flanking surfaces. Moreover, current models, whether 2D or 3D orthogonal, struggle to accurately capture shearing phenomena. To address these limitations, this study introduces a comprehensive 3D model that incorporates orthogonal cutting

constraints. Figure 1 illustrates the workflow of this study, which utilizes dynamic explicit temperature-displacement models to predict cutting forces and chip morphology. These predictions are then validated against experimental results, contributing to a more thorough understanding of micro- milling processes.

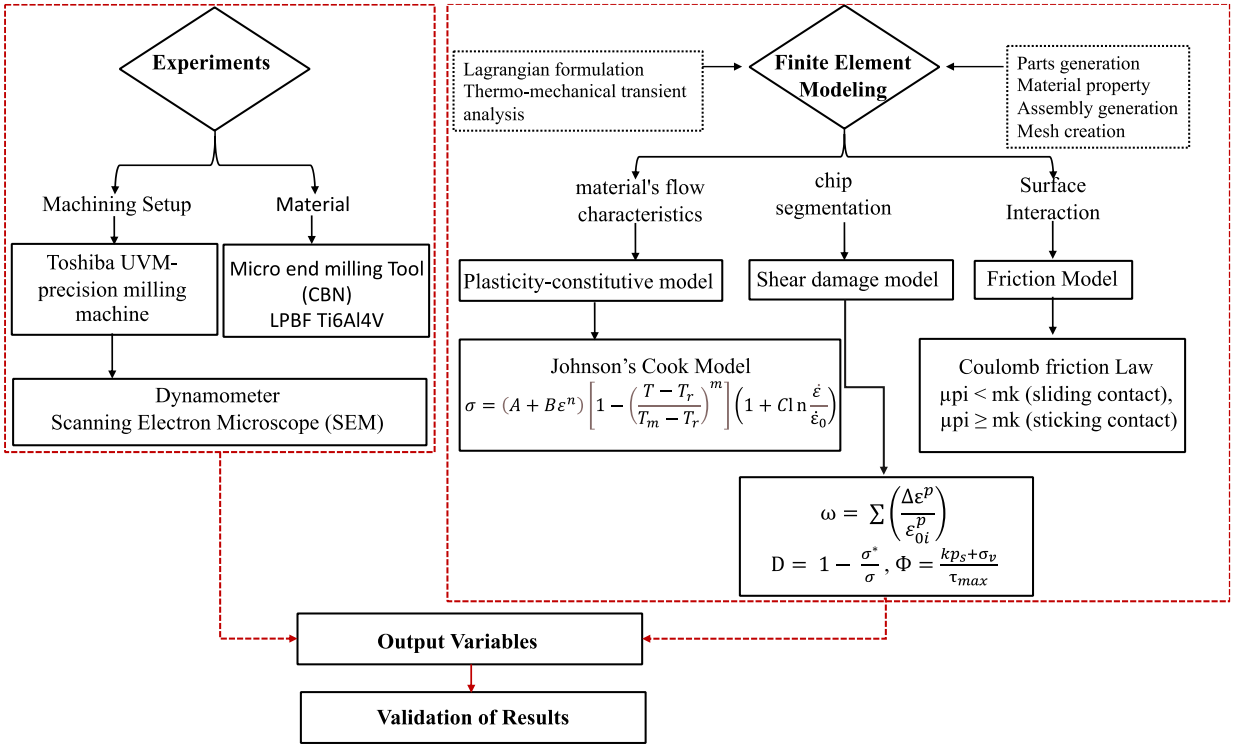

Figure 4. 1 The flow chart of this study

4.2 3D Finite Element Modeling

This investigation employs the ABAQUS software, a widely recognized tool in the realm of finite element analysis, to meticulously replicate and analyze the intricate dynamics of the high-speed micro-milling process associated with additively manufactured Ti6Al4V. Utilizing finite element models, the study aims to intricately capture and simulate the multifaceted aspects inherent in micro-milling operations. By employing the Lagrangian formulation in tandem with a thermo-mechanical transient analysis approach, the research endeavors to achieve a comprehensive understanding of the material response exhibited by SLM Ti-6Al-4V during micro-machining processes. Central to this analysis are fundamental components such as a

plasticity-based constitutive model, a chip segmentation damage model, and a friction model. These components are carefully integrated to encapsulate the intricate interactions occurring during the relative motion between different parts of the machining system. Notably, Johnson-Cook's material law is chosen for its suitability in addressing the influence of elevated strain rates and temperature variations on the flow characteristics of materials during plastic deformation.

4.2.1 Johnson-Cook's material law:

The simulation of material removal during micro machining poses a complex challenge in finite element analysis, given its dependence on numerous factors beyond mere material properties and cutting parameters. To address this intricacy, several methodologies are employed, including adaptive meshing, damage analysis, and failure criteria assessment. Adaptive meshing dynamically optimizes the mesh configuration throughout the chip formation process. In terms of material failure modeling, various approaches exist, among which the Johnson-Cook model, introduced by Johnson and Cook in 1983, stands out as particularly noteworthy [198, 199]. Johnson-Cook's material law stands as a prominent constitutive model within the field of material science and engineering, frequently employed to elucidate the responses of materials when subjected to high strain rates and increased temperatures. Its application extends across various industrial processes, including plastic deformation, machining operations, and impact loading scenarios. By furnishing a mathematical framework, this model enables the characterization of material flow stress, with dependencies on factors such as strain, strain rate, and temperature. Its utility becomes especially evident in dynamic conditions, where conventional models often fall short in capturing the nuanced intricacies of material behavior. This model characterizes flow stress as a function of strain, strain rate, and temperature, as delineated in Equation (5.2) within the present study [200, 201].

$$\sigma = (A + B\varepsilon^{n})\left[1 - \left(\frac{T - T_r}{T_m - T_r}\right)^{m}\right](1 + C\ln\frac{\dot{\varepsilon}}{\dot{\varepsilon}_0}) \quad (1)$$

The equation provided includes symbols representing various parameters: , ε, ε̇, and $\dot{\varepsilon}_0$ denote the equivalent plastic strain, equivalent plastic strain rates, and equivalent reference plastic strain rates, respectively. T signifies the temperature within the cutting zone, while Tm denotes the material's melting temperature, and T_r represents the ambient temperature. The coefficients *A, B, n, m,* and *C* correspond to the yield strength, strain rate, strain hardening index, thermal softening index, and strain rate sensitivities of the material, respectively [200]. The specific numerical values assigned to these constants for SLM Ti 6Al4V are detailed in Table 4.1.

Table 4. 1 Johnson Cook's coefficients for SLM Ti6Al4V *[138, 194, 202, 203]*

A (MPa)	**B (MPa)**	**n**	**m**	**C**	**ε̇₀(/sec)**	**T₀ (°C)**	**Tₘ (°C)**
1157.11	396.79	0.5246	1.35	0.009	1	25	1560

4.2.2 Chip separation criterion:

Chip separation initiates within the primary deformation zone, where high plastic strain and friction facilitate material removal. An assessment of the cutting process can be conducted through chip formation analysis. The elimination of excess material follows a sequential progression, commencing with the concentration of stresses at the interface between the cutting tool and the workpiece. This process persists as the cutting tool undergoes relative movement with respect to the workpiece. The onset of cutting action and subsequent material removal occur at the plastic point of the workpiece, with cutting performance traditionally evaluated through chip morphology analysis. It is noteworthy that each material exhibits distinct chip formation characteristics, thereby influencing the observed chip shape.

The chip formation mechanism, delineated by the evolution of damage within the workpiece, is elucidated through the application of the Johnson-Cook fracture model, as

expressed in Equations (2) and (3). The progression of the damage parameter, denoted as D, commences at zero during the initiation of failure and advances to a critical value of 1, indicating material failure and subsequent exclusion from the simulation. Utilization of the shear damage model facilitates the assessment and elimination of material damage throughout the deformation process. Equations (2) and (3) [197, 200] are employed for the calculation of both the damage initiation parameter, represented by ω, and the damage evaluation parameter, denoted as D.

$$\omega = \sum \left(\frac{\Delta \varepsilon^p}{\varepsilon_{0i}^p} \right) \qquad (2)$$

$$D = 1 - \frac{\sigma^*}{\sigma} \qquad (3)$$

Here ω= damage initiation parameter , $\Delta\varepsilon^p$ =cumulative failure stra*in,* ε_{0i}^p i=initial failure strain, *D*=damage evaluation parameter, σ= undamaged stress and σ^*= damaged stress. The cumulative failure strain ε_{0i}^p used in Equation 2 is a function of shear stress ratio Φ along with strain rate and fracture strain [197]. Shear stress ratio is represented in Equation (4):

$$\Phi = \frac{kp_s + \sigma_v}{\tau_{max}} \qquad (4)$$

In the provided context, *ps* denotes the pressure stress, *k* represents a material parameter, σv stands for Equivalent von Mises stress, and τmax signifies the critical shear stress. Additionally, table 4.2 contains the values utilized for the damage parameters within the model.

Table 4.2 Damage parameters during cutting [23]

Φ	**Reference plastic rate(mm/mm/sec)**	**Fracture strain(mm/mm)**
2	0.01	2

4.2.3 Friction and heat generation:

Friction is an inherent aspect of the cutting process, crucial for its successful execution as it ensures contact between the cutting tool and the workpiece. It stands as one of the most influential parameters in simulating cutting operations and serves as a primary source of heat generation. Given its role in inducing heat and altering material characteristics through inelastic deformation, friction emerges as a critical factor in understanding the cutting process. Consequently, our research primarily focuses on investigating heat generation, material stress, and temperature distribution during cutting. The complexity of friction between the tool-chip contact surfaces significantly impacts machining accuracy and surface integrity. Accurately depicting this interaction is vital for precise metal cutting simulations, necessitating the incorporation of a friction model between the tool and workpiece. Particularly in metal cutting, the interaction between the cutting tool and workpiece involves high stress, strain rates, and temperatures. Zorev (1963) delineated two distinct contact regions at the interface between the cutting tool and the chip: the sliding and sticking regions. The sliding region adheres to Coulomb's law of friction, while in the sticking region, the shear stress is directly proportional to the frictional stress. This relationship can be effectively described using a modified Coulomb friction model [188, 196, 199].

$$\text{If } \mu \times \sigma_n < K_{chip} \text{ Then } \tau_f = \mu \times \sigma_n \quad \text{Sliding region}$$

$$\text{If } \mu \times \sigma_n \geq K_{chip} \text{ Then } \tau_f = K_{chip} \quad \text{Sticking region}$$

Where: μ : friction coefficient, σ_n: normal stress, τ_f: friction stress, m_{Tresca} : Tresca factor, K_{chip}: shear flow stress.

4.2.4 Tool and workpiece interface and Meshing:

The workpiece exhibits elastic-plastic properties and is deformable, characterized by finite element meshes comprising linear tetrahedral elements. In contrast, the cutting tool is

represented by pre-defined linear tetrahedral elements within the software. To accurately determine cutting forces, the cutting tool is treated as a rigid, isothermal body, deviating from an elastic or elastoplastic model. Precision is ensured by designing the tool in CAD software to mirror the geometry of experimental micro- tools, featuring a diameter of 600μm, a 30-degree helix angle, and a cutting-edge radius of 3μm. Analytical integration within tetrahedral coordinates obviates the need for numerical integration when evaluating equations associated with both element types. Employing such elements, three-dimensional finite element models effectively address scenarios involving plastic deformation. The workpiece and cutting tool, depicted in Figure 4.2, are denoted as C3D8RT and 3D4T elements, respectively. A high mesh density in the cutting region guarantees machining precision, while a lower density in surrounding areas enhances computational efficiency. This meticulous mesh distribution enhances machining accuracy and efficiency by facilitating material flow with smaller meshes, yielding consistent outcomes. The workpiece comprises approximately 1.287x106 mesh elements. Conversely, the cutting tool consists of 3.134x105 mesh elements. The simulation framework is configured for dynamic explicit and temp-displacement (temp-disp) processes, owing to the thermal-mechanical dynamics inherent in ultra-precision milling employing micro tools at high velocities.

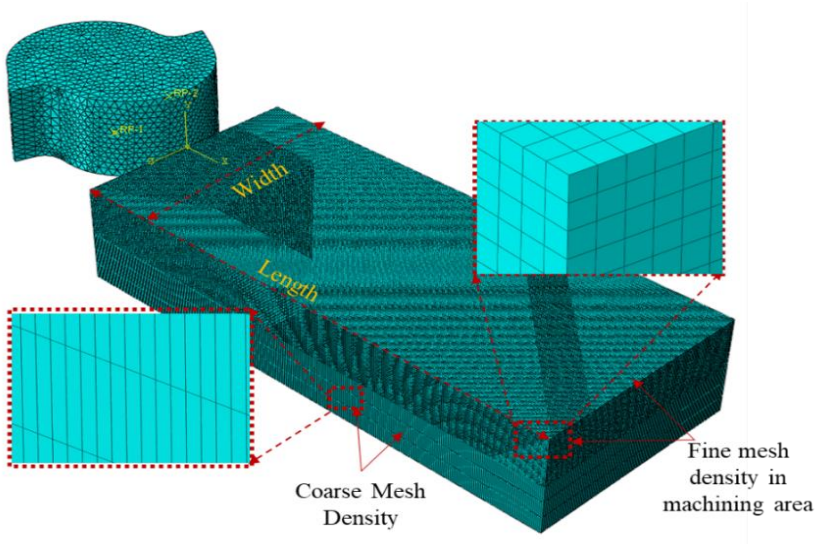

Figure 4.2 Features of simulation with mesh elements.

Conventional micromachining processes are characterized by significant plastic deformation along the shear plane, resulting in intricate nonlinear dynamics. These nonlinearities often lead to challenges related to convergence and computational stability during iterative procedures. To mitigate these issues, an explicit time increment scheme is adopted, which effectively reduces computational expenses and simplifies convergence complexities. Establishing contact between the tool and workpiece involves employing a surface-to-node interaction approach.

4.2.5 Constraints and boundary conditions:

Within the Abaqus tool, mechanical contact identification among assembly instances or regions necessitates explicit specification within the Interaction module. In this interaction scheme, slave body nodes (representing the workpiece) interact with a master body surface (representing the cutting tool). Throughout the cutting operation, this methodology ensures comprehensive tool-workpiece interaction, as depicted in Figure 4.3a.

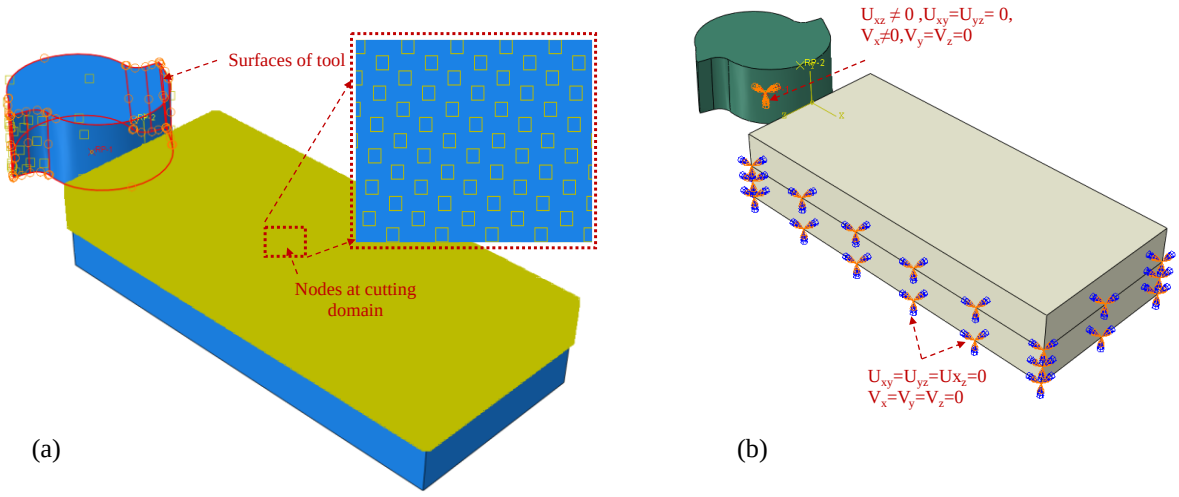

Figure 4. 3 3D-FE model of micro-milling; (a) Surface to node milling; (between tool and workpiece; (b) Boundary conditions on workpiece and cutting tool

The undersides of the workpiece are rigidly fixed in all potential directions, while the cutting tool has the capability to rotate both clockwise and anticlockwise around its axis and to move linearly. Figure 4.3b illustrates all constraints and boundary conditions pertaining to the workpiece and cutting tool. Initially, the temperature is set to match the ambient room temperature. Given the high-speed nature of the cutting process, it is regarded as adiabatic, thus excluding heat exchange through mechanisms of convection and radiation. Thermal transfer dynamics are governed solely by conduction. Thermal contact conductance of 107 $kWm^{-2}K^{-1}$ is established to ensure thermal connectivity at the interface between the tool and workpiece. The ambient temperature remains constant at 20°C, and thermal dissipation from both the workpiece and tool into the surroundings is managed through convection, governed by a coefficient of 0.02 $N\ s^{-1}\ mm^{-1}{\circ}C^{-1}$. Detailed mechanical and thermal properties of the materials used in the finite element simulations are provided in Table 4.3 [187, 204]. In 3D modelling, the element deletion criterion is employed to aid fracture analysis. Upon meeting fracture criteria, elements are assigned a predetermined maximum degradation value. These elements are subsequently removed from the model to prevent significant distortion errors.

Table 4.3 Mechanical and thermal properties of SLM Ti6Al4V and CBN tool [4, 30]

Material Properties	SLM Ti6Al4V	CBN Tool
Density (kg/m3)	4430	15000
Young's modulus (GPa)	0.7412 x T + 113,375	$6.52x10^{5}$
Thermal Conductivity ($W/m^{-1o}C^{-1}$)	7.039 x $e^{0.0011xT}$	100
Thermal expansion ($^{o}C^{-1}$)	3.109 x T + 7.10-^{6}	$5.2X10^{-6}$
Poisson's ratio	0.34	0.22
Heat Capacity $Nmm^{-1o}C^{-1}$	2.24 x $e^{0.0007\ x\ T}$	3.26

4.3 Validation and experiments of micro-milling of AM titanium alloys

Micro-milling experiments were conducted on a five-axis high-precision machine to compare and validate the established finite element model for AM Ti6Al4V using CBN micro-mills. Specimens with dimensions of 25mm x 25mm x 25mm were prepared using Selective laser melting(SLM). The chemical composition of the material is provided in Table 4. 1. The fabricated parts underwent post-heat treatment, including vacuum annealing at 800°C for 3 hours in an inert argon atmosphere, which simplifies the process of enhancing mechanical properties by refining the microstructure of the additively manufactured titanium alloys. The experiments utilized a Toshiba UVM-450C(V2) five-axis high-precision machine, which offers a resolution of 0.01µm on the X, Y, and Z axes. The experimental setup is shown in Figure 4.4. Micro-grooves, 10 mm in length and matching the tool diameter in width, were machined using two-fluted CBN micro-flat end mill cutters with a cutting diameter of 600µm and a cutting length of 1.5mm, provided by Changzhou Easy Joint Imports and Exports Co. Ltd. The morphology of the chips was examined using a scanning electron microscope (SEM) (Hitachi - TM3000) at various magnifications. To ensure a precise depth of cut and remove any oxide layers, the workpiece surface was prepared beforehand using a 2mm diameter two-fluted end mill cutter. During the experiments, cutting forces were measured using a Kistler 9256C1 dynamometer. The detailed experimental setup is illustrated in Figure 4.4.

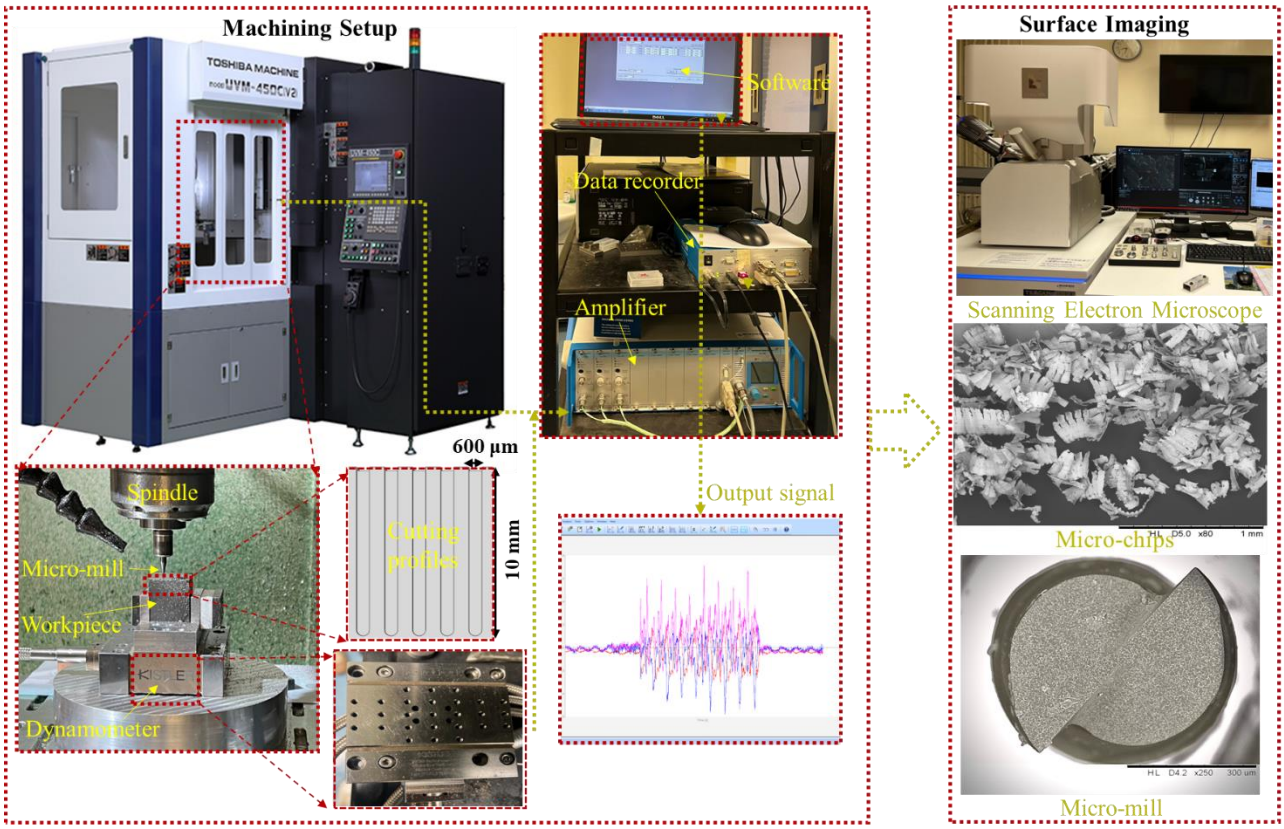

Figure 4. 4 Experimental Setup of micro-milling of SLM Ti6Al4V

4.4 Results and Discussions

4.4.1 Chip Morphology:

A distinct advantage of employing 3D simulations over their 2D counterparts is their enhanced capability to predict chip formation, particularly emphasizing the three-dimensional aspects of chip flow. In conventional 2D models, chip flow is restricted to the X-Y plane, leading to chip accumulation in front of the cutting tool. In contrast, 3D simulations offer a more comprehensive and realistic prediction of chip flow and curling, resulting in a more accurate representation of the machining process. Figure 4.5 illustrates the cutting phenomenon, depicting the path of tool engagement with SLM Ti6Al4V and the resulting micro slot as the CBN tool advances. During micro-milling of SLM Ti6Al4V, three types of phenomena can occur during tool engagement: rubbing, ploughing/extrusion, and shearing [197]. Rubbing and ploughing are observed if the interaction between the SLM workpiece and

the CBN tool is not fully established. Initially, the tool rubs against the workpiece due to insufficient penetration, as shown in the simulation model by Y. et al. As the tool advances, the material removal process transitions into a ploughing/extrusion mechanism, where material elimination occurs mainly through plastic deformation without forming chips. This stage results in the lateral displacement of the workpiece material due to plastic deformation. As the tool progresses further, the machining mechanism shifts to a shearing action, making the effects of rubbing and ploughing negligible. During this stage, material removal or chip formation occurs predominantly through shearing, eliminating lateral material displacement [197]. The dominance of shearing in chip formation during micro-milling is crucial for achieving superior surface quality, precise dimensional accuracy, and reduced tool wear. This is particularly important in the micro-scale machining of SLM Ti6Al4V, where the material hardness is higher compared to wrought Ti6Al4V. The absence of lateral material displacement becomes evident during the generation of micro-grooves, highlighting the minimal influence of rubbing and ploughing actions and confirming the prevalence of the shearing process and consequent chip formation.

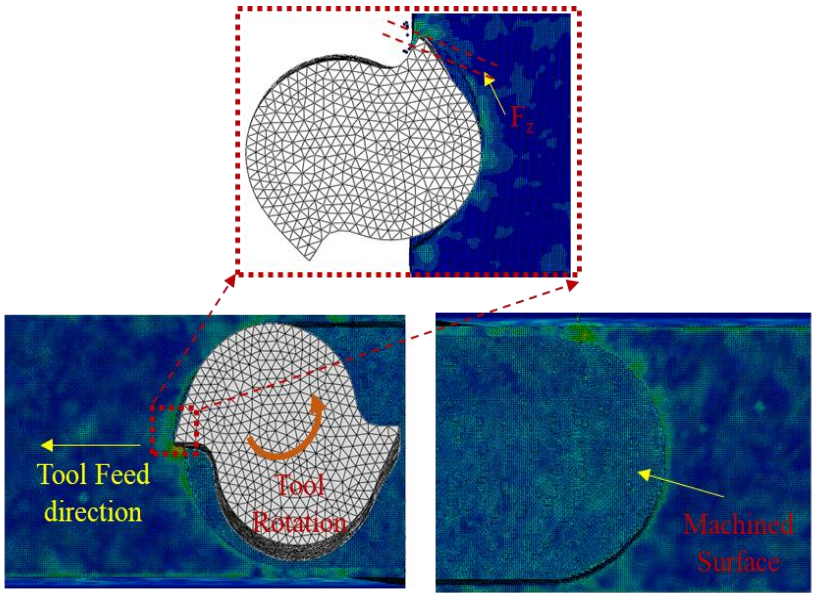

Figure 4. 5 Simulation of micro-milling

Figure 4.6 illustrates the shearing phenomenon during chip formation in the micro-milling of SLM Ti6Al4V, highlighting the distribution of von Mises stress throughout the machining zone. Effective micro-milling shearing necessitates methodical and precise extraction of material layers. The micro-mill cutter compresses the material, causing non-machined sections to protrude from the shear plane. When shear stresses exceed the material's fracture capacity, cracks form at the interface of the cutting edge and the workpiece, leading to material detachment and chip formation. The figure 4.6 shows the resulting micro groove, with no visible side material flow, indicating effective interaction between the workpiece and cutting tool. The shear damage criterion is employed to determine the extent of material damage. Complete material damage is indicated by a combination of red, orange, yellow, and green, while partial damage is represented similarly. The red line in the figure highlights the onset of the damage mechanism near the tooltip and free surface, influenced by loading and compression ahead of the cutting tool. As plastic strain within the element reaches the material's fracture strain, complete material stiffness degradation occurs, and the damage variable reaches unity. This results in the removal of the damaged element near the tooltip, leading to the formation of micro-cracks. These micro-cracks propagate within the shear zone, eventually reaching the chip's free surface, and this recurring mechanism results in the formation of new chips. Yadav et al. [200] described a similar mechanism for the orthogonal model. Our model, however, presents results using an authentic 3D simulation paradigm, demonstrating superior performance compared to previous studies. This enhanced model offers greater flexibility in tool rotation and feed rates.

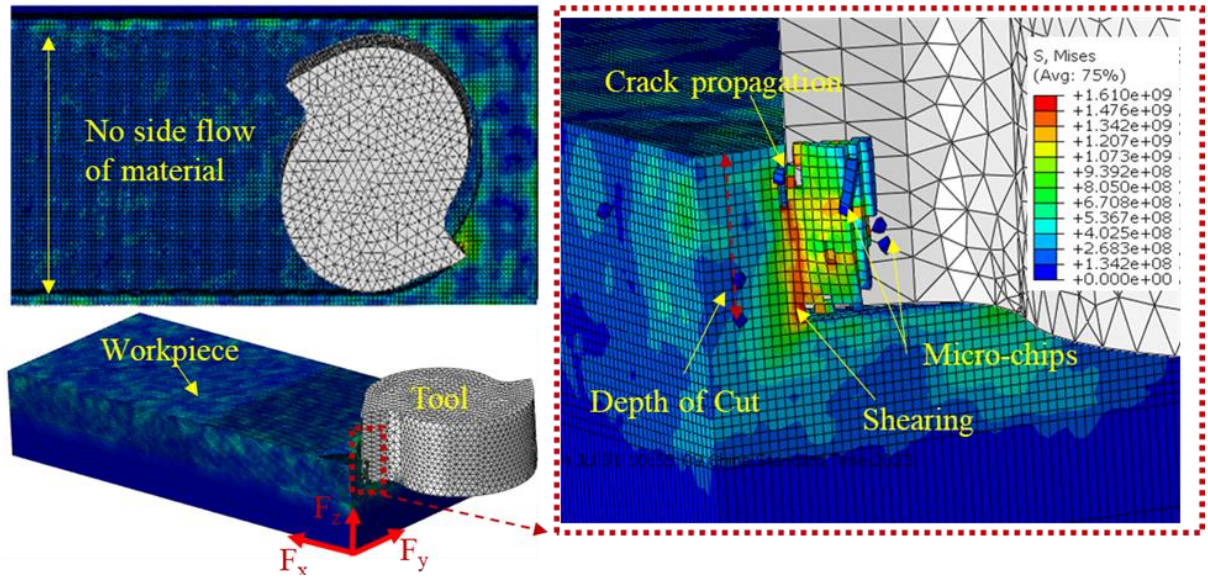

Figure 4. 6 Simulation of chip formation during micro-milling

The characteristics of chips generated during the cutting process are crucial for evaluating micro-machining performance. Chip morphology directly reflects surface quality, tool wear, and cutting forces. Figures 7 and 8 present a comparison between chips produced during the generation of micro grooves in SLM Ti6Al4V through experimentation and those predicted by simulation results. The profiles and morphological characteristics of the chips are remarkably similar in both cases. Two distinct chip types emerge: one characterized by short curls and a lamella structure, and the other by elongated curls with fractured cores and cracked edges. The formation of lamella structures is primarily caused by strain softening, which induces concentrated shearing within the band zone. This behavior is attributed to the poor thermal conductivity of SLM Ti6Al4V, which leads to mechanical strength loss as the temperature increases. Tearing in the central and edge portions of the chips, as seen in Figures 4.7a and 4.7b, results from the non-uniform distribution of strain, creating regions with high and low shear strains. When the depth of cut is increased, the produced chips are wider and exhibit fewer cracks and tears along the center. This improvement is due to the higher

magnitude of shear stress at greater cut depths. Thus, the depth of cut has a direct impact on chip properties.

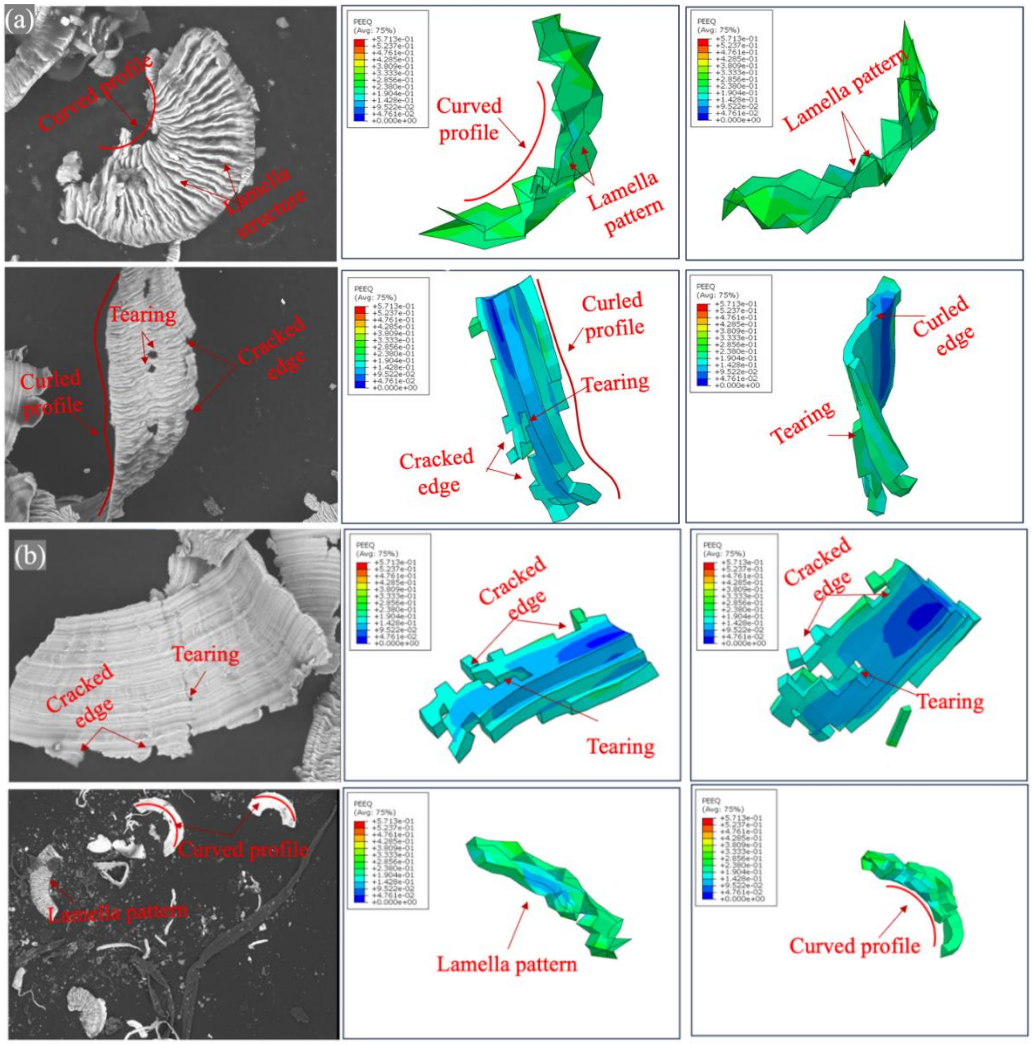

Figure 4. 7 Comparison of experimental and simulation results for Chips morphology under the machining condition (a)60000 rpm, 3µm/flute, 30µm, (b) Machining parameters: 60000 rpm, 3µm/flute, 45µm

The chip profiles and morphologies obtained from simulations closely match those observed in experimental results. The next stage involved simulations to investigate the effect of tool rotational speed on chip morphology. This further exploration aims to enhance the understanding of how different machining parameters influence chip formation and overall machining performance.

Figure 4.8a displays the chips obtained under a specific parameter configuration, while Figure 4.8b shows the results at a higher rotational speed. Notably, the simulation results closely resemble the experimental findings, especially in terms of chip type and characteristics. During the micro-milling of SLM Ti6Al4V, a consistent chip formation pattern is observed: the chips are elongated, curled, and narrow with distinct edge patterns. At higher rotational speeds, increased cutting temperatures lead to greater plastic flow, resulting in slightly longer chips compared to those produced at lower RPM settings. Additionally, the higher temperatures cause chip welding, leading to the formation of microchip clusters. This clustering is particularly evident at elevated speeds. The close alignment between experimental and simulation results validates the accuracy and reliability of our finite element modeling approach, confirming its effectiveness in predicting chip morphology under various machining conditions.

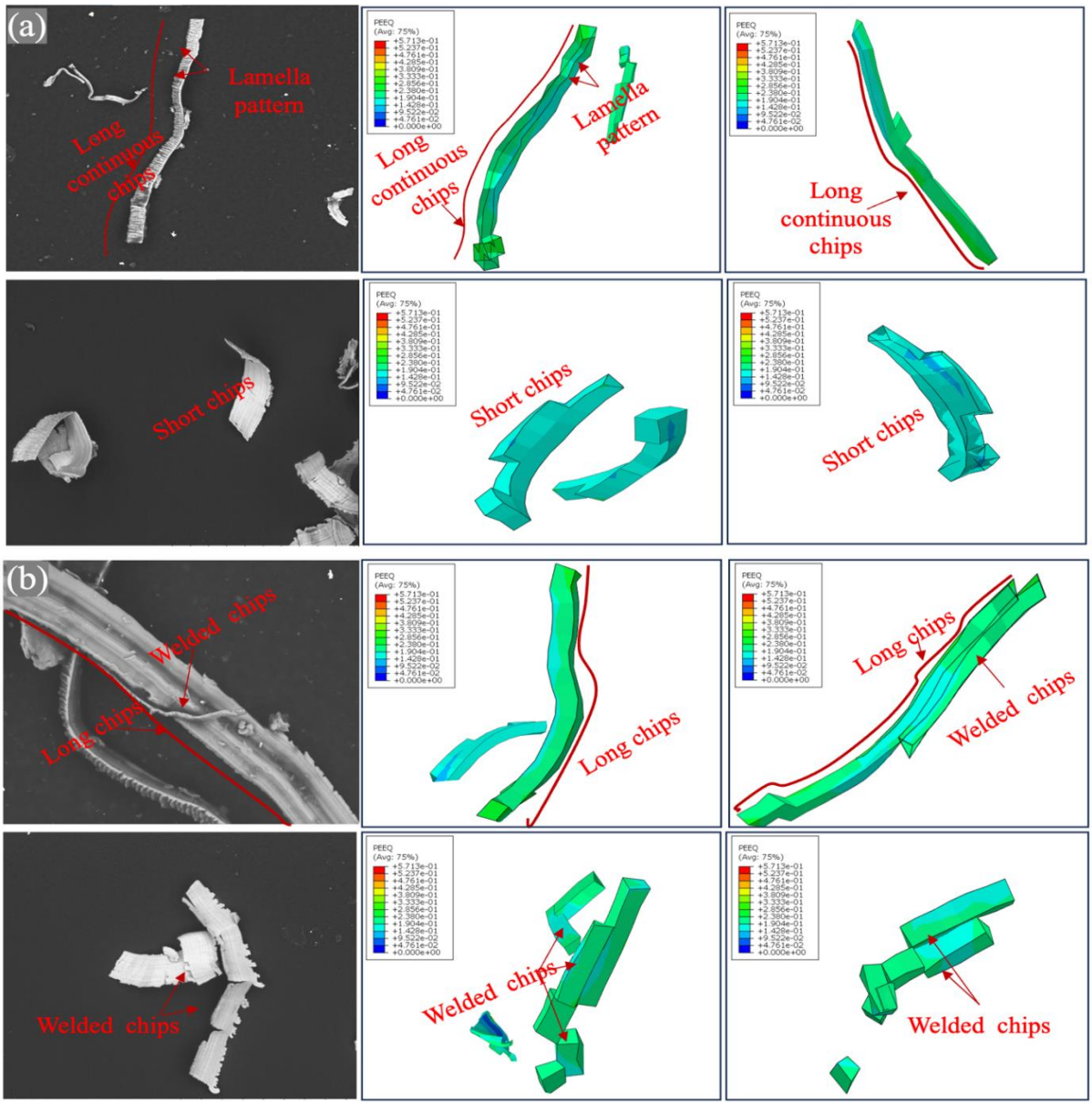

Figure 4. 8 Comparison of experimental and simulation results for Chips morphology under machining conditions, (a) 65000 rpm, 3µm/flute, 20µm, (b) Machining parameters: 80000 rpm, 3µm/flute, 20µm

4.4.2 Cutting forces:

SLM Ti6Al4V exhibits significant improvements in hardness, yield strength, and ultimate tensile strength compared to the conventional Ti6Al4V alloy. These enhancements result in noticeable changes in cutting force patterns, making it a valuable area for further investigation. In micro-milling processes, forces are exerted along the X, Y, and Z axes, denoted as Fx, Fy, and Fz, respectively. These forces are influenced by several factors, including the interaction between the cutting tool and the workpiece material, as well as specific milling parameters. Fx

primarily represents the cutting force parallel to the tool's movement, facilitating material removal. Fy signifies the force perpendicular to the tool's movement, arising from the shearing process between the tool and the workpiece material. Fz, the vertical force, acts normal to the workpiece surface, and its magnitude is influenced by factors such as tool geometry, feed rate, cutting depth, and material properties. Figure 4.9 provides a schematic representation of the micro-milling process, illustrating the corresponding forces. These distinct force patterns are critical for understanding the mechanics of micro-milling SLM Ti6Al4V, contributing to optimizing machining parameters and improving overall process efficiency. The advanced mechanical properties of SLM Ti6Al4V, compared to traditional Ti6Al4V, necessitate a deeper exploration of these forces to fully leverage the material's potential in precision machining applications.

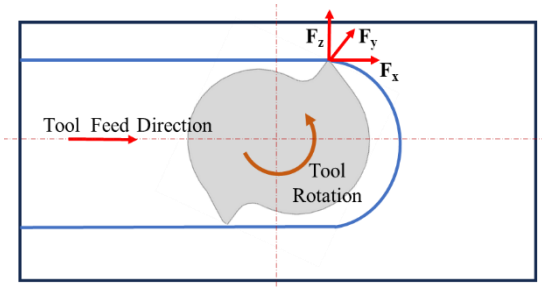

Figure 4. 9 schematic-micro milling process

Figures 4.10 and 4.11 present a comparison of cutting forces from experiments and simulations. The cutting forces recorded during the micro-milling of SLM Ti6Al4V were juxtaposed with the predictive cutting forces obtained from the 3D simulation model. During the experiments, cutting forces oscillated due to tool and workpiece vibrations. To maintain stability, the experimental results were filtered to smooth out peaks and fluctuations. A close examination of both charts reveals a satisfying coherence between the numerical and experimental cutting forces. Specifically, Figure 4.10 compares the forces (Fx, Fy, Fz) and the impact of cut depth on these forces during SLM Ti6Al4V micro-milling. The experimental and numerical results

exhibit a high degree of similarity. As the depth of cut increased, there was a corresponding increase in the average cutting forces. The analysis indicates that increasing the milling depth results in a greater amount of material being removed due to the larger shear area. This leads to increased internal friction between the tool and the cutting layer, as well as higher cutting resistance within the SLM Ti6Al4V workpiece material. Consequently, there is a positive relationship between cutting force, milling depth, and the associated parameters . Additionally, an increase in depth causes chip loading, which further amplifies the cutting force.

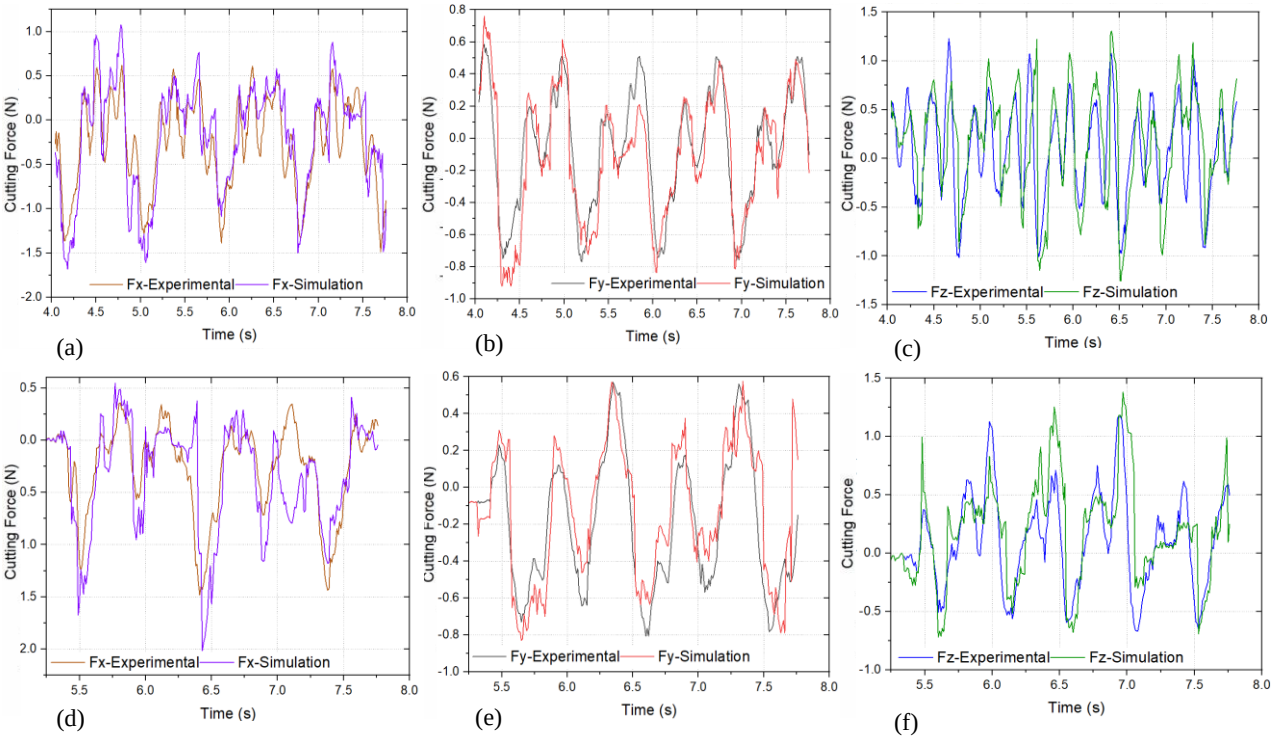

Figure 4. 10 Comparison of cutting force under the machining condition 60000 rpm, 3µm/flute, 45µm (a) x-axis , (b) y-axis and (c) z-axis; under the machining condition 60000 rpm, 3µm/flute, 30µm (d) x-axis, (e) y-axis and (f) z-axis

Figure 4.11 illustrates the effect of tool rotational speed on cutting forces during the micro-milling of SLM Ti6Al4V. The cutting forces increase as the rotational speed rises while maintaining the same depth of cut. The analysis reveals that increasing spindle speed leads to higher friction between the tool and the chip, thereby gradually increasing the material removal

rate per unit time.When comparing different spindle speeds, the cutting forces along the Y and Z axes show a significant increase at higher speeds. In contrast, due to the limited heat generation inherent in micro-milling, the cutting force along the X axis remains relatively stable as milling speed increases. Additionally, the micro-milling process of SLM Ti6Al4V encourages substantial plastic deformation and the accumulation of high-hardness chips at the tool edge when the tool rake face extrudes the workpiece material [205].The accuracy of friction models is critical for cutting simulations, as contact conditions directly impact the results [186]. The data demonstrate a high degree of convergence between the experimental and numerical values, reflecting that fine interaction conditions and an effective friction model were established during the simulations. Both experimental and simulation graphs align well, confirming the reliability of the simulation in predicting cutting forces under varying rotational speeds.

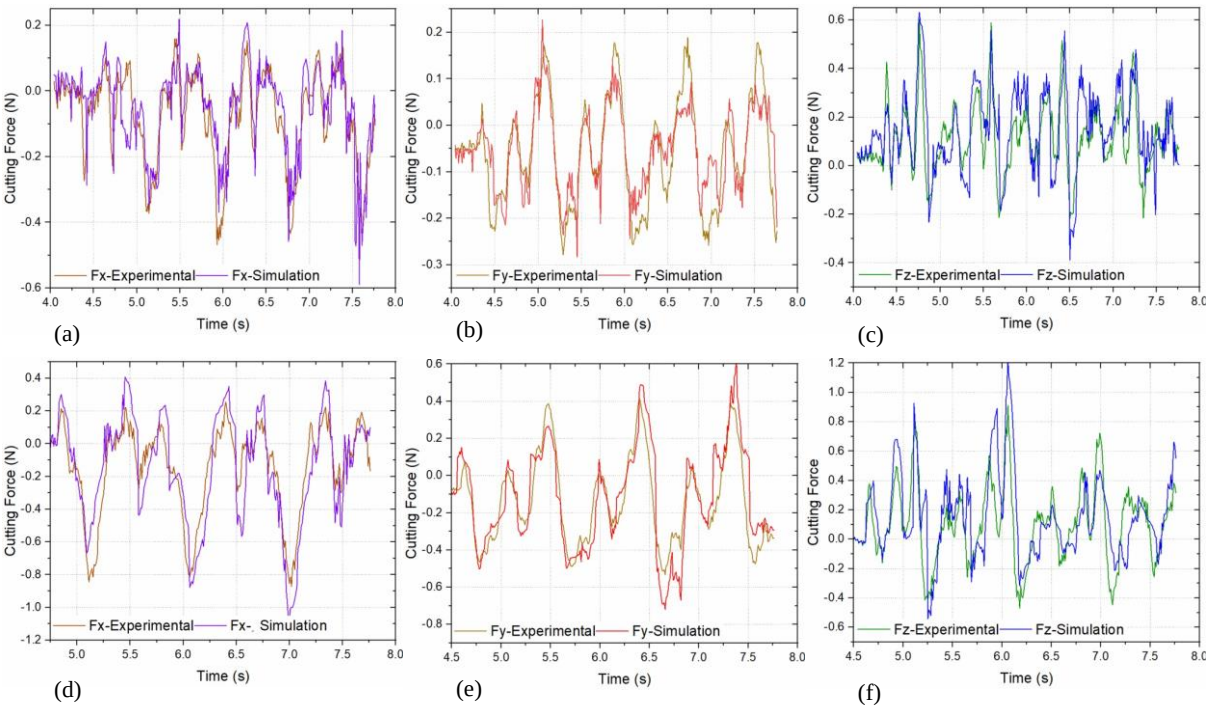

Figure 4. 11 Comparison of cutting forces under the machining condition 65000 rpm, 3μm/flute, 20μm (a) x-axis, (b) y-axis and (c) z-axis; under the machining condition 80000 rpm, 3μm/flute, 20μm (d) x axis, (e) y-axis and (f) z-axis

Cutting forces increase proportionally with the number of cutter rotations. This rise can be attributed to heightened tool wear and edge rounding caused by the high cutting temperatures encountered in the micro- milling of SLM Ti-6Al-4V alloy. Higher cutting speeds lead to increased deformation rates, which in turn amplify mechanical stresses due to strain hardening effects. Additionally, the elevated cutting speeds result in higher cutting temperatures, inducing thermal softening effects in the SLM Ti6Al4V alloy, which would typically reduce cutting forces. However, this study observed an opposing trend where cutting forces increased in tandem with cutting speed. The analysis suggests that the impact of strain hardening surpassed that of thermal softening. As a result, despite the thermal softening that might reduce cutting force, the strain hardening effect dominated, leading to an overall increase in cutting forces as cutting speed increased.

4.4.3 Surface Characterizations:

Surface quality in micro-milling is influenced by a variety of factors, including machining parameters, the materials of both the workpiece and tool, tool geometry, lubrication, and machining vibrations [111, 161]. Among these, machining parameters such as tool rotation, depth of cut, and feed rate play a crucial role in determining the surface quality of micro-milled parts. These parameters intricately control the milling process, directly affecting the resultant surface finish, precision, and overall quality of the machined components. Optimizing these machining parameters can significantly enhance surface characteristics, providing finer control and improvements in the final product's surface quality. This study specifically investigated the effects of tool rotation and depth of cut on surface quality through both finite element analysis and experimental methods. In both approaches, surface topography was analyzed to evaluate the resulting surface conditions, demonstrating the critical impact of these parameters on

micro-milling outcomes. The surface topologies produced by SLM Ti6Al4V micro-milling and finite element modeling (FEM) were compared, revealing a consistent presence of feed marks across all investigated machining conditions. Oliaei and Karpat [206] explored the formation of these marks in Ti6Al4V micro-milling, demonstrating the complex interplay between surface quality and machining parameters such as feed rate, built-up edge (BUE), and cutting speed. The increased occurrence of feed marks in SLM-manufactured Ti6Al4V primarily results from tool edge adherence to the surface, leading to the attachment of material fragments. Additionally, Wang et al. [172] attributed the formation of feed marks to the interaction between the milled surface and BUE. Subsequent machining processes increase adhesion and plowing along the tool flank face, enhancing friction at the tool-workpiece contact area, and significantly contributing to the prevalence of feed marks during Ti6Al4V micro-milling.

Figure 4.12 compares the machined surfaces between FEM and experimental results at 60,000 rpm, 3 µm/flute, and 30 µm depth of cut. The figure 4.12 a&b show good surface quality with consistent feed marks in both experimental and FEM outcomes. However, Figures 4.12c and 4.12d reveal noticeable defects alongside feed marks when machined at 60,000 rpm, 3 µm/flute, and 45 µm depth of cut. These defects could be attributed to scratches on the cross-sectional and machined surfaces caused by welded chip segments. These segments and micro-particles adhere to the tool's flank face due to the friction and heat generated during cutting.

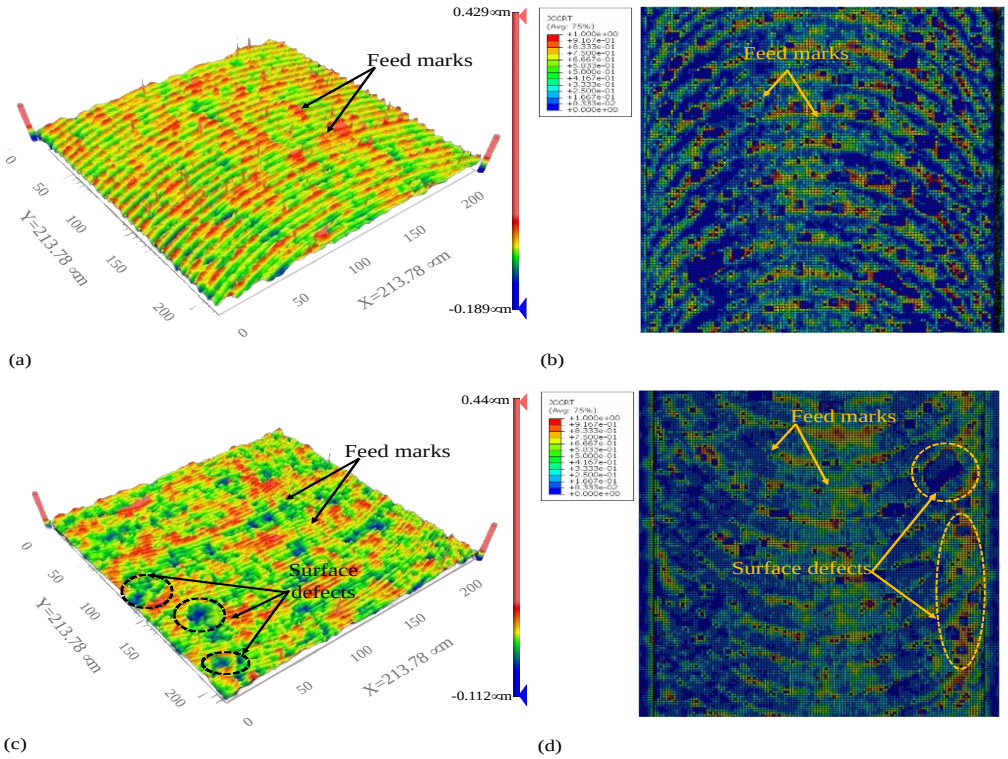

Figure 4. 12 Surface Topography of machined surface under the machining condition 60000 rpm, 3µm/flute, 30µm (a) Experimental (b) Simulation; 60000 rpm, 3µm/flute, 45µm (c) Experimental (d) Simulation

The chemical reactivity of SLM Ti6Al4V at elevated temperatures enhances material adhesion on the machined surface. Increasing the depth of cut leads to greater material removal, which amplifies cutting forces and potentially increases the cutting edge radius. This promotes plowing and induces defects on the machined surface. During tool rotation, the micro-chips produced disperse in various directions. These chips, along with built-up edge (BUE) formations, significantly contribute to surface degradation and the appearance of feed marks. Additionally, as tools wear out, surface quality deteriorates further. Tool rotation substantially influences the surface quality of micro-milled components.

Figure 4.13 compares the surface topographies between experimental and FEM results under high tool rotational speed conditions. Tool marks are consistently present in both sets of conditions, exhibiting a uniform pattern throughout. However, surface defects become more pronounced at higher rotational speeds (80,000 rpm). Defects are particularly noticeable on the

left sides of slots, representing the up-milling side. These defects primarily arise from phenomena such as BUE, adherence of micro-particles to the tool surface, and the plowing mechanism. Increased heat production at higher speeds promotes greater adhesion of micro-particles and chips onto the SLM Ti6Al4V surface and tool surface, thereby increasing BUE formation. Furthermore, surface quality degradation at higher speeds can be attributed to increased frictional heat generation during the rubbing action between the tool flank and the freshly machined surface.Figure 4.13 also highlights differences in surface quality between the slot edges, which are more pronounced on the up-milling sides, and the slot center. This variation indicates irregularities in the cutting process, particularly in areas with critical chip depth. When chip thickness falls below the critical value, especially at the beginning and end of the cut, a plowing effect occurs, indicating a sliding mechanism in the cutting process. Additionally, at higher speeds, the abrasion and chipping of the cutting edge emphasize the dominance of plowing over shearing. Consequently, the material forms chips elastically under the plowing action, resulting in a rougher surface and lower overall surface quality, as illustrated in Figure 4.13.According to Hojati et al. [104], the high ductility and hardness of SLM Ti6Al4V cause material wrapping around the cutting edge, further deteriorating surface quality. Moreover, higher rotational speeds increase cutting forces, accelerating the wear of micro-mill cutting edges and promoting material plowing towards the up-milling sides, ultimately contributing to the formation of a poor surface. Therefore, depth of cut and cutting rotation are critical factors in achieving high surface quality.

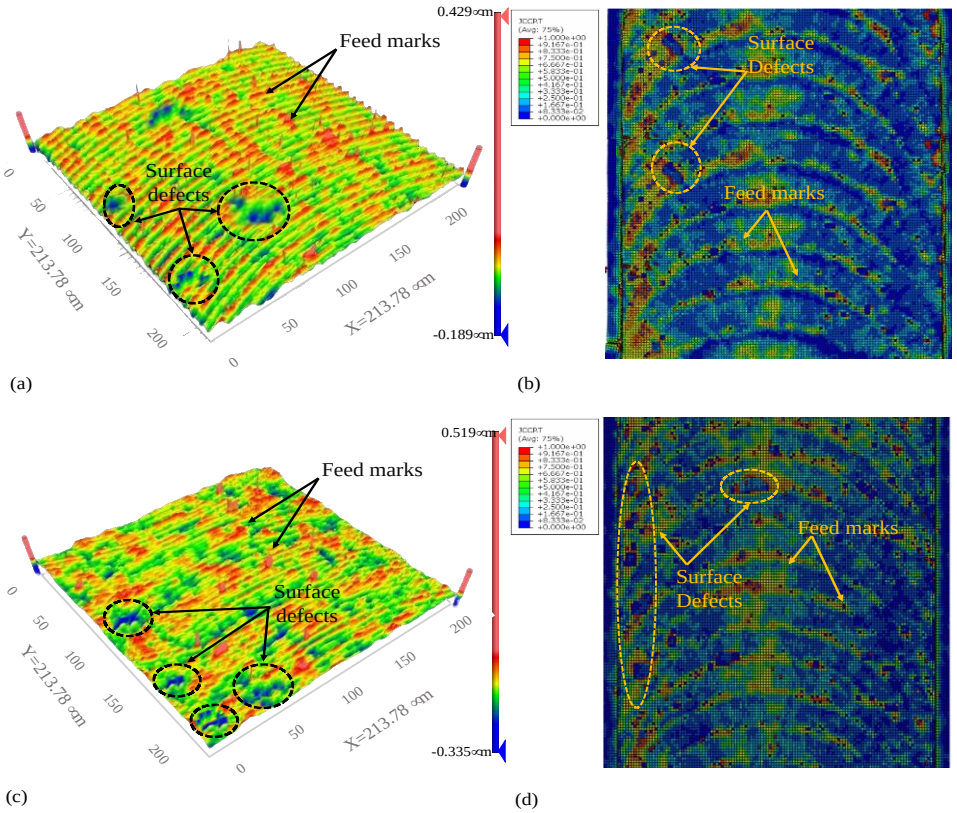

Figure 4. 13 Surface Topography; 65000 rpm, 3µm/flute, 20µm (a) Experimental (b) Simulation; 80000 rpm, 3µm/flute, 20µm. (c) Experimental (d) Simulation

4.5 Conclusion:

In conclusion, this study addresses the limitations of existing finite element (FE) models in predicting cutting forces and chip characteristics during the micro- milling of additively manufactured (AM) Ti6Al4V. Previous models were limited to orthogonal cutting and oversimplified the high-speed micro-milling process by neglecting tool rotation and the detailed interaction between the workpiece and cutting tool. Therefore, this study presents a comprehensive 3D FE model that accurately simulates shearing and orthogonal cutting processes. The experimental and simulation results for cutting forces and chip morphology matched well, validating the model's accuracy and reliability. The study also examined the influences of depth of cut and spindle speed on cutting forces. The highlights of this study are:

1- Cutting Phenomenon Representation: The cutting phenomenon observed in this model accurately represents the actual process of SLM Ti6Al4V micro- milling, particularly

the dominance of shearing. The interaction between the workpiece and the cutting tool, combined with tool rotation, results in pure shearing, effectively suppressing slipping, ploughing, and side flow of material.

2- Chip Morphology: At low depths of cut, two types of chips were generated: short curls with a lamella structure and elongated curls with fractured cores and cracked edges. As the depth of cut increased, wider chips with reduced cracking and tearing were produced due to greater shear magnitude. At high rotational speeds and reduced depths of cut, a consistent chip formation pattern emerged, characterized by elongated shapes, curled surfaces, and distinct edge patterns.
3- Cutting Force Analysis: The FEM model demonstrates alignment with the experimental results in chip formation, highlighting the relationship between cutting force, milling depth, and other parameters. Increasing the tool rotational speed while maintaining the same depth of cut leads to higher cutting forces, attributed to increased friction between the tool and the chip, resulting in a faster material removal rate.
4- Surface Quality: The comparison between the FEM model and experimental results shows substantial agreement in surface quality. Surface defects and degradation are significantly influenced by factors such as tool rotation speed, depth of cut, and material properties. The material's ductility and hardness also contribute to surface quality degradation. Therefore, careful consideration of these factors is essential for achieving high-quality surfaces in micro-milling processes.

Overall, this study provides a robust framework for understanding and improving the micro-milling process of SLM Ti6Al4V, paving the way for better prediction and control of cutting forces, chip formation, and surface quality. It is worth highlighting that this model has the potential to be generalized for other material systems in micro-milling. While each material system exhibits unique thermal, mechanical, and microstructural behaviors such as variations

in thermal conductivity, melting points, tensile strength, hardness, and ductility, these differences can significantly influence defect formation, microstructure evolution, and overall mechanical performance. The interactions, contact conditions, and boundary conditions in the model have been meticulously designed to ensure adaptability to other material systems, provided the necessary material characteristics are known. This flexibility allows the model to account for material-specific properties while maintaining its predictive accuracy. Additionally, the model is robust enough to accommodate tools with different geometries, offering reliable approximations for various tool designs. This adaptability further enhances the model's utility in diverse applications, making it a valuable tool for optimizing micro-milling processes across a wide range of materials and configurations.

Chapter 5: Magnetic field assisted micro-milling for improving machinability of selective laser melted titanium alloy

5.1 Introduction

Ultra-precision machining (UPM), a cutting-edge advancement in manufacturing following conventional methods, is pivotal for producing high-end optical products with nanometric features. The recent integration of magnetic manipulation techniques in ultra-precision machining has demonstrated significant enhancements in various aspects of the machining process[207, 208]. A strong magnetic field applied around the cutting zone can positively influence the process by improving the optical characteristics of the machined surface, optimizing machining conditions, and refining machining factors. Key improvements include damping passive vibrations, enhancing the material's thermal conductivity, and reducing tool wear. Magnetic field assistance has also proven beneficial in finishing procedures and processes such as micro-EDM, electro-discharge machining (EDM), and electrochemical discharge machining (ECDM), by improving surface finish quality and reducing tool wear [207-209]. Ti-6Al-4V is renowned for its better tensile strength, and corrosion resistance, making it versatile across various industry sectors. However, all titanium alloys exhibit poor thermal conductivity, complicating ultra-precision machining and resulting in poor machinability and relatively low-quality surface finishes. The challenges in ultra-precision machining of titanium alloys include high cutting temperatures, significant tool degradation, short tool life cycle, and suboptimal surface quality. These difficulties stem from titanium's tendency to sustain work hardening due to its lower heat conductivity and high cutting temperatures, especially during diamond turning [209-211] .While titanium(Ti6Al4V) has weaker magnetic characteristics as compared to other ferromagnetic materials, it still responds to magnetic fields. With a susceptibility of 14.6 ppm, titanium exhibits positive

paramagnetic behaviour, meaning its magnetic moments align with an externally applied magnetic field during magnetic field-assisted ultra-precision machining [207].

In purely mechanical ultra precision (SPDT) of Ti-6Al-4V, an average surface roughness above 30nm is typically achieved, which is relatively higher [208]. The-application of magnetic field assistance in ultra-precision SPDT is a relatively new area in-advanced manufacturing technologies. Recently, a few experimental studies have been conducted to evaluate the effects of-using magnetic field assistance with a magnetic flux density of 0.01 and 0.02 during ultra-precision SPDT of Ti-6Al-4V [209, 210] The results of these investigations indicate that increasing the strength of the magnetic field can positively impact machining conditions. In addition to these studies, it has been reported that applying a magnetic field during single-point diamond turning (SPDT) can facilitate dry machining of titanium alloys, significantly reducing tool wear compared to conventional methods [205, 211]. This technique has demonstrated promising improvements in machining parameters, turning conditions, and optical surface generation mechanisms. Despite these positive outcomes, the magnetic manipulation technique is still emerging, with limited studies exploring its effects during SPDT. Consequently, the full impact of magnetic assistance on SPDT remains not entirely understood.

5.2 Influence of magnetic field on thermal conductivity

The influence of magnetic fields on material properties, particularly thermal conductivity, is well-documented in materials science [216, 217]. This effect is notable across various materials, including those containing ferroparticles, magnetic particles, ferrometals, or thin films of ferrofluids, where exposure to a magnetic field causes ferroparticles to realign, enhancing thermal conduction [218-220]. Without a magnetic field, ferroparticles aggregate due to van der Waals forces and dipole-dipole interactions, resulting in an irregular distribution [221, 222]. A magnetic field shifts this balance, prioritizing magnetic dipolar energy over

thermal energy, causing ferroparticles to align in response to the field due to their positive magnetic susceptibility. This alignment forms conductive pathways that significantly enhance heat transfer [223, 224]. In the absence of a magnetic field, magnetic particles exhibit random orientations and Brownian motion, often described by a dimensionless Langevin number less than 1. The introduction of a magnetic field intensifies magnetic dipole interactions, aligning particles parallel to the field direction and forming chain-like structures that greatly improve thermal conductivity [225]. Aligned particles act as direct conduits for heat transfer, with chain lengths correlating to magnetic field strength. This phenomenon has been explained in figure 5.1 [226]. Higher magnetic field intensities align more particles in the field direction [222]. Similarly, magnetic fields influence paramagnetic particles, which typically show adhesive properties due to van der Waals forces and dipole-dipole interactions in the absence of a magnetic field. When a magnetic field is applied, these particles' inherent dipole moments align with the field, significantly altering material properties [220]. Building on these findings, magnetic field-induced particle alignment shows promise for enhancing thermal conductivity during titanium alloy machining. Titanium alloys, with a magnetic susceptibility of 14.6 ppm, are paramagnetic and respond to magnetic fields [35]. As these alloys melt during machining, suspended paramagnetic particles align with the magnetic field, forming conductive pathways that increase thermal conductivity [227, 228].

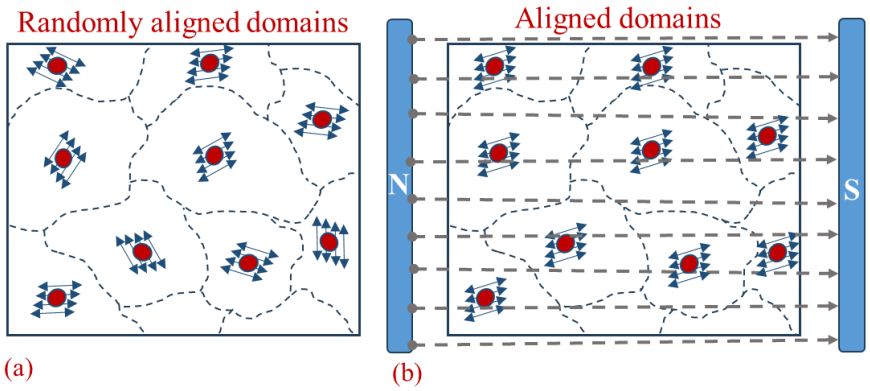

Figure 5. 1Magnetic domains of ferromagnetic materials in the absence (a) and presence (b) of an applied magnetic field

5.3 Magnetic field assisted micro machining of additively manufactured Ti6Al4V

The application of a magnetic field in ultra-precision machining has emerged as a promising technique to enhance machining performance and surface quality, particularly for challenging materials like Ti6Al4V. Yip and To [220] employed a magnetic field during single point diamond turning (SPDT) to mitigate the material swelling effect on the machined surface of Ti6Al4V, finding that the magnetic field significantly improved material recovery compared to setups without a magnetic field. Similarly, Khalil et al. [71] utilized a magnetic field to enhance the thermal conductivity of Ti6Al4V during micro turning, aiming to improve machinability and extend tool life. They developed a Finite Element Model using ABAQUS software to simulate micro-machining, analyzing the impact of the magnetic field on surface morphology and tool life due to improved thermal conductivity. The results showed a substantial increase in tool life and a significant improvement in machined surface quality, with an increase of over 60%, demonstrating the feasibility of sustainable diamond machining facilitated by a magnetic field. Additionally, Yip and To [229]explored the use of a magnetic field in SPDT to enhance material removal rate and surface quality when machining titanium alloys. This method aimed to achieve improvements without requiring complex equipment or additional resources. The magnetic field improved surface quality and extended diamond tool life, particularly at higher material removal rates. The sustainability assessment, measured using the Product Sustainability Index, showed that components machined with a magnetic field had an index 2.39 times higher than those machined with conventional SPDT, indicating significant advancements in product sustainability through this technology. In addition Shahrokh Hatefi* and Khaled Abou-El-Hossein [207] employed Magnetic field assistance in the single point diamond turning (SPDT) of Ti-6Al-4V alloy. The results indicated that this technique substantially enhance machining conditions and the quality of optical surface generation. Specifically, the use of magnetic field assistance with air coolant improves the

surface finish quality by 62.5% compared to non-magnetic, purely mechanical SPDT under dry cutting conditions. This passive, environmentally friendly machining technique promotes green manufacturing and clean production in ultra-precision SPDT applications.

By leveraging the magnetic field's ability to align ferroparticles and improve thermal conduction, this innovative approach not only enhances machinability but also contributes to the sustainability of the manufacturing process, as evidenced by substantial improvements in the Product Sustainability Index. The integration of magnetic fields into ultra-precision machining thus represents a significant advancement in manufacturing technology, offering a viable solution for achieving higher precision and efficiency in the machining of titanium alloys.

5.4 Magnetic field assisted micro milling of additively manufactured Ti6Al4V

The well-established theories on the impact of magnetic fields on upm, along with previous research, provide a solid foundation for investigating the specific effects of a magnetic field on the micro-milling process of Ti6Al4V fabricated by selective laser melting (SLM). This study conducts a comparative analysis, micro-milling SLM Ti6Al4V in the presence of a magnetic field using CBN tools, and then comparing the results to those obtained without the magnetic field. Additionally, the study explores the effect of depth of cut on micro-milling quality. Micro-milling, a dynamic material removal process, transitions from ploughing to shearing during tool rotation, impacting the machined surface quality. Unlike current practices that primarily focus on the central aspects of the milled slot for surface roughness assessments, this study meticulously examines the transverse distribution of surface roughness along the slot. This comprehensive approach aims to provide valuable insights into the micro-milling of SLM Ti6Al4V.

5.5 Development of the magnetic field assisted micro milling Setup

Enhancing the thermal conductivity of the workpiece material can significantly improve SPDT outcomes by lowering cutting temperatures and improving surface finish quality. Applying a magnetic field during SPDT of ferromagnetic and paramagnetic materials positively influences particle interactions. In purely mechanical SPDT, van der Waals' forces and dipole-dipole interactions cause paramagnetic particles to aggregate, reducing thermal conductivity. Titanium alloys, with a susceptibility of 14.6 ppm, benefit from magnetic fields, as these fields align paramagnetic particles with their direction, reducing dipole-dipole interactions and enhancing thermal conductivity [207].

Table 5. 1: Composition of SLM Ti6Al4V

Element	**Ti**	**Al**	**V**	**Fe**	**C**	**O**	**N**	**H**
Percentage Composition	Balance	6.01	4.08	0.042	0.006	0.097	0.005	0.003

To investigate the effect of a magnetic field the experiments were conducted using a Toshiba UVM-450C(V2) five-axis high-precision machine, which features a resolution of 0.01 μm for the X, Y, and Z axes. The experimental setup is depicted in Figure 5.1. To study the effect of a magnetic field, permanent magnets were employed in some experiments, as illustrated in Figure 5.1b, while comparative tests without a magnetic field were performed on the setup shown in Figure 5.1c. To establish a unique micro end milling platform assisted by a non-conventional magnetic field, a robust magnetic field with a precisely controlled flux density was generated. This involved positioning two powerful magnets strategically at the sides of the workpiece, as illustrated in Figure 5.1. Each magnet generates a magnetic field within the surrounding environment, with the intensity of the magnetic flux density increasing as the magnets approach each other. The magnetic flux density at the cutting zone can be accurately measured using a flux meter. For the milling operations, two-fluted CBN micro-flat end mill cutters (manufactured by Changzhou Easy Joint Imports and Exports Co. Ltd) with a diameter

of 600 µm and a length of 1.5 mm were used. The cross-section of the tool was examined with a scanning electron microscope (SEM, Hitachi TM3000) at various magnifications, and the images are provided in Figure 5.2 d. To ensure consistency in the experimental conditions, a new tool was utilized for each sample. Micro-grooves, each 10 mm in length and equal to the tool diameter in width, were machined both with and without the application of a magnetic field. The cutting parameters for each slot at their respective levels are listed in Table 5.2. Figure 5.2e shows the surface-cutting sequence used in the experiments. Before machining the micro-grooves, the surface of the workpiece was plane-milled using two-fluted end mill cutters with a 2 mm diameter. Klubercut CO (6-102), a biodegradable vegetable oil, was used as a lubricant during the milling process. Each machined groove was analyzed using an optical profiling system (Zygo NexviewTM) to measure surface roughness, generate surface topography, and profile the surface. Additionally, a Hitachi tabletop microscope (TM3000) was used to inspect the milling tool edge and the machined surface. The surface roughness of each groove was evaluated using a non-contact optical profiling system, with five measurements taken for each groove. The average surface roughness values are reported in this study.

Table 5. 2 Machining parameters of experiments

Slot	**spindle speed, *SS*** (rpm)	**feed rate, F_r** (mm/minute)	**depth of cut, D_{oc}** (mm)
1	60000	90	0.015
2	60000	90	0.03
3	60000	90	0.045
4	60000	90	0.06

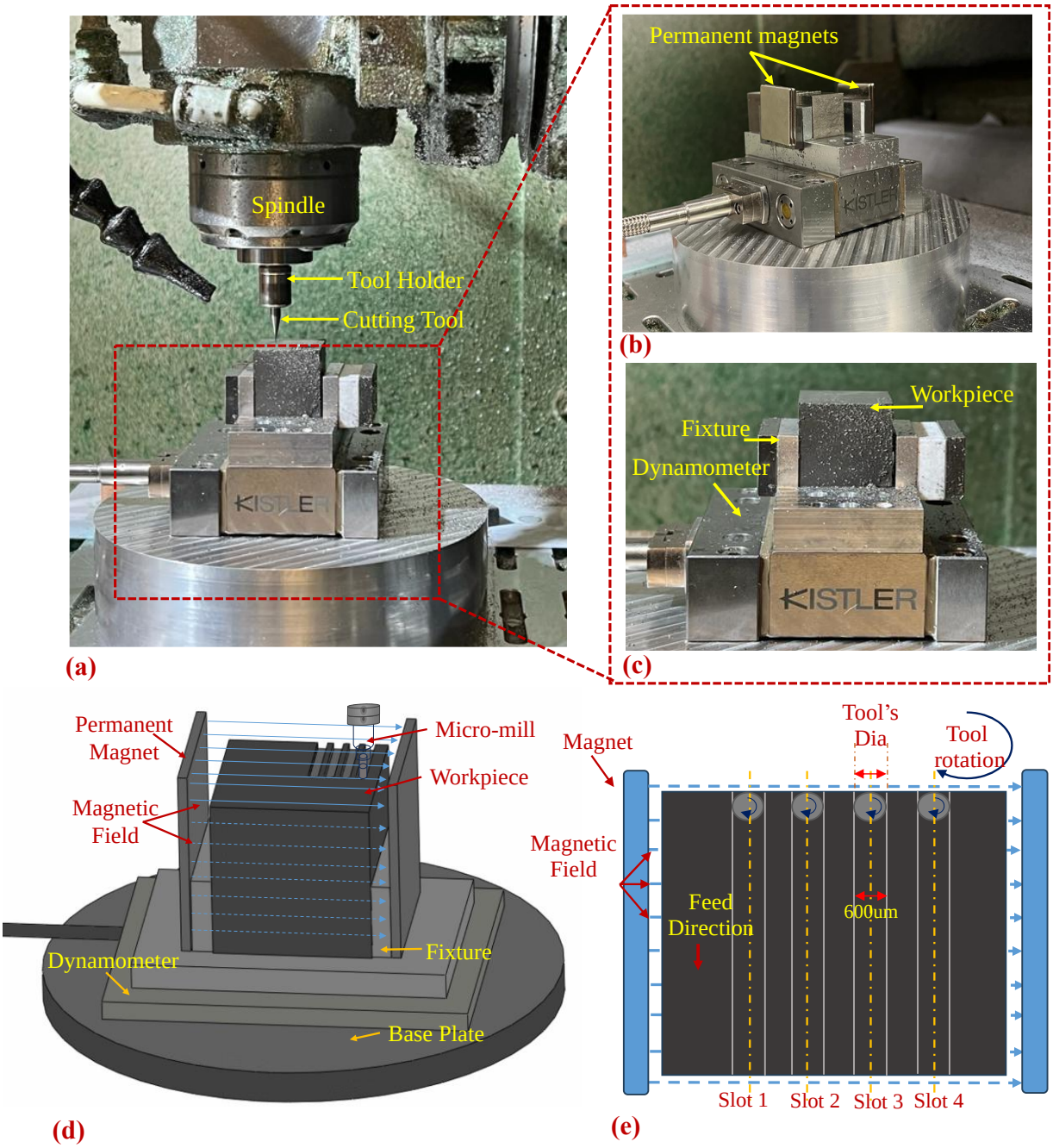

Figure 5. 2 (a) Experimental setup of (b) magnetic field setup (c) non-magnetic field setup (d) CAD design of system, and (e) schematic diagram of the cutting sequence

5.6 Results and Discussion

5.6.1 Surface roughness

Micro-milling, distinct from macro-milling due to its unique material removal mechanics, is influenced by several factors that impact surface quality. The intricacies of this process are governed by material properties, tool geometry, and process parameters such as cutting speed, feed rate, and depth of cut [230-232]. The small cutting edge of the micro-mill cutter complicates material removal compared to conventional milling. Surface quality is paramount in assessing the precision of micro-milled parts, particularly in applications requiring low surface roughness. It is typically evaluated using surface roughness measurements and is affected by machining parameters, the materials of the workpiece and tool, tool geometry, lubrication, and vibrations during machining [111, 161]. Among these factors, machining parameters, including tool rotation, depth of cut, and feed rate, along with material properties, play a crucial role in determining the surface quality of micro-milled components. This study specifically explores the impact of depth of cut in conjunction with the influence of an external magnetic field.

Applying a magnetic field in micro-milling significantly enhances surface quality, particularly when machining SLM Ti6Al4V. This improvement is attributed to the magnetic field's effect on thermal conductivity. The intensification of magnetic dipole interactions aligns particles along the field orientation, forming chain-like structures that act as efficient heat transfer conduits [222, 225]. These structures improve thermal conductivity, with a direct correlation between chain length and magnetic field strength [222, 225]. This phenomenon offers a promising approach to enhancing thermal conductivity during titanium alloy machining, especially for SLM Ti6Al4V. As illustrated in Figure 5.3a, the refined surface quality achieved through micro-milling under magnetic conditions, specifically at 60,000 rpm, 90 mm/min, and 0.015 mm, shows a 22% reduction in average surface roughness compared to

non-magnetic samples. In single-point diamond turning of Ti6Al4V, the eddy damping effect, caused by eddy currents, suppresses tool vibrations, reducing uncut material and concave areas on the machined surface and decreasing tool mark width. Consequently, surface quality during micro-machining improves in the presence of a magnetic field [233]

Figure 5.3 presents the average surface roughness values for both magnetic and non-magnetic setups across various parameters, indicating that non-magnetic (NM) SLM samples consistently exhibit higher average surface roughness than magnetic (M) SLM samples. Figure 5.3b demonstrates that as the depth of cut increases, surface roughness increases for both sample types, reaching its maximum at a depth of cut of 0.06 mm. Kumar and Avinash [234] reported a similar trend, noting that increased surface roughness at higher depths of cut during micro-milling of Ti-6Al-7Nb is due to excessive heat generation and material welding on the tool and machined surfaces. This increase in surface roughness is associated with intensified cutting forces and material removal at greater depths of cut. Wang et al. [235] explored the relationship between depth of cut and cutting forces, noting that cutting forces increase proportionally with the depth of cut. As the cutting edge wears under these higher forces, ploughing mechanisms become more dominant than shearing. This ploughing leads to elastic deformation of the chips, producing a rougher surface and increasing the average surface roughness. In milling, the continuous motion of the cutting tool results in dynamic shifts between different modes of material removal. According to the principles of minimum chip thickness and tool rotation, a single cutting pass can be divided into a central shear zone and a peripheral ploughing zone. Ploughing occurs when the instantaneous undeformed chip thickness is at the minimum chip thickness (h_{min}), while the shear zone dominates when the thickness exceeds hmin. This behaviour causes distinct surface morphologies and varying roughness levels across different transverse positions on the milled surface.

Researchers have traditionally concentrated on surface roughness at the center of micro-milled surfaces, often neglecting variations along the edges. However, the transverse distribution of surface roughness significantly influences the performance of components. This section thoroughly examines the transverse surface roughness and the impact of a magnetic field during micro milling. Figure 5.4 illustrates the transverse distribution of the milled slot, divided into five sections, with sections 1 and 5 representing the cut-in and cut-out sides, respectively, and sections 2, 3, and 4 comprising the middle. Figure 5.5 presents surface roughness trends at various points along the milled surface for both minimum and maximum depths of cut, comparing results with and without a magnetic field. The findings indicate that surface roughness is higher along the edges (sections 1 and 5) and lower and more consistent in the middle (sections 2, 3, and 4).

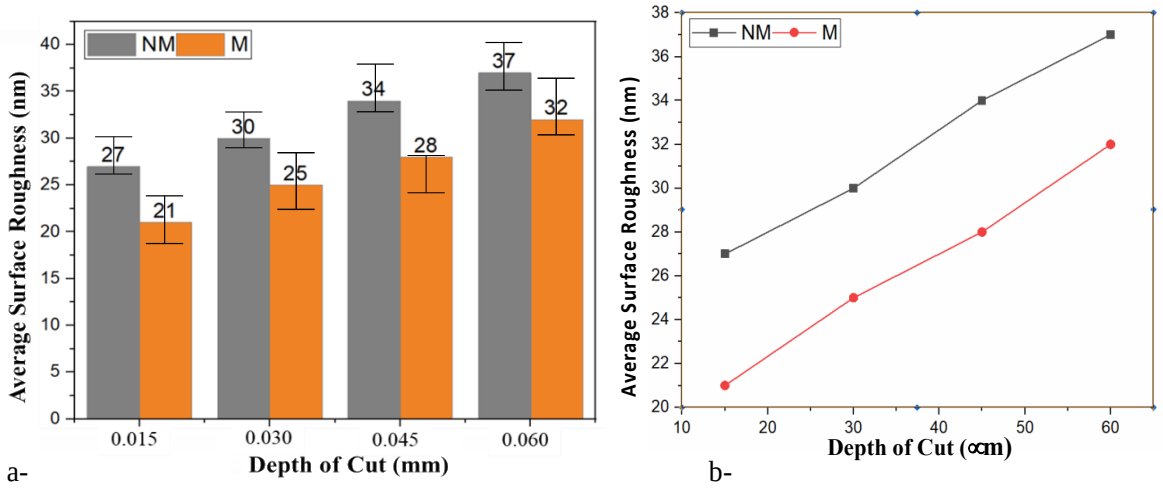

Figure 5. 3 a-Comparison of average surface roughness of non-magnetic (NM) and magnetic (M) samples, b- The effect of depth of cut on average surface roughness for NM and M samples

During the cut-in stage, the cutting tool initially contacts the workpiece material with a very small undeformed chip thickness, leading to ploughing as the dominant material removal mode. This results in an extremely rough transverse surface profile. As the process progresses to the middle stage, the undeformed chip thickness increases, shifting the material removal mode to shearing and cutting, which smooths and evens out the surface profile. In the cut-out

stage, the surface roughness deteriorates again as ploughing becomes predominant once more. Wu et al. [236]identified a distinctive W-shape pattern in the transverse distribution of surface roughness across the micro-milled slot of SLM Ti6Al4V, attributed to variations in undeformed chip thickness and material removal modes at different positions. This study highlighted that unstable cutting behaviors significantly influence surface roughness, contributing to the observed size effect.

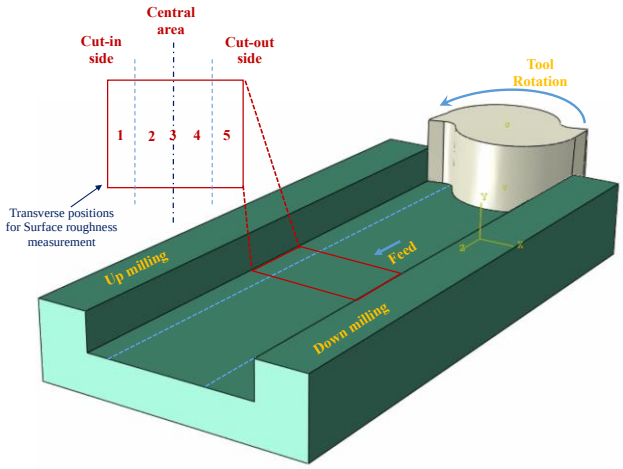

figure 5. 4 Positions of surface roughness along the machined surface

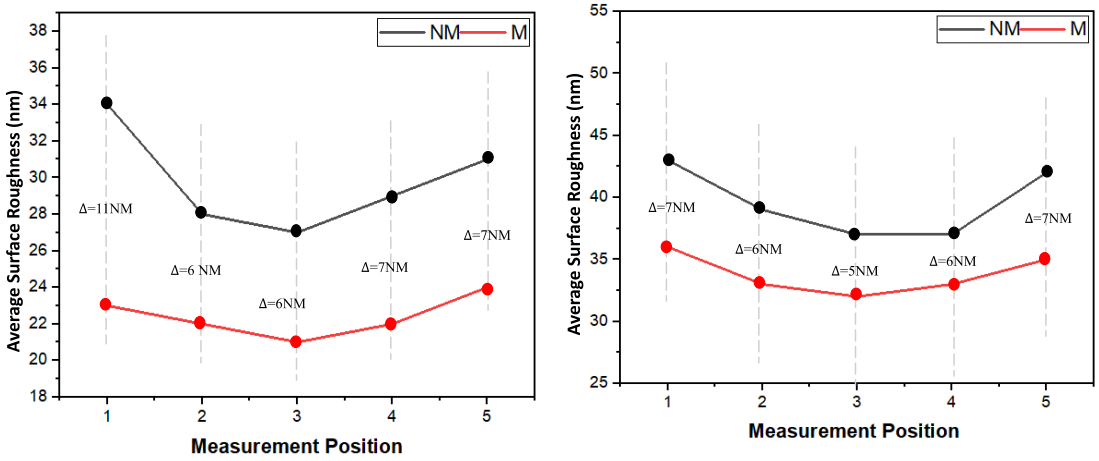

a- b-

figure 5. 5 Average surface roughness of (a) slot 1 at depth of cut 0.015mm; (b) slot 4 at depth of cut 0.06mm

5.6.2 Surface topology

Figure 5.6 depicts the surface topographies of each slot during the micro-milling process of SLM Ti6Al4V. Figures 5.6 a, b, c, and d illustrate surface topologies without the presence of a magnetic field, contrasting with figures e, f, g, and h, which display surface topologies under the influence of a magnetic field. Notably, in the absence of a magnetic field, distinct ploughing patterns are observed, particularly concentrated along the edges where ploughing dominates the material removal process. As the depth of cut (DOC) increases, these topographies exhibit decreased uniformity. Sun et al. [237] elucidated this phenomenon, attributing it to low surface roughness where shearing predominates and increased roughness along the edges dominated by ploughing. Their proposed mathematical model factors in alignment errors, material elastic recovery, tool sharpness, and ploughing effects to explain this variance. Additionally, micro-milled slots without magnetic field intervention exhibit deeper feed marks and built-up edge, induced by the scratching action of the built-up edge on the cutting edge. Moreover, the heat generated during material removal leads to microchips welding onto the flank face of the cutting tool, contributing to feed mark formation through rubbing action against the newly generated surface. Non-magnetic micro-milled surfaces exhibit sharper peaks and irregularities compared to surfaces influenced by a magnetic field, which demonstrate greater consistency and fewer irregularities. In the case of micro-milling SLM Ti6Al4V, a harder material, elevated temperatures between the tool and flank face cause material softening and chip fusion or welding. In the absence of a magnetic field, limited heat dissipation results in increased accumulation of micro-particles and chip welding on the tool cross-section, thereby compromising surface quality. Conversely, the presence of a magnetic field reduces the occurrence of feed marks by mitigating built-up edge, thereby minimizing the scratching effect and reducing feed mark formations.

The observed trends indicate a direct correlation between feedrate and resultant surface roughness. As the depth of cut increases gradually, there is a corresponding rise in actual surface roughness, reaching a peak at a depth of cut of 0.060mm, indicative of a characteristic size effect. With an increasing depth of cut, greater material removal is necessitated, leading to elevated shear stresses and heat generation. Consequently, more particles adhere to the cutting tool, resulting in the formation of deeper feed marks. In the absence of a magnetic field, restricted heat dissipation leads to heightened accumulation of microparticles and chip welding on the tool cross-section, consequently diminishing the quality of the machined surface. Concurrently, inadequate heat dissipation during tool rotation fosters the welding of microchips onto the newly formed surface, exacerbating surface irregularities. These findings align with Yip and To's [229] assertion that magnetic field-assisted micro-machining offers benefits for enhancing surface roughness, particularly in the context of magnetic and ferromagnetic materials.

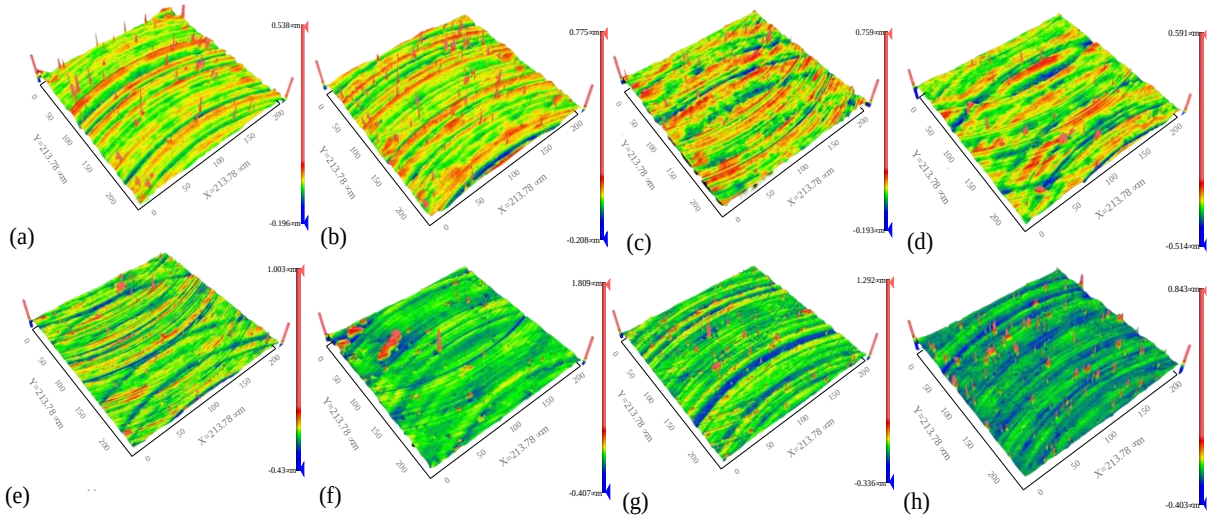

figure 5. 6 Surface topologies of non-magnetic samples in micro-milling of SLM Ti6Al4V at depth of cut (a) 0.015mm, (b) 0.030mm, (c) 0.045mm, (d) 0.06mm; and magnetic samples of micro-milling depth of cut, (e) 0.015mm, (f) 0.030mm, (g) 0.045mm, (h) 0.06mm

5.6.3 Surface profile

Figure 5.7 illustrates the transverse profile of a machined micro-milled surface for slots 1 and 4. Specifically, Figure 5.7a and Figure 5.7b depict the surface profiles of micro-milled slot 1 in the presence and absence of a magnetic field, respectively, while Figures 6c and 6d display the corresponding results for slot 4. These surface profile findings are consistent with the transverse distribution of surface roughness along the slot. Each surface profile exhibits three distinct sections: the cut-in side, the middle portion, and the cut-out side, each showcasing unique surface characteristics. During the cut-in stage, characterized by the penetration of the cutting tool into the SLM Ti6Al4V material, ploughing emerges as the primary material removal mode due to the small instantaneous undeformed chip thickness, resulting in a visibly rough transverse surface profile. Figure 5.7a exhibits irregularities and bulges, which manifest as prominent surface features contributing to suboptimal surface quality. Subsequently, in the middle stage, shearing and cutting actions prevail as the instantaneous undeformed chip thickness increases, yielding a smoother and more uniform transverse profile. Conversely, the cut-out stage mirrors the cut-in stage, showcasing a transverse profile marked by noticeable irregularities. This trend is echoed in Figure 5.7c, where the surface profile appears smooth in the middle but exhibits visible irregularities in the cut-in and cut-out stages. Moreover, the heightened depth of cut in slot 4 amplifies material removal and stresses, inducing tool vibrations and instability, culminating in a rougher surface at the edges, consistent with the qualitative results for surface roughness. Figures 5.7 b and d showcase the profiles of slots 1 and 4 in the presence of a magnetic field, highlighting notable enhancements in profile stability. The surfaces demonstrate remarkable smoothness and stability compared to those obtained without the magnetic field.

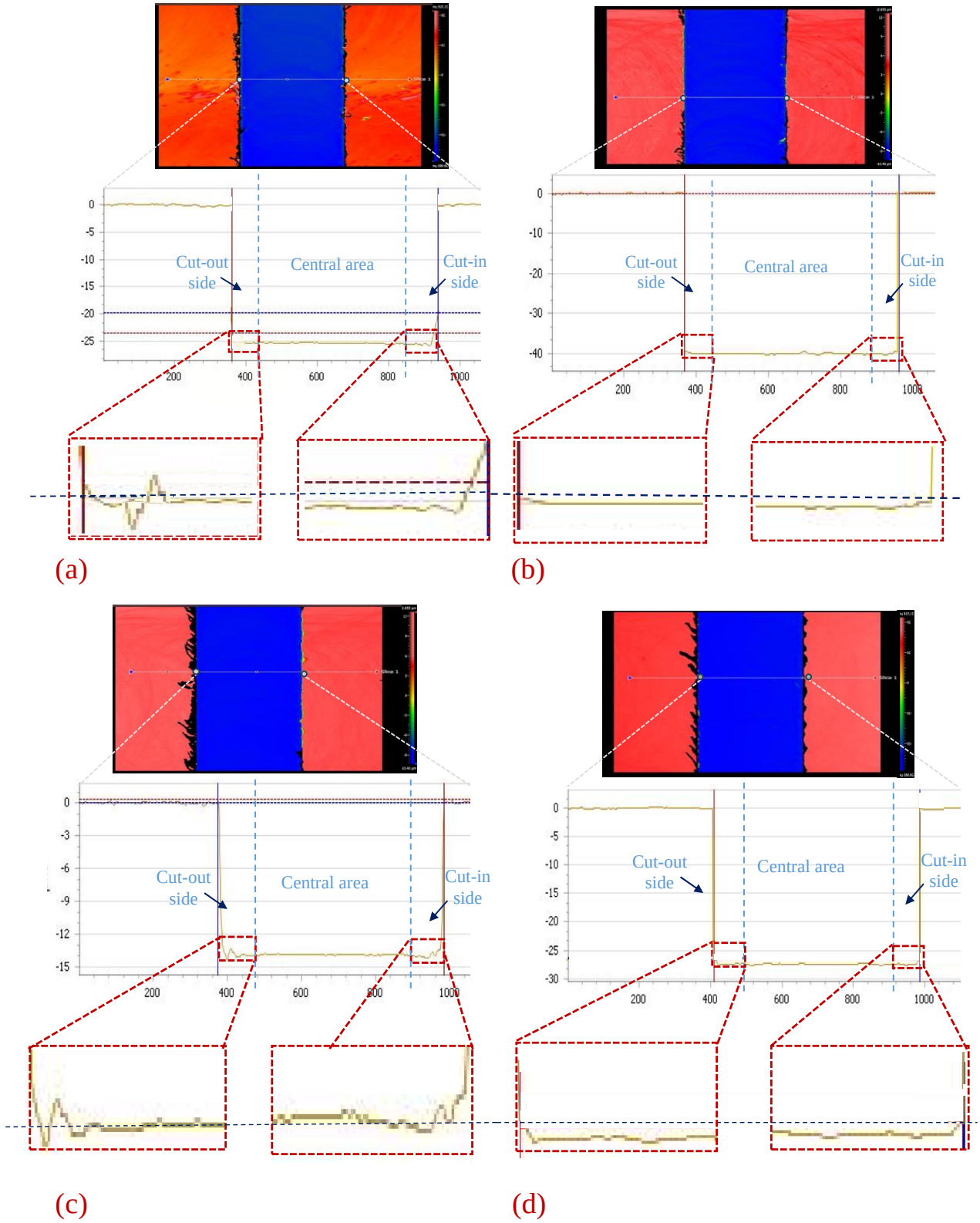

figure 5. 7 Surface profiles of (a) slot 1 of non-magnetic sample, (b) slot 1 of magnetic sample, (c) slot 4 of non-magnetic sample , (d) slot 1 of magnetic sample

5.6.4 Surface defects

To comprehensively assess the transverse surfaces produced during micro-milling experiments, each slot underwent further analysis utilizing Scanning Electron Microscopy (SEM), with the results depicted in Figure 5.8. Figures a, b, c, and 7d illustrate slots 1, 2, 3, and 4 milled without the application of a magnetic field, while Figures e, f, g, and h depict the same slots milled in the presence of a magnetic field. Notably, each slot exhibits distinct feed marks, with Figures 5.8 e and f displaying noticeably reduced prominence of such marks. Specifically, slots milled at shallower depths and under the influence of a magnetic field exhibit minimal feed marks, whereas deeper cuts accentuate their visibility. According to Chen et al. [238],, the persistence of feed marks along the micro-mill tool path arises from instability stemming from unaddressed feed resistance and micro-milling bending. Additionally, as posited by Liu et al. [239], the high adhesion and low thermal conductivity coefficient of Ti6Al4V contribute to feed mark formation, with micro-particles adhering to the tool face during high-temperature micro-milling, thereby inducing defect formation. This phenomenon results from enhanced bonding between the titanium alloy and the tool, or chips adhering to the tool during fabrication, consequently manifesting as observed chatter during machining and visible feed marks on the machined surface. Moreover, increasing cut depth correlates with the emergence of burrs on the machined slot, notably reducing surface roughness along slot edges, particularly on the cut-in and cut-out sides. Remarkably, burr length exhibits an inverse relationship with cut depth, yielding smaller burrs for shallower cuts and a burr-free surface. SEM inspections reveal surface defects such as chip fragments, material side flow, deep feed marks, and micro-particles. It is imperative to acknowledge the variability in surface roughness values across each slot, underscoring the dynamic nature of the tool-workpiece interaction during micro-milling, wherein the material removal mechanism oscillates between shearing and ploughing as the tool rotates. Concurrently, Figures 5.8 e, f, g, and h showcase the surfaces

generated under the influence of a magnetic field, indicating a significant enhancement in the quality of each slot compared to their non-magnetic counterparts. The attenuation in feed mark intensity, absence of material slide flow, and reduction in adhered particles and chip segments align with the findings of Yip and To, who observed improved surface quality during single point diamond turning of wrought titanium alloy [229]. Kamel et al. [240] also noted, through SEM analysis of machined surfaces during single point diamond turning, the emergence of flat surfaces devoid of scratches and featuring shallow feed marks when a magnetic field was employed. This underscores the significant improvement in machining outcomes facilitated by the presence of the magnetic field.

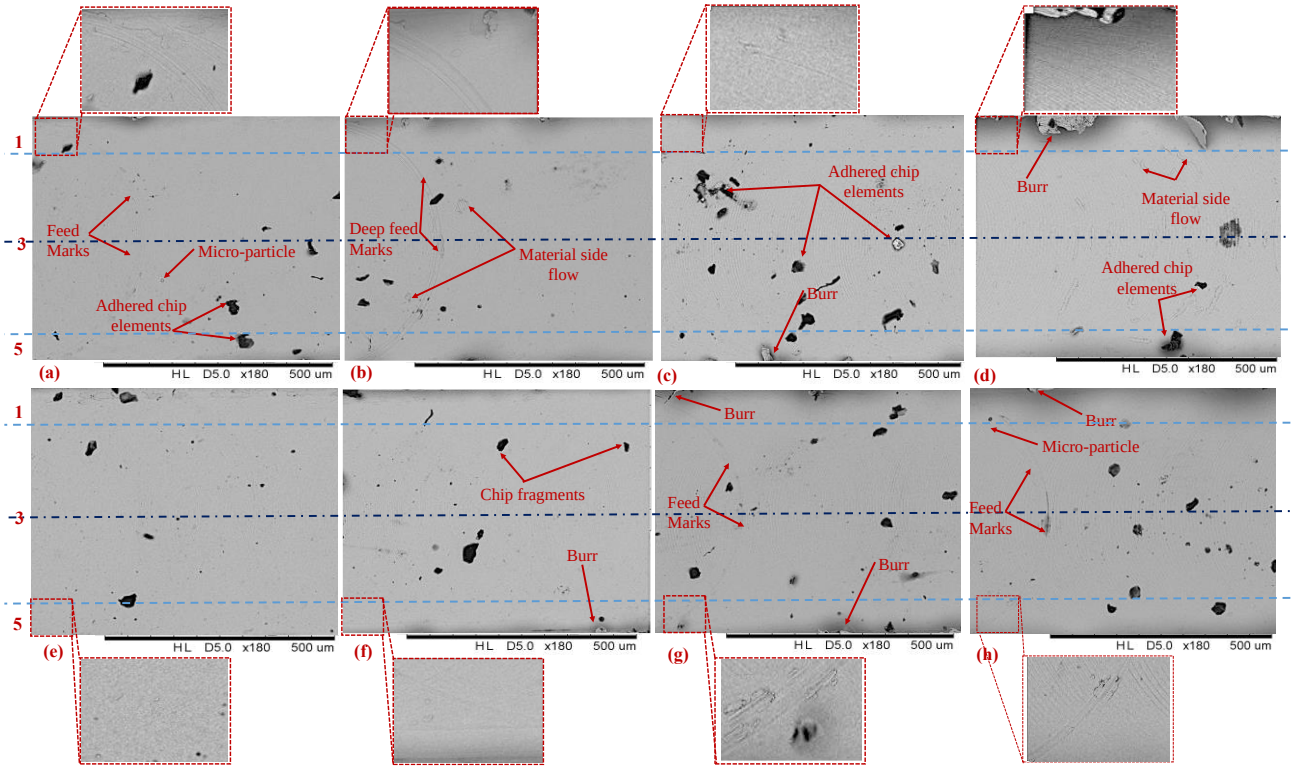

figure 5. 8 SEM of the non-magnetic field sample, (a) slot 1, (b) slot 2, (c) slot 3, (d) slot 4, and, SEM of the magnetic field sample, (e) slot 1, (f) slot 2, (g) slot 3, (h) slot 4

5.6.5 Tool Wear

Micro-milling SLM Ti6Al4V, renowned for its robustness, hardness, and low thermal conductivity, presents formidable challenges in machining. The cutting edges endure substantial cutting forces and temperatures during milling, leading to intricate interactions with the workpiece. This intricacy is compounded by the material's high hardness and tensile strength, which prompt plastic deformation during micro-milling. The resultant escalation in cutting forces and temperatures profoundly impacts tool wear [131, 180, 181]. As elucidated by Komanduri [241]and Ezugwu [242], micro-milling of Ti6Al4V yields elevated temperatures (approximately 500 °C) and intensified thrust forces (about 600-650 N), engendering high cutting pressures (approximately 1-1.5 GPa). Elevated spindle speed and feed rate correspondingly escalate cutting temperature and cutting-edge stress, hastening tool wear. This phenomenon is particularly pronounced with SLM Ti6Al4V, owing to its heightened hardness, which augments resistance to chip formation and, consequently, exacerbates flank wear. Sartory et al. [243] and Khanna et al. [52] have discerned that micro-machining of SLM Ti6Al4V precipitates heightene d flank and tool wear attributable to its heightened hardness. The micro-machining of SLM Ti6Al4V mandates augmented specific energy to induce plastic deformation and surmount resistance, expediting flank face deterioration, especially at elevated cutting velocities. Augmented heat at the tool-workpiece interface fosters rubbing, further hastening flank wear owing to inadequate heat conductivity.

Figures 9 and 10 depict the cross-sectional area and rake face of milling tools utilized in processing SLM Ti6Al4V, contrasting their conditions in the absence and presence of magnetic fields, respectively. Evidently, a notable disparity exists between the states of both tools. The tool processed sans a magnetic field exhibits significant deterioration, particularly evident in Figure 5.9b, showcasing adhesive wear in the tool's cross-sectional area. Adhesive wear occurs when material adhesion transpires upon the tool face due to challenging chip

removal, exacerbated when the uncut chip thickness falls below the critical threshold, promoting rubbing and hastening adhesive layer formation. Consequently, the fracturing of the adhesive material during progressive cutting results in small tool segment detachment, manifesting as flaking or chipping of the cutting edges. Cutting edge abrasion, primarily induced by the interaction between hard particles in Ti6Al4V and the cutting edge during machining, typically affects the flank and rake faces, with material adhesion on the flank face offering protection against abrasion [244]. Additionally, plowing at low feed rates instigates cutting edge abrasion, as observed in Figure 5.9b, showcasing micro chipping. The tool's low fracture toughness renders it susceptible to micro cracks formation and propagation during the ploughing stage, culminating in micro chipping of the tool material [235]. . Furthermore, the material's elevated temperature and reactivity prompt welded particles to adhere to the tool surface, resulting in the formation of a built-up edge (BUE), as evidenced in Figure 5.9c [206]. . Given that the feed operates within the micro range, BUE formation in micro-machining corresponds to the uncut chip thickness. BUE, being harder than the cutting material, can supplant it, diminishing sharpness and fostering workpiece material adhesion to the cutting edge, thereby exacerbating material side flow and compromising surface quality. Conversely, the tool processed on SLM Ti6Al4V in the presence of an external magnetic field exhibits notably enhanced performance (Figure 5.10 a & b), showcasing cutting edges devoid of BUE (Figure 5.10c) and retaining their original shape with minimal adhesive wear. This marked improvement can be attributed to the magnetic field's influence on material properties, particularly the augmentation of thermal conductivity in SLM Ti6Al4V by aligning its microstructure, thereby mitigating deformation resistance and facilitating heat dissipation. Consequently, the encountered cutting forces and temperatures are reduced, diminishing adhesive wear and micro chipping. Moreover, the magnetic field's impact on the material's magnetic domains renders it less rigid and more amenable to machining, potentially curbing

tool wear and enhancing machined surface quality. These discernments underscore the magnetic field application as a promising avenue for enhancing the machinability and overall quality of micro-milled SLM Ti6Al4V components, thereby heralding transformative prospects in machining challenging materials and fostering advancements in the manufacturing domain

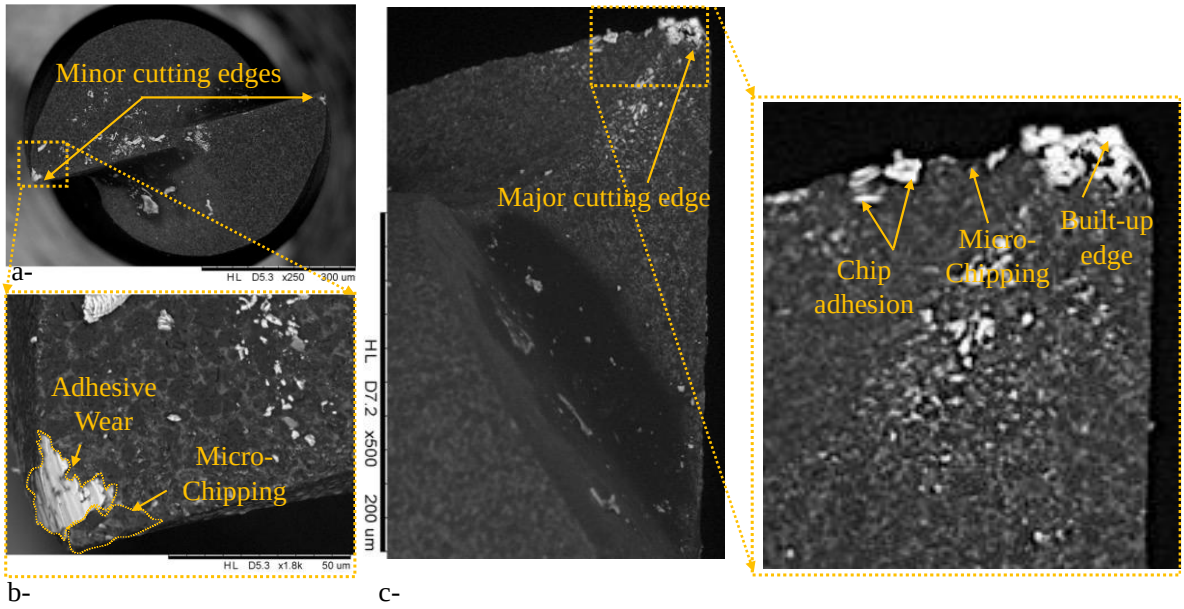

figure 5. 9 SEM of cutting tool in non-magnetic field, (a) cross sectional area, (b) cutting edge, (c) rake face

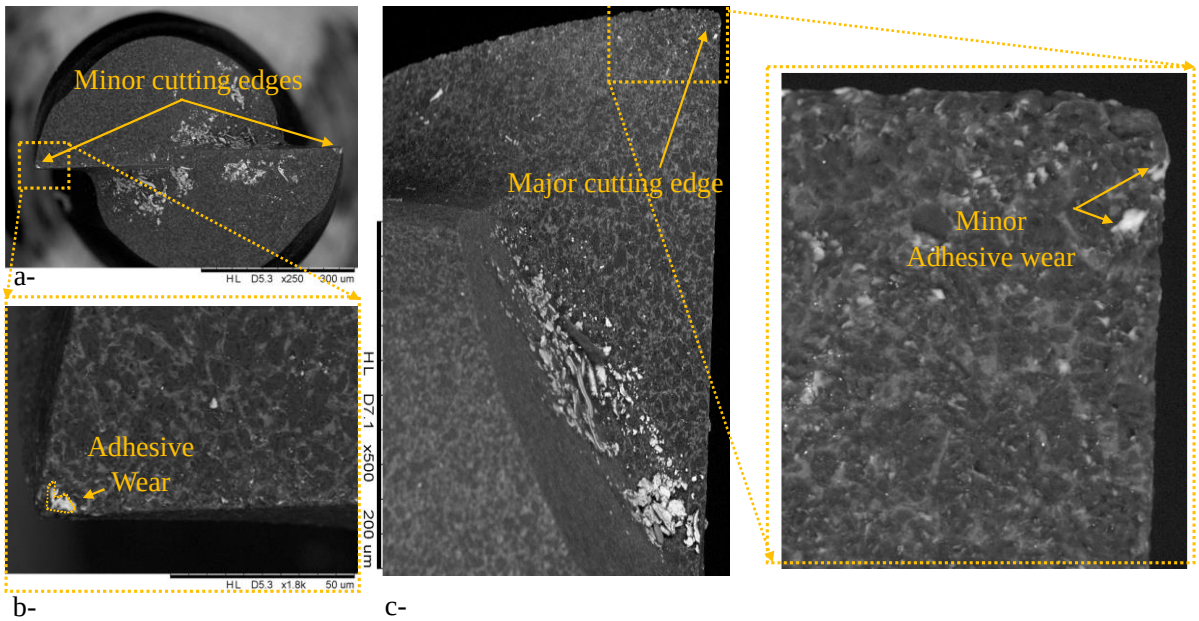

figure 5. 10 SEM of cutting tool in magnetic field (a) cross sectional area, (b) cutting edge, (c) rake face

5.7 Conclusion

This study undertook a systematic exploration of the magnetic field's influence on the micro-milling process of SLM Ti6Al4V. Leveraging established theories, we conducted a comprehensive comparative analysis to elucidate the nuanced dynamics inherent in micro-milling with and without a magnetic field. Crucially, our research addressed a significant void in current methodologies by meticulously examining the transverse distribution of surface roughness along the slot, elucidating the varying material removal processes during micro tool rotation. The findings contribute detailed and academically robust insights to the field of micro-milling, shedding light on the interplay between magnetic field application, tool dynamics, and surface quality in the machining of SLM Ti6Al4V. Specifically, the key highlights of our study are outlined below:

1. Employing an external magnetic field for micro-milling SLM Ti6Al4V yields a substantial enhancement in surface quality, underscoring the practical utility of magnetic field assistance in micro-milling of additively fabricated titanium alloys. Under specified machining parameters of 60000 rpm, 90mm/min, and 15 μm/tooth, magnetic field-assisted micro-milling of SLM titanium alloys reduces surface roughness by 22% compared to non-magnetic samples.
2. Observable and consistent feed marks are evident on the surface topography of each milled slot under both magnetic and non-magnetic conditions, attributed to the scratching effect of a built-up edge (BUE) on the cutting edge. Micro-milled slots machined without a magnetic field exhibit deeper and more pronounced feed marks.
3. The transverse distribution of surface roughness unveils distinct regions with specific milling surface patterns based on instantaneous chip thickness and cutting modes, i.e., plowing and shearing. The middle section exhibits a smooth and consistent surface roughness due to shearing, whereas cut-in and cut-out sections display plowing. SEM

images corroborate these findings by revealing surface imperfections such as chip fragments, material side flow, deep feed marks, and microparticles.

4. SEM analysis of tools processed on SLM Ti6Al4V in the absence of a magnetic field reveals the presence of BUE, micro chipping, and adhesive wear. Conversely, in the presence of a magnetic field, a significant reduction in tool wear is evident, indicating a notable improvement in tool condition facilitated by the external magnetic field.

Chapter 6: Conclusions and suggestions for future studies

6.1 Conclusions

Ti6Al4V (grade 5) is a widely utilized titanium alloy, extensively applied in the aerospace, marine, power generation, automotive, and chemical industries. Its exceptional properties are attributed to its unique crystalline structure, distinguishing it from other materials in its class. At room temperature, Ti6Al4V primarily consists of a hexagonal closest packed (HCP) α phase, with a minor proportion of body-centered cubic (BCC) β phase. This crystalline composition endows Ti6Al4V with exceptional strength and superior mechanical properties, including corrosion resistance, fatigue resistance, and toughness, even at high temperatures. Additionally, the alloy demonstrates high hardness. These attributes collectively make Ti6Al4V an ideal choice for applications in the aforementioned sectors. Advanced manufacturing technologies have introduced additive manufacturing (AM) as a transformative field, revolutionizing the industry by offering unparalleled design flexibility and significantly reducing product lead times. For metals such as Ti6Al4V, AM facilitates the creation of near-net-shape, complex geometrical parts. In recent years, a plethora of enhanced AM technologies have emerged, offering numerous advantages over conventional machining methods. These advantages include faster production times, elimination of molds and tooling, efficient material utilization, and the ability to create complex shapes and customize products. Industries requiring lightweight components, such as power production, automotive, aerospace, and medical sectors, often necessitate the inclusion of thin-walled features in their designs to meet strength and fatigue requirements. Subtractive methods, however, typically involve removing nearly 95% of bulk material to achieve the final product geometry, resulting in significant material wastage, particularly for expensive materials like titanium and nickel alloys. Moreover, machining harder materials like Ti6Al4V is associated with drastic tool wear. AM addresses these challenges by enabling the deposition of only the necessary amount of material

to create thin features, thereby significantly controlling material wastage. This method not only conserves material but also minimizes tool wear, making it a highly efficient alternative to traditional manufacturing processes.

The properties of Ti6Al4V alloy produced by additive manufacturing (AM) differ significantly from those produced by traditional methods such as forging and casting. Specifically, Ti6Al4V fabricated via Selective Laser Melting (SLM) is characterized by α' martensite with a hexagonal close-packed structure. This transformation results from the rapid cooling that converts the stable β phase into α' martensite. In contrast, conventionally manufactured Ti6Al4V exhibits equiaxed α grains and intergranular β phases, with directional alignment due to deformation in processes like forging. The slower cooling rates in traditional methods lead to coarser grains, allowing for more significant grain growth. While components fabricated using AM technologies often demonstrate superior mechanical properties compared to those produced by forging or rolling, they frequently show deviations from the specified surface finish and geometric tolerances required for critical and precision applications. Therefore, post-processing of as-fabricated components is essential to overcome these limitations and achieve the desired surface finish and dimensional accuracy using current AM technology. Despite the numerous benefits and potential applications of Ti6Al4V, machining this titanium alloy remains challenging due to its low thermal conductivity, strain hardening, high strength at elevated temperatures, and high chemical reactivity. Machining additively manufactured (AM) metallic parts introduces additional challenges when compared to wrought alloys. The intricacies of the powder bed, molten pool, and laser beam dynamics during AM processes complicate the understanding of the underlying thermophysical and metallurgical phenomena. These complexities are further intensified in micro-machining due to increased sensitivity to variations in AM process parameters and cooling rates, which can significantly impact the microstructure. Moreover, micro-machining encounters issues related to size effects, machine

tool vibrations, and tool-workpiece interactions. Size effects stem from factors such as workpiece characteristics, microstructure, process variables, and tool geometry. Additionally, chip formation in micro-machining alters process behavior. The machinability of a material is closely tied to its mechanical properties, which are influenced by the manufacturing method and the resulting microstructural characteristics.

One of the challenges in machining Ti6Al4V is its limited thermal conductivity, which hinders heat dissipation during the machining process. This accumulation of heat at the shearing point leads to tool wear and deteriorates surface quality. Recently, the application of a magnetic field in ultra-precision machining has emerged as a promising technique to enhance performance and surface quality, particularly for challenging materials like Ti6Al4V. The influence of magnetic fields on material properties, especially thermal conductivity, is well-documented in materials science. This phenomenon is observed across various materials, including those containing ferroparticles, magnetic particles, ferrometals, or thin films of ferrofluids. When exposed to a magnetic field, ferroparticles realign, thereby enhancing thermal conduction. Without a magnetic field, ferroparticles tend to aggregate due to van der Waals forces and dipole-dipole interactions, resulting in an irregular distribution. The application of a magnetic field shifts this balance, causing ferroparticles to align according to their positive magnetic susceptibility. This alignment forms conductive pathways that significantly improve heat transfer. In the absence of a magnetic field, magnetic particles exhibit random orientations and Brownian motion, which is often described by a dimensionless Langevin number of less than 1. Introducing a magnetic field intensifies magnetic dipole interactions, aligning particles parallel to the field direction and forming chain-like.

To address these issues, a comprehensive study was conducted, detailed in Chapter 3, which compares the machinability of wrought Ti6Al4V and SLM Ti6Al4V. The experimental results revealed distinct differences in surface topologies, chip morphology, burr formation,

and tool wear between the samples. Micro-milling of AM Ti6Al4V achieved a surface roughness of 19.2 nm, which is 13.9% lower than that of wrought workpieces, and exhibited reduced tool wear. Additionally, SLM Ti6Al4V produced continuous chips, whereas the wrought Ti6Al4V resulted in shorter chips. Furthermore, SLM Ti6Al4V demonstrated smaller burrs after micro-milling. Despite its higher hardness, SLM Ti6Al4V showed superior machinability, resulting in improved surface quality with lower tool wear and reduced burr heights. This study provides valuable insights for future research on post-processing AM titanium parts, particularly through micro-milling techniques. Furthermore, as the mechanical characteristics of materials are dependent on their microstructure and grain orientation, this chapter includes a detailed analysis of how these factors affect micro-milling performance. The effect of microstructure on cutting forces during micro-milling has been specifically examined.

Finite element (FE) simulation has been utilized to study machining processes for many years. One of the key advantages of FE simulation is its ability to predict and estimate critical machining process parameters, including cutting temperature, strain, strain rate, and stress. Advances in computing power have enabled FE-based process simulations to model and simulate complex problems with high efficiency and accuracy. Consequently, these simulations have become viable alternatives to physical experiments, providing significant time and resource savings while enhancing process performance. Three-dimensional FE simulations are particularly valuable for developing and refining cutting tool micro-geometries. However, there remain several challenges in FE process simulation research. Specifically, 3D modeling strategies and the representation of micro-scale processes face difficulties in obtaining comprehensive material and friction data, as well as in implementing sophisticated meshing techniques to optimize simulation precision and computational efficiency. Most current studies focus on orthogonal cutting, which oversimplifies high-speed micro-milling by neglecting factors such as tool rotation and the interaction between the workpiece and the cutting tool's

rake and flank surfaces. Both 2D and 3D orthogonal models have limitations in accurately capturing the shearing process. To address these gaps, Chapter 4 of this study introduces an advanced 3D finite element model (FEM) that incorporates orthogonal cutting constraints and accurately simulates the shearing process. This model accounts for the complexities of the micro-milling process, including tool rotation and interactions between the cutting tool and workpiece surfaces. Experimental results demonstrate that increasing the depth of cut results in larger cutting forces and enhanced material removal, while increasing rotational speed at a constant depth of cut leads to higher cutting forces due to increased friction. Additionally, machining parameters such as tool rotation speed, depth of cut, and material properties, particularly ductility and hardness, significantly influence surface defects and degradation. This study successfully developed and validated a 3D finite element model, showing a high level of agreement between experimental and simulation results regarding cutting forces, chip morphology, and surface topologies. The findings underscore the model's accuracy and reliability, offering valuable insights for manufacturers to optimize micro-milling strategies for SLM Ti6Al4V components.

The final section of this study (Chapter 5) explores the impact of a magnetic field on the micro-milling process of SLM Ti6Al4V, building on existing theories that suggest its advantages. Comparative experiments were conducted under milling conditions both with and without a magnetic field. These experiments demonstrated a significant enhancement in surface quality, evidenced by a 22% reduction in average surface roughness for the machined surface when a magnetic field was applied. The study also investigates the transverse distribution of surface roughness in micro-milling with a magnetic field. Scanning Electron Microscope (SEM) images corroborate these findings, revealing that micro-milling of SLM titanium alloys with a magnetic field result in fewer surface defects, such as welded chips, material side flow, deep feed marks, and micro-particles. Moreover, the application of an external magnetic field

during the micro-milling of SLM Ti6Al4V notably reduces tool wear, including built-up edge (BUE), micro chipping, and adhesive wear. These insights provide valuable information for the implementation of magnetic fields in the micro-milling of additively manufactured parts, suggesting potential improvements in surface finish and tool longevity.

6.2 Suggestions for the future work

The insights gained from this research will advance the post-processing methods for titanium parts produced via additive manufacturing. Future studies should focus on optimizing micro-milling parameters to enhance surface quality and prolong tool life. Additionally, employing advanced monitoring systems to mitigate tool vibrations and improve tool-workpiece interactions could yield superior results. Developing specialized cutting tools designed for the unique properties of additively manufactured materials will address current machining challenges. By pursuing these avenues, we can expand the capabilities of micro-milling as a finishing process for AM components, ensuring they meet the stringent standards required in aerospace, automotive, and medical device industries.

Furthermore, extending finite element modelling (FEM) to gain deeper insights into the micro-milling process is crucial. This extension could facilitate the accurate measurement and observation of critical parameters such as temperature, shear stresses, and residual stresses, which are challenging to measure experimentally. Additionally, FEM could be utilized to better understand and evaluate tool wear, incorporating the effects of heat generation and microstructural changes. This comprehensive approach has been largely overlooked in previous FEM research. Exploring the impact of magnetic fields on the micro-milling of various additively manufactured materials, such as high-temperature superalloys or composite materials, will help assess the broader applicability of magnetic field-assisted micro-milling. Investigating different magnetic field strengths and orientations will aid in identifying the optimal parameters for specific machining conditions. Enhancing the magnetic field effect

could also improve micro-pattern generation and form accuracy. Some researchers have explored the use of magnetic fields as an alternative to lubricants in single-point diamond turning of Ti6Al4V; this concept could be tested for micro-milling to advance clean manufacturing practices. Finally, collaborating with industry partners to pilot and implement the findings of this study in real-world manufacturing environments is essential. This collaboration will bridge the gap between academic research and practical applications, facilitating the adoption of advanced machining techniques.

References

1. Alojaly, H.M., A. Hammouda, and K.Y. Benyounis, *Review of recent developments on metal matrix composites with particulate reinforcement.* 2023.
2. Kang, I., et al., *A mechanistic model of cutting force in the micro end milling process.* Journal of Materials Processing Technology, 2007. **187**: p. 250-255.
3. Varghese, A., et al., *Experimental investigation of the correlation between surface roughness and tool-life in micromilling.* Advances in Materials and Processing Technologies, 2019. **5**(1): p. 67-77.
4. Ansari, P., et al., *Selective laser melting of 316l austenitic stainless steel: Detailed process understanding using multiphysics simulation and experimentation.* Metals, 2021. **11**(7): p. 1076.
5. He, T., et al., *3D printing for ultra-precision machining: current status, opportunities, and future perspectives.* Frontiers of Mechanical Engineering, 2024. **19**(4): p. 23.
6. Chen, N., et al., *Advances in micro milling: From tool fabrication to process outcomes.* International Journal of Machine Tools and Manufacture, 2021. **160**: p. 103670.
7. Zhang, S., et al., *Advances in ultra-precision machining of micro-structured functional surfaces and their typical applications.* International Journal of Machine Tools and Manufacture, 2019. **142**: p. 16-41.
8. Taniguchi, N., *Current status in, and future trends of, ultraprecision machining and ultrafine materials processing.* CIRP annals, 1983. **32**(2): p. 573-582.
9. Zhang, S.J., et al., *A review of surface roughness generation in ultra-precision machining.* International Journal of Machine Tools and Manufacture, 2015. **91**: p. 76-95.
10. Yuan, J., et al., *Review on the progress of ultra-precision machining technologies.* Frontiers of mechanical engineering, 2017. **12**: p. 158-180.

11. Goel, S., et al., *Diamond machining of silicon: a review of advances in molecular dynamics simulation.* International Journal of Machine Tools and Manufacture, 2015. **88**: p. 131-164.

12. Fang, F., et al., *Manufacturing and measurement of freeform optics.* CIRP Annals, 2013. **62**(2): p. 823-846.

13. Cheung, C.F. and W.B. Lee, *A theoretical and experimental investigation of surface roughness formation in ultra-precision diamond turning.* International Journal of Machine Tools and Manufacture, 2000. **40**(7): p. 979-1002.

14. Liu, D., et al., *Mechanisms of enhancing the machining performance in micro abrasive waterjet drilling of hard and brittle materials by vibration assistance.* International Journal of Machine Tools and Manufacture, 2020. **151**: p. 103528.

15. Thepsonthi, T. and T. Özel, *Multi-objective process optimization for micro-end milling of Ti-6Al-4V titanium alloy.* The International Journal of Advanced Manufacturing Technology, 2012. **63**: p. 903-914.

16. Srinivasa, Y. and M. Shunmugam, *Mechanistic model for prediction of cutting forces in micro end-milling and experimental comparison.* International Journal of Machine Tools and Manufacture, 2013. **67**: p. 18-27.

17. Boswell, B., M. Islam, and I.J. Davies, *A review of micro-mechanical cutting.* The International Journal of Advanced Manufacturing Technology, 2018. **94**: p. 789-806.

18. Blázquez, J., et al., *Ball milling as a way to produce magnetic and magnetocaloric materials: a review.* Journal of Materials Science, 2017. **52**: p. 11834-11850.

19. Pereira, R.B.D., et al., *A review of helical milling process.* International Journal of Machine Tools and Manufacture, 2017. **120**: p. 27-48.

20. Arsecularatne, J., *On tool-chip interface stress distributions, ploughing force and size effect in machining.* International Journal of Machine Tools and Manufacture, 1997. **37**(7): p. 885-899.

21. Johnson, K.L., *Contact mechanics*. 1987: Cambridge university press.

22. Jun, M.B., R.E. DeVor, and S.G. Kapoor, *Investigation of the dynamics of microend milling—part II: model validation and interpretation.* 2006.

23. Malekian, M., et al., *Modeling of minimum uncut chip thickness in micro machining of aluminum.* Journal of Materials Processing Technology, 2012. **212**(3): p. 553-559.

24. Jardret, V., et al., *Understanding and quantification of elastic and plastic deformation during a scratch test.* Wear, 1998. **218**(1): p. 8-14.

25. Jaffery, S. and P. Mativenga, *Assessment of the machinability of Ti-6Al-4V alloy using the wear map approach.* The International Journal of Advanced Manufacturing Technology, 2009. **40**: p. 687-696.

26. Yuan, Y., et al., *Modeling of cutting forces in micro end-milling.* Journal of Manufacturing Processes, 2018. **31**: p. 844-858.

27. Bao, W. and I. Tansel, *Modeling micro-end-milling operations. Part II: tool run-out.* International Journal of Machine Tools and Manufacture, 2000. **40**(15): p. 2175-2192.

28. Sutherland, J. and R.E. Devor, *An improved method for cutting force and surface error prediction in flexible end milling systems.* 1986.

29. Abellan-Nebot, J.V. and F. Romero Subirón, *A review of machining monitoring systems based on artificial intelligence process models.* The International Journal of Advanced Manufacturing Technology, 2010. **47**: p. 237-257.

30. Bissacco, G., H.N. Hansen, and J. Slunsky, *Modelling the cutting edge radius size effect for force prediction in micro milling.* CIRP annals, 2008. **57**(1): p. 113-116.

31. Ramsden, J.J., et al., *The design and manufacture of biomedical surfaces.* CIRP annals, 2007. **56**(2): p. 687-711.

32. Mian, A., N. Driver, and P. Mativenga, *Micromachining of coarse-grained multi-phase material.* Proceedings of the Institution of Mechanical Engineers, Part B: Journal of Engineering Manufacture, 2009. **223**(4): p. 377-385.

33. Horsch, C., V. Schulze, and D. Löhe, *Deburring and surface conditioning of micro milled structures by micro peening and ultrasonic wet peening.* Microsystem technologies, 2006. **12**: p. 691-696.

34. Jin, X. and Y. Altintas, *Slip-line field model of micro-cutting process with round tool edge effect.* Journal of Materials Processing Technology, 2011. **211**(3): p. 339-355.

35. Rehan, M., et al., *Microstructure and machinability of selective laser melted titanium alloy in micro-milling.* Journal of Materials Research and Technology, 2024. **33**: p. 8491-8502.

36. Rehan, M., W.S. Yip, and S.S. To. *Experimental investigation of microstructure, tool wear, and burr formation of micro-milling of selective laser melting Ti6Al4V*. in *Seventh International Conference on Mechanical Manufacturing and Industrial Engineering (MMIE 2024)*. 2024. SPIE.

37. Rehan, M., et al., *Experimental Investigation of the Micro-Milling of Additively Manufactured Titanium Alloys: Selective Laser Melting and Wrought Ti6Al4V.* Chinese Journal of Mechanical Engineering, 2024. **37**(1): p. 136.

38. Pirozzi, C., et al., *The effect of post-processing on the mechanical behavior of Ti6Al4V manufactured by electron beam powder bed fusion for general aviation primary structural applications.* Aerospace, 2020. **7**(6): p. 75.

39. Liu, S. and Y.C. Shin, *Additive manufacturing of Ti6Al4V alloy: A review.* Materials & Design, 2019. **164**: p. 107552.

40. Li, P., et al., *Critical assessment of the fatigue performance of additively manufactured Ti–6Al–4V and perspective for future research.* International Journal of Fatigue, 2016. **85**: p. 130-143.

41. Kasperovich, G. and J. Hausmann, *Improvement of fatigue resistance and ductility of TiAl6V4 processed by selective laser melting.* Journal of Materials Processing Technology, 2015. **220**: p. 202-214.

42. Silva, T.E., et al. *Machinability of the 18Ni300 additively manufactured maraging steel based on orthogonal cutting tests*. in *Innovations in Mechanical Engineering*. 2022. Springer.

43. Kaynak, Y. and O. Kitay, *The effect of post-processing operations on surface characteristics of 316L stainless steel produced by selective laser melting.* Additive Manufacturing, 2019. **26**: p. 84-93.

44. Bonaiti, G., et al., *Micro-milling machinability of DED additive titanium Ti-6Al-4V.* Procedia Manufacturing, 2017. **10**: p. 497-509.

45. Javidrad, H., M. Riahi, and M. Larky, *Utilization of metal additive manufacturing (AM) in precision oriented mechanical part production.*

46. Bai, Y., et al., *Additively manufactured CuCrZr alloy: Microstructure, mechanical properties and machinability.* Materials Science and Engineering: A, 2021. **819**: p. 141528.

47. Ni, C., et al., *Effect of material anisotropy on ultra-precision machining of Ti-6Al-4V alloy fabricated by selective laser melting.* Journal of Alloys and Compounds, 2020. **848**: p. 156457.

48. Huang, R., et al., *Energy and emissions saving potential of additive manufacturing: the case of lightweight aircraft components.* Journal of cleaner production, 2016. **135**: p. 1559-1570.

49. Ni, C., et al., *Effects of machining surface and laser beam scanning strategy on machinability of selective laser melted Ti6Al4V alloy in milling.* Materials & Design, 2020. **194**: p. 108880.

50. Park, E., et al., *Evaluation of tool life in the dry machining of inconel 718 parts from additive manufacturing (AM).* International Journal of Precision Engineering and Manufacturing, 2020. **21**: p. 57-65.

51. Grossi, N., et al., *Process parameters optimization of thin-wall machining for wire arc additive manufactured parts.* Applied Sciences, 2020. **10**(21): p. 7575.

52. Khanna, N., et al., *Review on machining of additively manufactured nickel and titanium alloys.* Journal of materials research and technology, 2021. **15**: p. 3192-3221.

53. Gong, X., T. Anderson, and K. Chou, *Review on powder-based electron beam additive manufacturing technology.* Manufacturing Review, 2014. **1**: p. 2.

54. Körner, C., *Additive manufacturing of metallic components by selective electron beam melting—a review.* International Materials Reviews, 2016. **61**(5): p. 361-377.

55. Udroiu, R., *POWDER BED ADDITIVE MANUFACTURING SYSTEMS AND ITS APPLICATIONS.* Academic journal of manufacturing engineering, 2012. **10**(4).

56. Babu, J.J., et al., *An experimental study of downfacing surfaces in selective laser melting.* Advanced Engineering Materials, 2022. **24**(8): p. 2101562.

57. Fereiduni, E., A. Ghasemi, and M. Elbestawi, *Selective laser melting of aluminum and titanium matrix composites: recent progress and potential applications in the aerospace industry.* Aerospace, 2020. **7**(6): p. 77.

58. Jing, L.-l., et al. *Application of selective laser melting technology based on titanium alloy in aerospace products*. in *IOP Conference Series: Materials Science and Engineering*. 2020. IOP Publishing.

59. Mishra, A.K., et al., *Identification of a suitable volumetric heat source for modelling of selective laser melting of Ti6Al4V powder using numerical and experimental validation approach.* The International Journal of Advanced Manufacturing Technology, 2018. **99**: p. 2257-2270.

60. Ali, H., H. Ghadbeigi, and K. Mumtaz, *Effect of scanning strategies on residual stress and mechanical properties of Selective Laser Melted Ti6Al4V.* Materials Science and Engineering: A, 2018. **712**: p. 175-187.

61. Lu, P., et al., *Study on corrosion resistance and bio-tribological behavior of porous structure based on the SLM manufactured medical Ti6Al4V.* Metals and Materials International, 2020. **26**: p. 1182-1191.

62. Al-Rubaie, K.S., et al., *Machinability of SLM-produced Ti6Al4V titanium alloy parts.* Journal of Manufacturing Processes, 2020. **57**: p. 768-786.

63. Toptan, F., et al., *Corrosion and tribocorrosion behaviour of Ti6Al4V produced by selective laser melting and hot pressing in comparison with the commercial alloy.* Journal of Materials Processing Technology, 2019. **266**: p. 239-245.

64. Yan, C., et al., *Ti–6Al–4V triply periodic minimal surface structures for bone implants fabricated via selective laser melting.* Journal of the mechanical behavior of biomedical materials, 2015. **51**: p. 61-73.

65. Zhao, Z. and S. To, *An investigation of resolved shear stress on activation of slip systems during ultraprecision rotary cutting of local anisotropic Ti-6Al-4V alloy: Models and experiments.* International Journal of Machine Tools and Manufacture, 2018. **134**: p. 69-78.

66. Musa, N., J.B. Saedon, and M. Adenan. *An investigation on the surface integrity of grade 5 titanium alloy proceeding the wire electro-discharge machining (WEDM) process*. in *Applied Mechanics and Materials*. 2020. Trans Tech Publ.

67. Dong, Y., et al., *Additive manufacturing of pure Ti with superior mechanical performance, low cost, and biocompatibility for potential replacement of Ti-6Al-4V.* Materials & Design, 2020. **196**: p. 109142.

68. Rehan, M., et al., *Experimental investigation of the influence of wire offset and composition on complex profile WEDM of Ti6Al4V using trim-pass strategy.* The International Journal of Advanced Manufacturing Technology, 2023. **127**(3): p. 1209-1224.

69. Du, Y., et al., *Microstructures and mechanical properties of as-cast and as-extruded Mg-4.50 Zn-1.13 Ca (wt%) alloys.* Materials Science and Engineering: A, 2013. **576**: p. 6-13.

70. Alabort, E., et al., *Alloys-by-design: application to titanium alloys for optimal superplasticity.* Acta Materialia, 2019. **178**: p. 275-287.

71. Khalil, A.K., et al., *A novel magnetic field assisted diamond turning of Ti-6Al-4 V alloy for sustainable ultra-precision machining.* Materials Today Communications, 2023. **35**: p. 105829.

72. Sun, Y., et al., *Microstructure, mechanical properties and reinforcement mechanism of dual-scale TC4 titanium alloy prepared by cryomilling and plasma activated sintering.* Materials Science and Engineering: A, 2018. **736**: p. 120-129.

73. Singh, P., H. Pungotra, and N.S. Kalsi, *On the characteristics of titanium alloys for the aircraft applications.* Materials today: proceedings, 2017. **4**(8): p. 8971-8982.

74. Zhao, D., et al., *Improvement on mechanical properties and corrosion resistance of titanium-tantalum alloys in-situ fabricated via selective laser melting.* Journal of Alloys and Compounds, 2019. **804**: p. 288-298.

75. Wang, J., et al., *Optimization of mechanical property, antibacterial property and corrosion resistance of Ti-Cu alloy for dental implant.* Journal of materials science & technology, 2019. **35**(10): p. 2336-2344.

76. Shunmugavel, M., A. Polishetty, and G. Littlefair, *Microstructure and mechanical properties of wrought and additive manufactured Ti-6Al-4 V cylindrical bars.* Procedia Technology, 2015. **20**: p. 231-236.

77. Murr, L., et al., *Microstructures and mechanical properties of electron beam-rapid manufactured Ti–6Al–4V biomedical prototypes compared to wrought Ti–6Al–4V.* Materials characterization, 2009. **60**(2): p. 96-105.

78. Shunmugavel, M., et al., *Metallurgical and machinability characteristics of wrought and selective laser melted Ti-6Al-4V.* Journal of Metallurgy, 2016. **2016**.

79. Shunmugavel, M., et al., *A comparative study of mechanical properties and machinability of wrought and additive manufactured (selective laser melting) titanium alloy–Ti-6Al-4V.* Rapid Prototyping Journal, 2017. **23**(6): p. 1051-1056.

80. Murr, L., et al., *Microstructure and mechanical behavior of Ti–6Al–4V produced by rapid-layer manufacturing, for biomedical applications.* Journal of the mechanical behavior of biomedical materials, 2009. **2**(1): p. 20-32.

81. Zhao, X., et al., *Comparison of the microstructures and mechanical properties of Ti–6Al–4V fabricated by selective laser melting and electron beam melting.* Materials & Design, 2016. **95**: p. 21-31.

82. Edwards, P. and M. Ramulu, *Fatigue performance evaluation of selective laser melted Ti–6Al–4V.* Materials Science and Engineering: A, 2014. **598**: p. 327-337.

83. Cain, V., et al., *Crack propagation and fracture toughness of Ti6Al4V alloy produced by selective laser melting.* Additive Manufacturing, 2015. **5**: p. 68-76.

84. Pramanik, A., et al., *Optimizing dimensional accuracy of titanium alloy features produced by wire electrical discharge machining.* Materials and Manufacturing Processes, 2019. **34**(10): p. 1083-1090.

85. Usman, M., et al., *An in-depth evaluation of surface characteristics and key machining responses in WEDM of aerospace alloy under varying electric discharge environments.* The International Journal of Advanced Manufacturing Technology, 2023. **124**(7): p. 2437-2449.

86. Arikatla, S.P., K.T. Mannan, and A. Krishnaiah, *Parametric optimization in wire electrical discharge machining of titanium alloy using response surface methodology.* Materials Today: Proceedings, 2017. **4**(2): p. 1434-1441.

87. Manjaiah, M., S. Narendranath, and S. Basavarajappa, *A review on machining of titanium based alloys using EDM and WEDM.* Rev. Adv. Mater. Sci, 2014. **36**(2): p. 89-111.

88. Hu, K., et al., *Study on influence of ultrasonic vibration on the ultra-precision turning of Ti6Al4V alloy based on simulation and experiment.* IEEE Access, 2019. **7**: p. 33640-33651.

89. Lou, Y. and H. Wu, *Improving machinability of titanium alloy by electro-pulsing treatment in ultra-precision machining.* The International Journal of Advanced Manufacturing Technology, 2017. **93**(5): p. 2299-2304.

90. Tan, R., et al., *Sustainable production of dry-ultra-precision machining of Ti–6Al–4V alloy using PCD tool under ultrasonic elliptical vibration-assisted cutting.* Journal of Cleaner Production, 2020. **248**: p. 119254.

91. Zareena, A. and S. Veldhuis, *Tool wear mechanisms and tool life enhancement in ultra-precision machining of titanium.* Journal of Materials Processing Technology, 2012. **212**(3): p. 560-570.

92. Pramanik, A., *Problems and solutions in machining of titanium alloys.* The International Journal of Advanced Manufacturing Technology, 2014. **70**(5): p. 919-928.

93. Atkins, C., et al. *Additively manufactured mirrors for CubeSats*. in *Astronomical Optics: Design, Manufacture, and Test of Space and Ground Systems II*. 2019. International Society for Optics and Photonics.

94. Carroll, B.E., T.A. Palmer, and A.M. Beese, *Anisotropic tensile behavior of Ti–6Al–4V components fabricated with directed energy deposition additive manufacturing.* Acta Materialia, 2015. **87**: p. 309-320.

95. Edwards, P., A. O'conner, and M. Ramulu, *Electron beam additive manufacturing of titanium components: properties and performance.* Journal of Manufacturing Science and Engineering, 2013. **135**(6).

96. Chan, K.S., et al., *Fatigue life of titanium alloys fabricated by additive layer manufacturing techniques for dental implants.* Metallurgical and Materials Transactions A, 2013. **44**: p. 1010-1022.

97. Koike, M., et al., *Evaluation of titanium alloys fabricated using rapid prototyping technologies—electron beam melting and laser beam melting.* Materials, 2011. **4**(10): p. 1776-1792.

98. Leuders, S., et al., *On the mechanical behaviour of titanium alloy TiAl6V4 manufactured by selective laser melting: Fatigue resistance and crack growth performance.* International journal of fatigue, 2013. **48**: p. 300-307.

99. Bejjani, R., et al., *Variations in the surface integrity of Ti-6Al-4V by combinations of additive and subtractive manufacturing processes.* Materials, 2020. **13**(8): p. 1825.

100. Pragana, J., et al., *Hybrid metal additive manufacturing: A state–of–the-art review.* Advances in Industrial and Manufacturing Engineering, 2021. **2**: p. 100032.

101. Ming, W., et al., *Chip formation and hole quality in dry drilling additive manufactured Ti6Al4V.* Materials and Manufacturing Processes, 2020. **35**(1): p. 43-51.

102. Dang, J., et al., *New observations on wear characteristics of solid Al2O3/Si3N4 ceramic tool in high speed milling of additive manufactured Ti6Al4V.* Ceramics International, 2020. **46**(5): p. 5876-5886.

103. Rysava, Z. and S. Bruschi. *Comparison between EBM and DMLS Ti6Al4V machinability characteristics under dry micro-milling conditions*. in *Materials Science Forum*. 2016. Trans Tech Publ.

104. Hojati, F., et al., *Study on machinability of additively manufactured and conventional titanium alloys in micro-milling process.* Precision Engineering, 2020. **62**: p. 1-9.

105. de Oliveira Campos, F., et al., *The influence of additive manufacturing on the micromilling machinability of Ti6Al4V: A comparison of SLM and commercial workpieces.* Journal of Manufacturing Processes, 2020. **60**: p. 299-307.

106. Rysava, Z., *MICRO-CUTTING OF DIFFICULT-TO-CUT-MATERIALS.* 2017.

107. Varghese, V. and S. Mujumdar, *Micromilling-induced Surface Integrity of Porous Additive Manufactured Ti6Al4V Alloy.* Procedia Manufacturing, 2021. **53**: p. 387-394.

108. Su, Y., L. Li, and G. Wang, *Machinability performance and mechanism in milling of additive manufactured Ti6Al4V with polycrystalline diamond tool.* Journal of Manufacturing Processes, 2022. **75**: p. 1153-1161.

109. Sommer, D., et al., *Tool Wear and Milling Characteristics for Hybrid Additive Manufacturing Combining Laser Powder Bed Fusion and In Situ High-Speed Milling.* Materials, 2022. **15**(3): p. 1236.

110. Khaliq, W., et al., *Tool wear, surface quality, and residual stresses analysis of micro-machined additive manufactured Ti–6Al–4V under dry and MQL conditions.* Tribology International, 2020. **151**: p. 106408.

111. Danish, M., et al., *An experimental investigations on effects of cooling/lubrication conditions in micro milling of additively manufactured Inconel 718.* Tribology International, 2022. **173**: p. 107620.

112. Bordin, A., et al., *Analysis of tool wear in cryogenic machining of additive manufactured Ti6Al4V alloy.* Wear, 2015. **328**: p. 89-99.

113. Bruschi, S., et al., *Influence of the machining parameters and cooling strategies on the wear behavior of wrought and additive manufactured Ti6Al4V for biomedical applications.* Tribology International, 2016. **102**: p. 133-142.

114. Bruschi, S., et al., *Environmentally clean micromilling of electron beam melted Ti6Al4V.* Journal of Cleaner Production, 2016. **133**: p. 932-941.

115. Airao, J., H. Kishore, and C.K. Nirala, *Comparative analysis of tool wear in micro-milling of wrought and selective laser melted Ti6Al4V.* Wear, 2023. **523**: p. 204788.

116. Lizzul, L., et al., *Influence of additive manufacturing-induced anisotropy on tool wear in end milling of Ti6Al4V.* Tribology International, 2020. **146**: p. 106200.

117. Lizzul, L., et al., *Anisotropy effect of additively manufactured Ti6Al4V titanium alloy on surface quality after milling.* Precision Engineering, 2021. **67**: p. 301-310.

118. Zhao, Z., et al., *Effects of microstructures on the material removal energy in ultraprecision machining of Ti6Al4V alloys.* Materials Letters, 2021. **300**: p. 130231.

119. Liu, X., P.K. Chu, and C. Ding, *Surface modification of titanium, titanium alloys, and related materials for biomedical applications.* Materials Science and Engineering: R: Reports, 2004. **47**(3-4): p. 49-121.

120. Tshephe, T.S., et al., *Additive manufacturing of titanium-based alloys-A review of methods, properties, challenges, and prospects.* Heliyon, 2022. **8**(3).

121. Herzog, D., et al., *Additive manufacturing of metals.* Acta Materialia, 2016. **117**: p. 371-392.

122. Nguyen, H.D., et al., *A critical review on additive manufacturing of Ti-6Al-4V alloy: Microstructure and mechanical properties.* Journal of Materials Research and Technology, 2022. **18**: p. 4641-4661.

123. Liu, F., H. Xie, and W. He, *Multi-field coupling fatigue behavior of laser additively manufactured metallic materials: A review.* Journal of Materials Research and Technology, 2022.

124. Chen, C., et al., *Quasicrystal-strengthened biomedical magnesium alloy fabricated by laser additive manufacturing.* Journal of Alloys and Compounds, 2023. **947**: p. 169555.

125. Zhang, B., Y. Li, and Q. Bai, *Defect formation mechanisms in selective laser melting: a review.* Chinese Journal of Mechanical Engineering, 2017. **30**: p. 515-527.

126. Zhu, L., et al., *Investigation on synergism between additive and subtractive manufacturing for curved thin-walled structure.* Virtual and Physical Prototyping, 2022. **17**(2): p. 220-238.

127. Gupta, M.K., et al., *Tool wear patterns and their promoting mechanisms in hybrid cooling assisted machining of titanium Ti-3Al-2.5 V/grade 9 alloy.* Tribology International, 2022. **174**: p. 107773.

128. Sourd, X., et al., *Plain water jet cleaning of titanium alloy after abrasive water jet milling: Surface contamination and quality analysis in the context of maintenance.* Wear, 2021. **477**: p. 203833.

129. Liu, J., et al., *A review of low-temperature plasma-assisted machining: from mechanism to application.* Frontiers of Mechanical Engineering, 2023. **18**(1): p. 18.

130. Xiao, G., et al., *Thermal-Mechanical Effect and Removal Mechanism of Ti-6Al-4V During Laser-Assisted Grinding.* Chinese Journal of Mechanical Engineering, 2023. **36**(1): p. 118.

131. Airao, J., H. Kishore, and C.K. Nirala, *Measurement and analysis of tool wear and surface characteristics in micro turning of SLM Ti6Al4V and wrought Ti6Al4V.* Measurement, 2023. **206**: p. 112281.

132. Guo, S., et al., *Surface integrity of ultrasonically-assisted milled Ti6Al4V Alloy manufactured by selective laser melting.* Chinese Journal of Mechanical Engineering, 2021. **34**(1): p. 1-14.

133. Gomes, M.C., et al., *Micro-machining of additively manufactured metals: a review.* The International Journal of Advanced Manufacturing Technology, 2021: p. 1-20.

134. Sharma, S. and A. Meena, *Microstructure attributes and tool wear mechanisms during high-speed machining of Ti-6Al-4V.* Journal of Manufacturing Processes, 2020. **50**: p. 345-365.

135. Ji, H., et al., *Microstructure and machinability evaluation in micro milling of selective laser melted Inconel 718 alloy.* Journal of Materials Research and Technology, 2021. **14**: p. 348-362.

136. Han, C., et al., *Recent advances on high-entropy alloys for 3D printing.* Advanced Materials, 2020. **32**(26): p. 1903855.

137. Le Coz, G., et al., *Micro cutting of Ti-6Al-4V parts produced by SLM process.* Procedia Cirp, 2017. **58**: p. 228-232.

138. Zheng, Z., et al., *Microstructure and anisotropic mechanical properties of selective laser melted Ti6Al4V alloy under different scanning strategies.* Materials Science and Engineering: A, 2022. **831**: p. 142236.

139. Bedmar, J., et al., *Impact of Remelting in the Microstructure and Corrosion Properties of the Ti6Al4V Fabricated by Selective Laser Melting.* Coatings, 2022. **12**(2): p. 284.

140. Wang, J., Y. Wang, and J. Shi, *Solid-state diffusion joining of Ti6Al4V parts produced by selective laser melting: joint characteristics and bonding mechanism.* The

International Journal of Advanced Manufacturing Technology, 2021. **115**(4): p. 1037-1048.

141. Song, J., et al., *Temperature sensitivity of mechanical properties and microstructure during moderate temperature deformation of selective laser melted Ti-6Al-4V alloy.* Materials Characterization, 2020. **165**: p. 110342.

142. Karimi, J., et al., *Selective laser melting of Ti6Al4V: Effect of laser re-melting.* Materials Science and Engineering: A, 2021. **805**: p. 140558.

143. Ducato, A., et al. *An automated visual inspection system for the classification of the phases of Ti-6Al-4V titanium alloy*. in *Computer Analysis of Images and Patterns: 15th International Conference, CAIP 2013, York, UK, August 27-29, 2013, Proceedings, Part II 15*. 2013. Springer.

144. Yang, J., et al., *Formation and control of martensite in Ti-6Al-4V alloy produced by selective laser melting.* Materials & Design, 2016. **108**: p. 308-318.

145. Cao, Z., et al., *A machine learning method to quantitatively predict alpha phase morphology in additively manufactured Ti-6Al-4V.* npj Computational Materials, 2023. **9**(1): p. 195.

146. Sallica-Leva, E., et al., *Ductility improvement due to martensite α' decomposition in porous Ti–6Al–4V parts produced by selective laser melting for orthopedic implants.* Journal of the mechanical behavior of biomedical materials, 2016. **54**: p. 149-158.

147. Rautio, T., et al., *Laser welding of selective laser melted Ti6Al4V: Microstructure and mechanical properties.* Materials Today: Proceedings, 2020. **28**: p. 907-911.

148. Vrancken, B., et al., *Heat treatment of Ti6Al4V produced by Selective Laser Melting: Microstructure and mechanical properties.* Journal of Alloys and Compounds, 2012. **541**: p. 177-185.

149. Kim, Y.-K., et al., *Improvement in the high-temperature creep properties via heat treatment of Ti-6Al-4V alloy manufactured by selective laser melting.* Materials Science and Engineering: A, 2018. **715**: p. 33-40.

150. Neikter, M., *Microstructure and texture of additive manufactured Ti-6Al-4V*. 2017, Luleå University of Technology.

151. Murgau, C.C., *Microstructure model for Ti-6Al-4V used in simulation of additive manufacturing.* Luleatekniska universitet, 2016.

152. de Formanoir, C., et al., *Micromechanical behavior and thermal stability of a dual-phase α+ α'titanium alloy produced by additive manufacturing.* Acta materialia, 2019. **162**: p. 149-162.

153. Krakhmalev, P., et al., *Deformation behavior and microstructure of Ti6Al4V manufactured by SLM.* Physics Procedia, 2016. **83**: p. 778-788.

154. Galindo-Fernández, M., et al., *A microstructure sensitive model for deformation of Ti-6Al-4V describing Cast-and-Wrought and Additive Manufacturing morphologies.* Materials & Design, 2018. **160**: p. 350-362.

155. Lütjering, G., et al., *Commercially pure (CP) titanium and alpha alloys.* Titanium, 2003: p. 149-175.

156. Hayes, B.J., *Characterization of Ti-6Al-4V produced via electron beam additive manufacturing*. 2015: University of North Texas.

157. Shahsavari, M., et al., *Corrosion evaluation of Ti–6Al–4V manufactured by electron beam melting in Ringer's physiological solution: an in vitro study of the passive film.* Journal of Applied Electrochemistry, 2022. **52**(6): p. 1003-1019.

158. Mironov, S., et al., *Microstructure evolution during warm working of Ti–6Al–4V with a colony-α microstructure.* Acta Materialia, 2009. **57**(8): p. 2470-2481.

159. Beladi, H., Q. Chao, and G.S. Rohrer, *Variant selection and intervariant crystallographic planes distribution in martensite in a Ti–6Al–4V alloy.* Acta Materialia, 2014. **80**: p. 478-489.

160. Airao, J., H. Kishore, and C.K. Nirala, *Comparative analysis of tool wear in micro-milling of wrought and selective laser melted Ti6Al4V.* Wear, 2023: p. 204788.

161. Gupta, M.K., et al., *Tribological performance based machinability investigations in cryogenic cooling assisted turning of α-β titanium alloy.* Tribology International, 2021. **160**: p. 107032.

162. Kou, Z., et al., *Burr controlling in micro milling with supporting material method.* Procedia Manufacturing, 2015. **1**: p. 501-511.

163. Kumar, P., et al., *Recent advances in characterization, modeling and control of burr formation in micro-milling.* Manufacturing Letters, 2017. **13**: p. 1-5.

164. Kumar, M. and V. Bajpai, *Experimental investigation of top burr formation in high-speed micro-milling of Ti6Al4V alloy.* Proceedings of the Institution of Mechanical Engineers, Part B: Journal of Engineering Manufacture, 2020. **234**(4): p. 730-738.

165. Zheng, L., W. Chen, and D. Huo, *Experimental investigation on burr formation in vibration-assisted micro-milling of Ti-6Al-4V.* Proceedings of the Institution of Mechanical Engineers, Part C: Journal of Mechanical Engineering Science, 2019. **233**(12): p. 4112-4119.

166. Erçetin, A., K. Aslantas, and Ö. Özgün, *Micro-end milling of biomedical TZ54 magnesium alloy produced through powder metallurgy.* Machining Science and Technology, 2020. **24**(6): p. 924-947.

167. Balogun, V.A. and P.T. Mativenga, *Impact of un-deformed chip thickness on specific energy in mechanical machining processes.* Journal of Cleaner Production, 2014. **69**: p. 260-268.

168. Ducobu, F., E. Filippi, and E. Rivière-Lorphèvre. *Chip formation and minimum chip thickness in micro-milling*. in *Proceedings of the 12th CIRP conference on modeling of machining operations*. 2009.

169. Zhang, S. and Y. Guo, *An experimental and analytical analysis on chip morphology, phase transformation, oxidation, and their relationships in finish hard milling.* International Journal of Machine Tools and Manufacture, 2009. **49**(11): p. 805-813.

170. Airao, J., C.K. Nirala, and N. Khanna, *Novel use of ultrasonic-assisted turning in conjunction with cryogenic and lubrication techniques to analyze the machinability of Inconel 718.* Journal of Manufacturing Processes, 2022. **81**: p. 962-975.

171. Komanduri, R. and B. Von Turkovich, *New observations on the mechanism of chip formation when machining titanium alloys.* Wear, 1981. **69**(2): p. 179-188.

172. Wang, Y., et al., *Effect of the progressive tool wear on surface topography and chip formation in micro-milling of Ti–6Al–4V using Ti (C7N3)-based cermet micro-mill.* Tribology International, 2020. **141**: p. 105900.

173. Yang, J., et al., *Effect of crystallographic orientation on mechanical anisotropy of selective laser melted Ti-6Al-4V alloy.* Materials Characterization, 2017. **127**: p. 137-145.

174. Wu, M.-W., P.-H. Lai, and J.-K. Chen, *Anisotropy in the impact toughness of selective laser melted Ti–6Al–4V alloy.* Materials Science and Engineering: A, 2016. **650**: p. 295-299.

175. Wilson-Heid, A.E., et al., *Quantitative relationship between anisotropic strain to failure and grain morphology in additively manufactured Ti-6Al-4V.* Materials Science and Engineering: A, 2017. **706**: p. 287-294.

176. Rafi, H., et al., *Microstructures and mechanical properties of Ti6Al4V parts fabricated by selective laser melting and electron beam melting.* Journal of materials engineering and performance, 2013. **22**: p. 3872-3883.

177. Simonelli, M., Y.Y. Tse, and C. Tuck, *Effect of the build orientation on the mechanical properties and fracture modes of SLM Ti–6Al–4V.* Materials Science and Engineering: A, 2014. **616**: p. 1-11.

178. Antonysamy, A.A., J. Meyer, and P. Prangnell, *Effect of build geometry on the β-grain structure and texture in additive manufacture of Ti6Al4V by selective electron beam melting.* Materials characterization, 2013. **84**: p. 153-168.

179. Oyelola, O., et al., *On the machinability of directed energy deposited Ti6Al4V.* Additive Manufacturing, 2018. **19**: p. 39-50.

180. Hong, H., et al., *Machinability of steels and titanium alloys under lubrication.* Wear, 1993. **162**: p. 34-39.

181. Ginting, A. and M. Nouari, *Surface integrity of dry machined titanium alloys.* International Journal of Machine Tools and Manufacture, 2009. **49**(3-4): p. 325-332.

182. Mamedov, A. and I. Lazoglu, *Thermal analysis of micro milling titanium alloy Ti–6Al–4V.* Journal of Materials Processing Technology, 2016. **229**: p. 659-667.

183. Pratap, T., K. Patra, and A.A. Dyakonov, *Modeling cutting force in micro-milling of ti-6al-4 v titanium alloy.* Procedia Engineering, 2015. **129**: p. 134-139.

184. Ahmadi, M., et al., *Microstructure effects on process outputs in micro scale milling of heat treated Ti6Al4V titanium alloys.* Journal of Materials Processing Technology, 2018. **252**: p. 333-347.

185. Chen, W., et al., *Finite element simulation and experimental investigation on cutting mechanism in vibration-assisted micro-milling.* The International Journal of Advanced Manufacturing Technology, 2019. **105**: p. 4539-4549.

186. Ucun, İ., K. Aslantas, and F. Bedir, *Finite element modeling of micro-milling: Numerical simulation and experimental validation.* Machining Science and Technology, 2016. **20**(1): p. 148-172.

187. Özel, T., et al., *Experiments and finite element simulations on micro-milling of Ti–6Al–4V alloy with uncoated and cBN coated micro-tools.* CIRP annals, 2011. **60**(1): p. 85-88.

188. Attanasio, A., et al., *Finite element simulation of high speed micro milling in the presence of tool run-out with experimental validations.* The International Journal of Advanced Manufacturing Technology, 2019. **100**: p. 25-35.

189. Jing, X., et al., *Modelling and experimental analysis of the effects of run out, minimum chip thickness and elastic recovery on the cutting force in micro-end-milling.* International Journal of Mechanical Sciences, 2020. **176**: p. 105540.

190. Jin, X. and Y. Altintas, *Prediction of micro-milling forces with finite element method.* Journal of Materials Processing Technology, 2012. **212**(3): p. 542-552.

191. Afazov, S., S. Ratchev, and J. Segal, *Modelling and simulation of micro-milling cutting forces.* Journal of Materials Processing Technology, 2010. **210**(15): p. 2154-2162.

192. Thepsonthi, T. and T. Özel, *3-D finite element process simulation of micro-end milling Ti-6Al-4V titanium alloy: experimental validations on chip flow and tool wear.* Journal of Materials Processing Technology, 2015. **221**: p. 128-145.

193. Uçak, N., et al., *Constitutive modelling of Ti6Al4V alloy fabricated by laser powder bed fusion and its application to micro cutting simulation.* Mechanics of Materials, 2023: p. 104756.

194. Liu, D., et al., *Modified material constitutive model with activation energy for machining of selective laser melted Ti6Al4V alloys fabricated by different scanning strategies.* Journal of Materials Research and Technology, 2023. **24**: p. 9612-9629.

195. Zhao, Z., S. To, and Z. Zhuang, *Serrated chips formation in micro orthogonal cutting of Ti6Al4V alloys with equiaxial and martensitic microstructures.* Micromachines, 2019. **10**(3): p. 197.

196. Liu, D., et al., *Serrated chip characteristics and formation mechanism in high-speed machining of selective laser melted Ti6Al4V alloys.* Science China Technological Sciences, 2023: p. 1-16.

197. Rahul, Y., K. Vipindas, and J. Mathew, *Methodology for prediction of sub-surface residual stress in micro end milling of Ti-6Al-4V alloy.* Journal of Manufacturing Processes, 2021. **62**: p. 600-612.

198. Wu, H. and S. Zhang, *3D FEM simulation of milling process for titanium alloy Ti6Al4V.* The International Journal of Advanced Manufacturing Technology, 2014. **71**(5): p. 1319-1326.

199. Ruibin, X. and H. Wu, *Study on cutting mechanism of Ti6Al4V in ultra-precision machining.* The International Journal of Advanced Manufacturing Technology, 2016. **86**(5): p. 1311-1317.

200. Yadav, R., N. Chakladar, and S. Paul, *A dynamic recrystallization based constitutive flow model for micro-machining of Ti-6Al-4V.* Journal of Manufacturing Processes, 2022. **77**: p. 463-484.

201. Gupta, M.K., et al., *Cutting forces and temperature measurements in cryogenic assisted turning of AA2024-T351 alloy: An experimentally validated simulation approach.* Measurement, 2022. **188**: p. 110594.

202. Ducobu, F., E. Rivière-Lorphèvre, and E. Filippi, *On the importance of the choice of the parameters of the Johnson-Cook constitutive model and their influence on the results of a Ti6Al4V orthogonal cutting model.* International Journal of Mechanical Sciences, 2017. **122**: p. 143-155.

203. Ucun, İ., et al., *3D numerical modelling of micro-milling process of Ti6Al4V alloy and experimental validation.* Advances in Materials and Processing Technologies, 2017. **3**(3): p. 250-260.

204. Zheng, Z., et al., *Research on the Cutting Force and Serrated Chips in Ultra-Precision Micro-Grooving of SLM Ti6Al4V Alloy.* Micromachines, 2023. **14**(3): p. 533.

205. Zhang, P., et al., *Investigation on the mechanism of micro-milling CoCrFeNiAlX high entropy alloys with end milling cutters.* Vacuum, 2023. **211**: p. 111939.

206. Oliaei, S.N.B. and Y. Karpat, *Investigating the influence of built-up edge on forces and surface roughness in micro scale orthogonal machining of titanium alloy Ti6Al4V.* Journal of Materials Processing Technology, 2016. **235**: p. 28-40.

207. Hatefi, S. and K. Abou-El-Hossein, *Experimental investigation on the effects of magnetic field assistance on the quality of surface finish for sustainable manufacturing of ultra-precision single-point diamond turning of titanium alloys.* Frontiers in Mechanical Engineering, 2022. **8**: p. 1037372.

208. Xiao, J., et al., *Experimental investigation for ultra-precision cutting of nickel based superalloy with the assistance of magnetic field.* Science China Technological Sciences, 2022. **65**(9): p. 2170-2177.

209. Hatefi, S. and K. Abou-El-Hossein, *Review of magnetic-assisted single-point diamond turning for ultra-high-precision optical component manufacturing.* The International Journal of Advanced Manufacturing Technology, 2022. **120**(3): p. 1591-1607.

210. Arrazola, P.-J., et al., *Machinability of titanium alloys (Ti6Al4V and Ti555. 3).* Journal of materials processing technology, 2009. **209**(5): p. 2223-2230.

211. Zhang, Y., et al., *Diamond tool wear in precision turning of titanium alloy.* Materials and Manufacturing Processes, 2013. **28**(10): p. 1061-1064.

212. Lou, Y. and H. Wu, *Effect of parameters on surface roughness during the ultra-precision polishing of titanium alloy.* PloS one, 2022. **17**(8): p. e0272387.

213. Yip, W. and S. To, *Effects of magnetic field on microstructures and mechanical properties of titanium alloys in ultra-precision diamond turning.* Materials Research Express, 2019. **6**(5): p. 056553.

214. Yip, W.S. and S. To, *Reduction of tool tip vibration in single-point diamond turning using an eddy current damping effect.* The International Journal of Advanced Manufacturing Technology, 2019. **103**: p. 1799-1809.

215. Yip, W. and S. To, *An application of eddy current damping effect on single point diamond turning of titanium alloys.* Journal of Physics D: Applied Physics, 2017. **50**(43): p. 435002.

216. Gavili, A., et al., *The thermal conductivity of water base ferrofluids under magnetic field.* Experimental Thermal and Fluid Science, 2012. **41**: p. 94-98.

217. Altan, C.L., et al., *Enhancement of thermal conductivity upon application of magnetic field to Fe3O4 nanofluids.* Journal of Applied Physics, 2011. **110**(9).

218. Sundar, L.S., M.K. Singh, and A.C. Sousa, *Investigation of thermal conductivity and viscosity of Fe3O4 nanofluid for heat transfer applications.* International communications in heat and mass transfer, 2013. **44**: p. 7-14.

219. Younes, H., et al., *Effects of alignment, pH, surfactant, and solvent on heat transfer nanofluids containing Fe2O3 and CuO nanoparticles.* Journal of Applied Physics, 2012. **111**(6).

220. Yip, W. and S. To, *Reduction of material swelling and recovery of titanium alloys in diamond cutting by magnetic field assistance.* Journal of Alloys and Compounds, 2017. **722**: p. 525-531.

221. Nkurikiyimfura, I., Y. Wang, and Z. Pan, *Heat transfer enhancement by magnetic nanofluids—a review.* Renewable and Sustainable Energy Reviews, 2013. **21**: p. 548-561.

222. Lajvardi, M., et al., *Experimental investigation for enhanced ferrofluid heat transfer under magnetic field effect.* Journal of Magnetism and Magnetic Materials, 2010. **322**(21): p. 3508-3513.

223. Nkurikiyimfura, I., Y. Wang, and Z. Pan, *Effect of chain-like magnetite nanoparticle aggregates on thermal conductivity of magnetic nanofluid in magnetic field.* Experimental Thermal and Fluid Science, 2013. **44**: p. 607-612.

224. Philip, J., P. Shima, and B. Raj, *Evidence for enhanced thermal conduction through percolating structures in nanofluids.* Nanotechnology, 2008. **19**(30): p. 305706.

225. Philip, J., P. Shima, and B. Raj, *Enhancement of thermal conductivity in magnetite based nanofluid due to chainlike structures.* Applied physics letters, 2007. **91**(20).

226. Rehan, M., et al., *Magnetic field assisted micro-milling of selective laser melted titanium alloy.* Journal of Manufacturing Processes, 2025. **134**: p. 494-504.

227. Wichmann, W., et al., *Aneurysm clips made of titanium: magnetic characteristics and artifacts in MR.* American journal of neuroradiology, 1997. **18**(5): p. 939-944.

228. Collings, E., *A sourcebook of titanium alloy superconductivity*. 2012: Springer Science & Business Media.

229. Yip, W. and S. To, *Sustainable manufacturing of ultra-precision machining of titanium alloys using a magnetic field and its sustainability assessment.* Sustainable Materials and Technologies, 2018. **16**: p. 38-46.

230. Dai, Y. and K. Zhu, *A machine vision system for micro-milling tool condition monitoring.* Precision engineering, 2018. **52**: p. 183-191.

231. Miao, J., et al., *Review of dynamic issues in micro-end-milling.* The International Journal of Advanced Manufacturing Technology, 2007. **31**: p. 897-904.

232. Bai, W., et al., *Improved analytical prediction of chip formation in orthogonal cutting of titanium alloy Ti6Al4V.* International Journal of Mechanical Sciences, 2017. **133**: p. 357-367.

233. Yip, W. and S. To, *Tool life enhancement in dry diamond turning of titanium alloys using an eddy current damping and a magnetic field for sustainable manufacturing.* Journal of Cleaner Production, 2017. **168**: p. 929-939.

234. Leo Kumar, S. and D. Avinash, *Influence of cutting conditions on surface characteristics in micro-milling of Ti-6Al-7Nb alloy.* Materials and Manufacturing Processes, 2019. **34**(16): p. 1783-1791.

235. Wang, Y., et al., *Feasibility study of the Ti (C7N3)-based cermet micro-mill based on dynamic fatigue behavior and modeling of the contact stress distribution on the round cutting edge.* International Journal of Mechanical Sciences, 2019. **155**: p. 143-158.

236. Wu, X., et al., *Investigation on surface quality in micro milling of additive manufactured Ti6Al4V titanium alloy.* Journal of Manufacturing Processes, 2023. **101**: p. 446-457.

237. Sun, Z., et al., *Theoretical and experimental investigation into non-uniformity of surface generation in micro-milling.* International Journal of Mechanical Sciences, 2018. **140**: p. 313-324.

238. Chen, N., et al., *Design, optimization and manufacturing of polycrystalline diamond micro-end-mill for micro-milling of GH4169.* Diamond and Related Materials, 2020. **108**: p. 107915.

239. Liu, H., et al., *Experimental research of milling force and surface quality for TC4 titanium alloy of micro-milling.* The International Journal of Advanced Manufacturing Technology, 2015. **79**: p. 705-716.

240. Khalil, A.K., W. Yip, and S. To, *Theoretical and experimental investigations of magnetic field assisted ultra-precision machining of titanium alloys.* Journal of Materials Processing Technology, 2022. **300**: p. 117429.

241. Komanduri, R., *Some clarifications on the mechanics of chip formation when machining titanium alloys.* Wear, 1982. **76**(1): p. 15-34.

242. Ezugwu, E. and Z. Wang, *Titanium alloys and their machinability—a review.* Journal of materials processing technology, 1997. **68**(3): p. 262-274.

243. Sartori, S., et al., *On the tool wear mechanisms in dry and cryogenic turning Additive Manufactured titanium alloys.* Tribology International, 2017. **105**: p. 264-273.

244. Vipindas, K. and J. Mathew, *Wear behavior of TiAlN coated WC tool during micro end milling of Ti-6Al-4V and analysis of surface roughness.* Wear, 2019. **424**: p. 165-182.